Spatio-temporal organisation of plasma membrane proteins in budding yeast

FELIX SPIRA

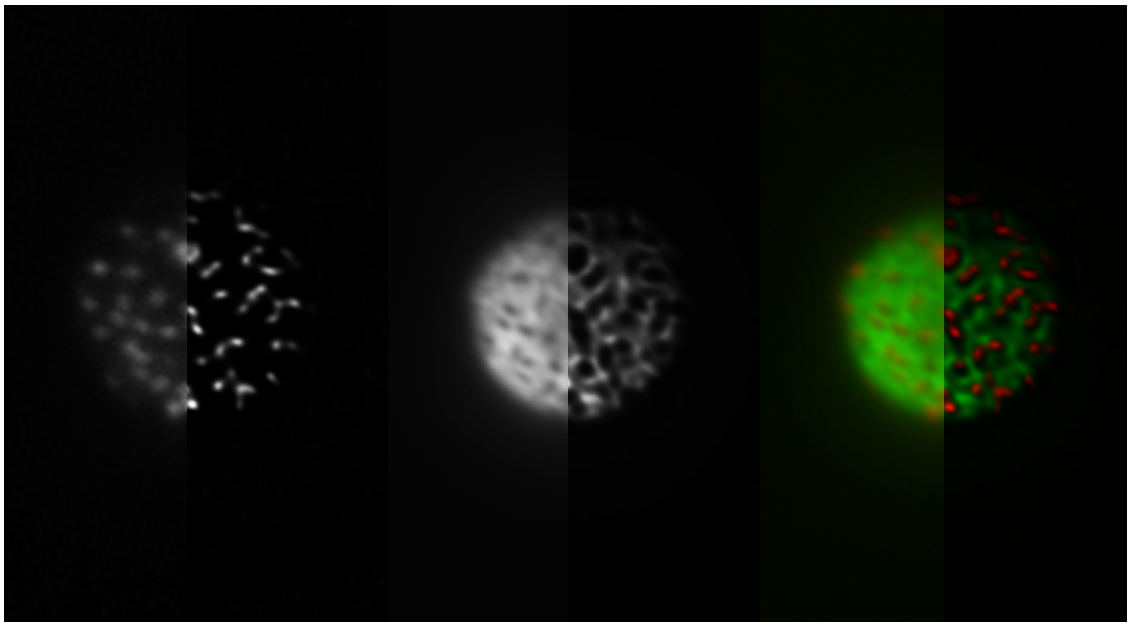

Dissertation
der Fakultät für Biologie
der Ludwig-Maximilians-Universität München

Spatio-temporal organisation of plasma membrane proteins in budding yeast

FELIX SPIRA

Dissertation
der Fakultät für Biologie
der Ludwig-Maximilians-Universität München

vorgelegt von
Felix Spira
aus Dillenburg
München, den 19. März 2012

Erstgutachter:	Prof. Dr. Stefan Jentsch
Zweitgutachter:	Prof. Dr. Charles David

Tag der mündlichen Prüfung: 21.6.2012

Für meine Eltern

Another Athens shall arise,
And to remoter time
Bequeath, like sunset to the skies,
The splendour of its prime;
And leave, if naught so bright may live,
All earth can take or Heaven give.
Percy Bysshe Shelly (1792-1822)

Contents

Chapter 1

Abstract

The plasma membrane (PM) is a complex system of lipids and proteins, which provides a selective barrier to the cell's environment as well as a localisation platform for signalling molecules. Many plasma membrane proteins have been shown to be laterally segregated into different domains and the mechanisms underlying this segregation have been the subject of intense debate. In this work we used the model organism *Saccharomyces cerevisiae* to systematically evaluate distribution and dynamics of plasma membrane proteins in living cells. To obtain reliable data we examined a comprehensive set of integral and peripheral PM proteins and used Total Internal Fluorescence Reflection Microscopy (TIRFM) which allows to obtain images with a high contrast and allows fast acquisition times. A semi-automated workflow was implemented for unbiased data analysis and to facilitate the handling of large datasets. The observed proteins localised to a large number of distinct or partially overlapping domains. Remarkably, segregation of proteins was directly driven by the sequence of their respective transmembrane segments and proteins were predictably relocated by swapping transmembrane regions. In addition we could show that lipid composition had a strong and selective effect on PM protein pattern. We also demonstrated that correct domain association of proteins was essential for their biological function. These results suggest a simple model for self organisation of biological membranes through weak interactions between proteins and lipids. After describing the PM as a highly segregated and organised multi-domain system, we examined the spatio-temporal relationship between PM domains and endocytic sites. Interestingly, we found no extensive co-localisation between endocytic patch marker proteins and any of our identified PM domains. In particular, we could show a general low turnover of PM proteins. To enable endocytosis, the eisosomal

amino acid transporter Mup1, first had to leave the eisosomal domain. In a second step, ubiquitylation of Mup1 led to the recruitment to endocytic sites. Artificially tethering Mup1 to eisosomes completely abolished endocytic uptake, indicating that cargo was not sufficient for recruitment of the endocytic machinery. Strikingly, directed re-localisation of proteins of the early endocytic coat module led to productive assembly of endocytic sites at the chosen domain. In conclusion, we provide new insights into the spatio-temporal regulation of early endocytosis and could clearly separate cargo selection and internalisation. In addition we identified endocytic master regulators sufficient for endocytic site selection. This study not only is a first representative characterisation of the yeast PM revealing numerous co-existing domains but also shed light on the spatio-temporal dependencies of domain association and endocytosis.

Chapter 2

Introduction

The plasma membrane (PM) is a semi-permeable barrier separating the inside of a cell from the environment. This highly specialised organelle selectively mediates the uptake of molecules required for cellular function while being impermeable for others. Additionally, the PM is used as a platform for many different signalling pathways. To fulfil these essential tasks, the cell not only has to orchestrate many different transport and signalling proteins, but also has to respond quickly to environmental changes.

In order to understand the PM, it is important to revisit lipids, proteins and protein-lipid interactions, as well as membrane organisation principles.

2.1 Lipids

The PM is a fluid bilayer composed of hundreds of different lipid species which has an average thickness of about 35Å. The thickness of the bilayer is influenced by the acyl chain length of the lipids and by the amount of cholesterol which leads to an increased bilayer thickness (Lee, 2005) and influences the fluidity of the membrane (see section 2.5). The building blocks of the lipid bilayer are phospholipids, sphingolipids and sterols (Fig. 2.1 A-C). Phospholipids and sphingolipids differ greatly in acyl chain length, acyl chain saturation and headgroups. Lipids are amphiphilic molecules with long hydrophobic aliphatic chains and a hydrophilic head group. In an aqueous environment like the cytoplasm, lipids minimise the area exposed to water molecules by assembling into a bilayer with hydrophobic tails pointing towards the core of the membrane and headgroups pointing towards the

solvent. The average length of the aliphatic chains of phospholipids is either 16 or 18 carbon atoms and sphingolipids are with 18 or 20 carbons on average longer. In contrast to flexible saturated acyl chains, unsaturated chains contain a “kink”, therefore they are less flexible and can not be packed as tight as flexible saturated chains (Fig. 2.1 A).

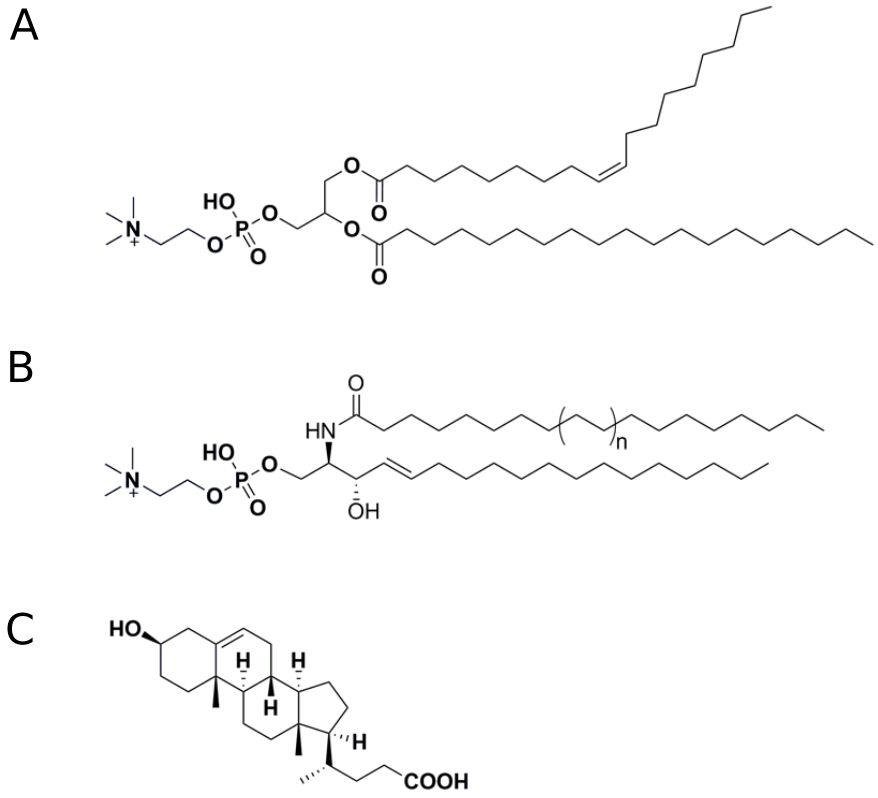

Figure 2.1: Main lipid classes. A) Phospholipid (Phosphatidylcholine) B) Sphingolipid (Sphingomyelin) C) Sterol (Cholesterol)

2.1.1 Phospholipids

Phospholipids contain a glycerol molecule as a backbone, which is esterified with fatty acyl chains on carbon 1 and 2. The acyl chain in position C1 is often unsaturated and 16 or 18 carbons in length and on average shorter than the usually unsaturated chain in position C2 (Fig. 2.1 A). The biophysical properties of phospholipids are very diverse in terms of charge and size. Phosphatidylserine (PS), phosphatidylinositol 4,5 bisphosphosphate (PIP2) and phosphatidylinositol (PI) contain a negative net charge and are major contributors to the

overall negative net charge of the PM. PS levels can rise to 30%, while PIP2 is less abundant and accounts for only 1% of total lipids (McLaughlin and Murray, 2005).

The reactive amines of PE and PS can undergo hydrogen bonding with interfacial water molecules, other lipid headgroups or membrane proteins. In addition to charge or hydrogen bonding, the lipid bilayer is influenced by steric constrains of the lipids. The bulky phospholipids phosphatidylinositol (PI) and phosphatidylchline (PC) affect the packing of the PM due to steric hindrance, while the wedge shaped and small phosphoethanolamine (PE) can introduce membrane curvature (Carman and Han, 2011) (see section 2.1.4).

Phospholipids are synthesised within the endoplasmic reticulum (ER), the mitochondrial inner membrane and the golgi apparatus Natter et al. (2005) via the canonical CDP-DAG pathway (Fig. 2.2). Within this pathway the phosphatidyl moiety of CDP-DAG is linked with serine resulting in PS. In budding yeast this reaction is carried out by the phosphatidylserine synthase Cho1. PS is decarboxylated by the decarboxylases Psd1/2 to PE. Cho2 and Opi3 catalyse three consecutive methylation steps which converts PE into PC. If enzymes of the canonical CDP-DAG pathway are missing phospholipids can be synthesised via the alternative Kennedy pathway, but only in the presence of appropriate precursors (Carman and Han, 2011).

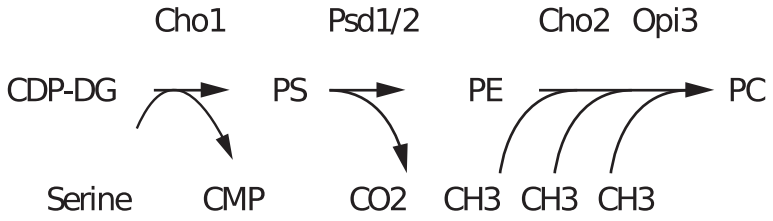

Figure 2.2: CDP-DAG Pathway. Scheme showing the necessary steps and enzymes of the canonical phospholipid synthesis pathway. The phosphatidyl moiety of CDP-DAG becomes linked with serine resulting in PS. PS is then de-carboxylated to PE, which becomes converted into PC by three consecutive methylation reactions.

2.1.2 Sphingolipids

Sphingolipids contain a sphingosine instead of a glycerol backbone which is linked via an amide bond to an acyl chain to form a ceramide (Coskun and Simons, 2011). In general sphingolipids are saturated and range from 18 to 24 carbon atoms and are on average longer than phospholipids (Fig. 2.1 B). Three different classes of glyco-sphingolipids are

present in *Saccharomyces cerevisiae* and all use a ceramide as a precursors and are interchangable. The single inositol phosphate containing inositolphosphoceramide (IPC), mannose-inositol-phosphoceramide (MIPC) and the main sphingolipid in yeast, mannose-(inositol-P)2-ceramide ($M(IP)_2C$) (van der Rest et al., 1995; Ejsing et al., 2009). Similar to phospholipids different chains and headgroups can generate thousands of different sphingolipids (Coskun and Simons, 2011; Yetukuri et al., 2008). The first and rate limiting step of sphingolipid biosynthesis is the condensation of a fatty acid CoA with serine, this reaction is catalysed by a serine palmitoyltransferase generating C18 or C20 products (Reggiori et al., 1997). This first step can be blocked by the drug myriocine (van der Rest et al., 1995) and abolishes long chain bases biogenesis completely. Synthesis of sphingolipids is carried out in the ER and the golgi apparatus (van der Rest et al., 1995).

2.1.3 Sterols

Sterols are rigid hydrophobic molecules with a polar hydroxyl group and are only present in eukaryotic membranes (Fig. 2.1 C). In mammalian cells cholesterol is the dominant sterol, while yeast membranes mainly contain ergosterol. Cholesterol and ergosterol are almost identical and differ only in minor features (see section 2.6.4). Sterols are synthesised in the ER and are delivered via the secretory pathway to the PM (Cowart and Obeid, 2007) and account for 30% of all PM lipids in budding yeast (Coskun and Simons, 2011). The rigid backbone of cholesterol can align between saturated acyl chains of sphingolipids, thereby increasing the conformational order of adjacent lipids resulting in a tight packing. Interestingly, cells can balance changes in the sterol content. In *Saccharomyces cerevisiae* the single knockout of a gene required for ergosterol synthesis has only mild defects on cellular function, while a multiple deletion of genes involved in ergosterol biosynthesis lead to drastic growth defects and detectable alterations in protein and lipid composition (Guan et al., 2009; Ganguly et al., 2009; Abe and Hiraki, 2009).

2.1.4 Lipid and membrane phases

Lipids organise spontaneously into a lamellar phase which corresponds to the classical planar bilayer. But some lipids organise into different phases like the cubic or inverted hexagonal phase. The conical PE can form spontaneously tubes, with head groups pointing

towards the solvent and the aliphatic backbone facing the inner of the tube. Interestingly, PC which differs from PE in only three additional methyl groups forms a planar lamellar bilayer while PE forms a hexagonal phase. This different behaviour can be explained by steric constrains of the additional methyl groups in PC and the capacity of PE to undergo intermolecular hydrogen bonding with other lipids. Intermolecular bonding will lead to a decreased hydration of the lipids which promotes tube formation (Lee, 2004). Embedded within a complex bilayer PE will not induce a hexagonal phase, but introduce membrane curvature. On the one hand this helps to quickly respond to hydrophobic mismatch, on the other hand curvature is also required for many processes like endo– and exocytosis or lateral domain formation.

Because of their cooperative behaviour, even simple lipid mixtures have a strong tendency to phase separate or to form lateral domains (Bagatolli et al., 2010b). The range of this co-operativity is reflected by the coherence length and depends on the composition and properties of the constituent lipids such as orientation, chain length and chain order. The most important phase transition with respect to lateral domain formation is the "main transition" from the liquid-ordered (L_O) to the liquid-disordered (L_D) phase.

Sphingolipids in combination with sterols can undergo a phase transition if mixed with phospholipids. Sphingolipids/sterols form crystalline or liquid ordered domains (L_O), while phospholipids are less tightly ordered and form liquid disordered (L_D) domains. These L_O/L_D domains are the basis of the lipid raft membrane organisation concept, which is discussed in section 2.5.

2.1.5 Lipid asymmetry of the plasma membrane

Although lipid synthesis is asymmetrical, lipids are randomly distributed between the two leaflets of the ER membrane (van Meer, 2011). Special enzymes facilitate the unspecific exchange of lipids between the two leaflets without requiring energy (Sanyal et al., 2008). Lipid asymmetry of the PM is introduced during the transit along the secretory pathway towards the PM and is actively maintained by specialised enzymes called flippases. This energetically unfavourable exchange of lipids between the leaflets requires the hydrolysis of ATP. Sphingolipids are enriched in the outer leaflet (up to 6 fold), while phospholipids like PS and PE are more abundant in the inner leaflet. Sterols can move freely between

the two leaflets, however, they have a preference to co-cluster with sphingolipids and are therefore more abundant in the outer PM leaflet (Sharom, 2011).

In *Saccharomyces cerevisiae* the flippase complexes Dnf1 or Dnf2 and Lem3 are required to keep aminophospholipids at the inner leaflet (Devaux, 1992; van Meer, 2011). If Lem3 is deleted PE can not be “flipped” to the inner leaflet and remains exposed to the environment. This in turn keeps the Rho GTPase and cell polarity protein Cdc42 at the polarised tip and renders the cells unable to switch from polarized to an isotropic growth (Saito et al., 2007). Another study showed a modulation of Cdc42 membrane association in dependence on flippase activity. Cdc42 membrane association is mediated by prenylation of the protein and additionally vie electrostatic protein lipid interactions. Inward movement of uncharged PE “dilutes" the negatively charged PS, reducing the negative net charge of the PM and therefore lowering the membrane affinity of Cdc42 (Das et al., 2012). These examples show the importance of lipid asymmetry for polarisation of the cell.

Lipid asymmetry is also known to occur in mammalian cells. Apoptosis for example is triggered by flipping PS to the PM leaflet. (Armstrong and Ravichandran, 2011; Elliott et al., 2005). Another example of the importance of phospholipids in domain formation and cellular function is given by the phospholipid PE. During abscission the last step of cell division, a large intercellular bridge is formed which is highly enriched in PE that is “flopped” to the outer leaflet during this event. As long as PE is located at the outer leaflet of the membrane, abscission cannot be completed (Emoto and Umeda, 2000). Whether this intercellular bridge is formed by the accumulation of PE or whether it is an indirect effect is currently unknown.

2.2 Plasma membrane proteins

Biomembranes are not only a “sea” of lipids with a few freely diffusing proteins but represent a rather crowded environment. A protein content of 80% was observed in some cell types (Luckey, 2008). Several different types of integral membrane and membrane associated proteins are known (Fig. 2.3). PM proteins can be either integral with one or more TMS, anchored with a lipid moiety or bind via specialised domains to lipid headgroups. Proteins localising to the membrane via Lipid binding domains (LBDs) are considered to be peripheral proteins. Integral TM-proteins which account for the largest group of PM

proteins, fulfil a broad variety of different tasks ranging from “house keeping” functions like the import/export of molecules to signalling platforms or sensors.

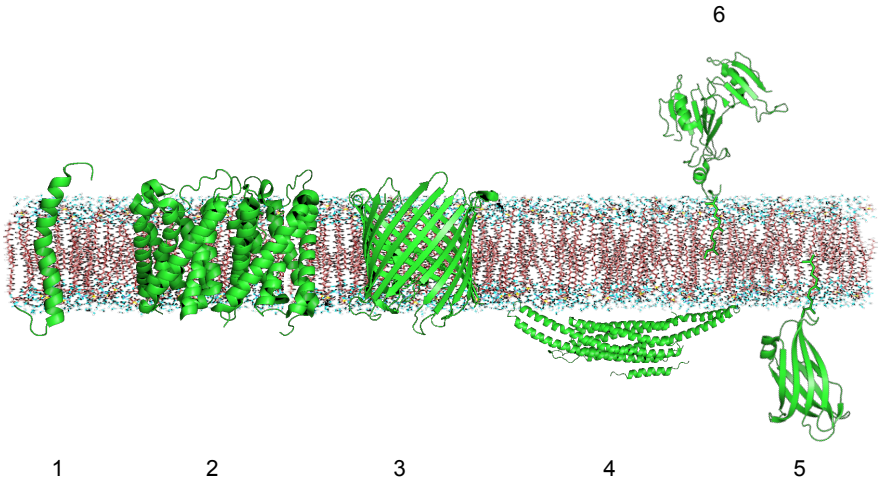

Figure 2.3: PM proteins classes. 1. Single spanning TM protein 2. Multi spanning TM protein 3. Beta barrel membrane protein 4. Lipid binding protein 5. Lipid anchored membrane protein 6. GPI anchored protein

2.2.1 Integral membrane proteins

Most integral TM proteins are co-translationally inserted into the ER membrane. During translation the signal peptide of a protein is bound by the signal recognition particle (SRP) which mediates the insertion of the nascent amino acid chain into the lipid bilayer. The synthesised peptide transits through the golgi and is packed into a secretory vesicle and eventually delivered to the PM. Transmembrane sequences of integral membrane proteins are longer the further a protein progresses through the secretory pathway. The TMS of PM proteins are on average longer than the TMS of integral ER or golgi proteins (Sharpe et al., 2010). Besides the canonical SRP mediated co-translational insertion of membrane proteins another pathway was identified, in which proteins become post translationally inserted into the PM. These tail anchored proteins bind to a soluble chaperon which mediates an ATP dependent transfer of the protein to the the membrane (High and Abell, 2004). Computational analysis predict 2%-5% of all membrane proteins to be tail anchored proteins (Hegde and Keenan, 2011).

TM proteins are classified according to the orientation of the N-terminus and the number of membrane spanning segments. Type I membrane proteins, the most common class of single spanning membrane proteins, have their amino terminus exposed to the extracellular space. Type II membrane proteins have their amino terminal exposed to the cytoplasm and Type III proteins are multi pass TM proteins (Luckey, 2008).

Roughly 300 proteins are annotated to be integral or PM associated proteins in *Saccharomyces cerevisiae*, of which 150 are present at the PM at a given time. The largest group of TM proteins are transporters (Type III), which account for 50% of all PM proteins (van der Rest et al., 1995). Transport proteins can be divided into two groups: Primary-transport-systems, in which light or chemical energy is converted into electrochemical energy and secondary-transport-systems which couples the transport of a molecule to the translocation of a second. Typical primary-systems are ATPases or ATP-binding-cassette (ABC) transporters. An electrochemical gradient established by an ATPase is often used to drive secondary-transporter-systems. Two molecules can be either transported in the same direction (symport) or in opposite directions (antiport). In some cases the electrochemical gradient of the transported molecule does not require further energy (uniport), the major function of this type of transport is facilitated diffusion.

Most transporters rely on the establishment and maintenance of a proton (H^+) gradient. As described above, the establishment of a proton gradient requires energy (primary-transport-system). The main ATPase in budding yeast Pma1 is crucial to maintain this proton gradient and is essential for survival of the cell. It is a highly abundant protein and accounts for 50% of all Type III membrane proteins (Serrano, 1978). The arginine permease Can1 is a typical secondary-symport-transport-system, that requires the proton gradient established by Pma1 to translocate the amino acid arginine against a gradient across the PM into the cell (Wipf et al., 2002; Ahmad and Bussey, 1986).

2.2.2 Peripheral membrane proteins

Proteins without membrane spanning sequences use either lipid anchors or lipid binding motifs to localise to the plasma membrane. These proteins bind often transiently to the PM and are used as signalling modules.

2.2.3 Lipid anchored PM proteins

Lipid modifications such as N-terminal N-myristoylation, C-terminal glycosyl phosphatidylinositol (GPI) anchor, S-acetylation or S-prenylation can mediate attachment of proteins to the PM. While S-prenylation is restricted to cysteins at the C-terminus, S-acetylation occurs on serins or cysteins throughout the protein (Walsh, 2006). In total five different lipid groups can be transferred to a protein (Fig. 2.4 A-D and Tab. 2.1).

While palmitoylation is a type of S-acetylation, which requires a palmitoyl (C_{16}) to be covalently linked to a serine or cysteine within the protein (Fig. 2.4 A), myristoylation requires the attachment of a myristoyl (C_{14}) group (Fig. 2.4 B). Palmitoylation and myristoylation are by far the most common forms of S-acetylation but different acyl chains, like stearic acid, or arachidonic acid can also be transferred to a protein.

S-prenylation occurs exclusively at the last C-terminal amino acid of a protein and requires either a farnesyl (C_{15}) or a geranylgeranyl (C_{20}) group linked to a cystein (Fig. 2.4 C). Prenylated proteins contain a C-terminal CaaX box, whereby the amino acids at position X determines the kind of modification (farnesylated or geranylgeranylated) (Didsbury et al., 1990). The C-terminus is often cleaved after prenylation to increase the membrane affinity of the protein.

The Glycophosphatidylinositol (GPI) anchor is a form of post-translational modification in which a pre-assembled GPI anchor becomes covalently linked to the C-terminus of a protein. The anchor is very complex and contains ethanolamine, sugars and phosphatidylinositol (Fig. 2.4 D). Before the GPI anchor is transferred to the protein the C-terminus becomes cleaved by an endopetidase at the ER (Walsh, 2006). Proteins containing this type of membrane attachment are exclusively targeted to the outer leaflet of the PM and are associated with sphingolipid and sterol enriched membrane domains.

Protein lipidation is carried out posttranslational in the cytoplasm with the exception of N-myristoylation, which occurs co-translationally.

Except for GPI anchored proteins a single lipid anchor is not sufficient to stably attach a protein to the PM. Therefore proteins contain frequently more than one lipid anchor and additional positive charged patches, which interact with the negative lipid headgroups of

PM lipids. Lipid modifications are not restricted to cytoplasmic proteins, S-acetylation and N- myristoylation can be also found within integral TM proteins (Casey, 1995).

Protein lipidation is important for many signalling pathways that emanate at the PM. Most of the early effector proteins contain lipid modifications. If lipidation is blocked, downstream signalling of the pathway is impaired. For example, small Rho-GTPases like Ras or Cdc42 require a lipid anchor to localise to the PM. Miss-localisation can lead to cell death. This is exploited by anti cancer drugs which block steps in the prenylation pathway of Rho GTPases such as N– and K-Ras, eventually resulting in apoptosis (Roberts et al., 2008; Prendergast, 2000).

Table 2.1: Protein lipidation

lipid	length	postion
N-Myristoyl	C_{14} Myristoyl	N-terminus
S-Palmitoyl	C_{16} Palmitoyl	Internal
S-Prenyl	C_{15} Farnesyl	C-terminus
	C_{20} Geranylgeranyl	
GPI	complex containing ethanolamine, sugars and phosphatidylinositol	C-terminus

2.2.4 Lipid binding domains

Beside integral transmembrane stretches and lipid anchors, membrane binding of proteins can be achieved via lipid-binding domains (LBDs). These modular domains bind reversibly to membranes and are frequently found in signalling molecules. LBDs usually complement negatively charged lipid headgroups with positively charged pockets as it is the case of the PIP2 binding domain of Plc δ (Stauffer et al., 1998), or the binding of C2 domains to PS (Yeung et al., 2008). The first C2 domain was identified within protein kinase C, which is localises to membranes in the presence of Ca^{2+} ions. Unlike other LBDs C2 domains contain no charged patches, instead the negatively charged lipid is attracted by a positive

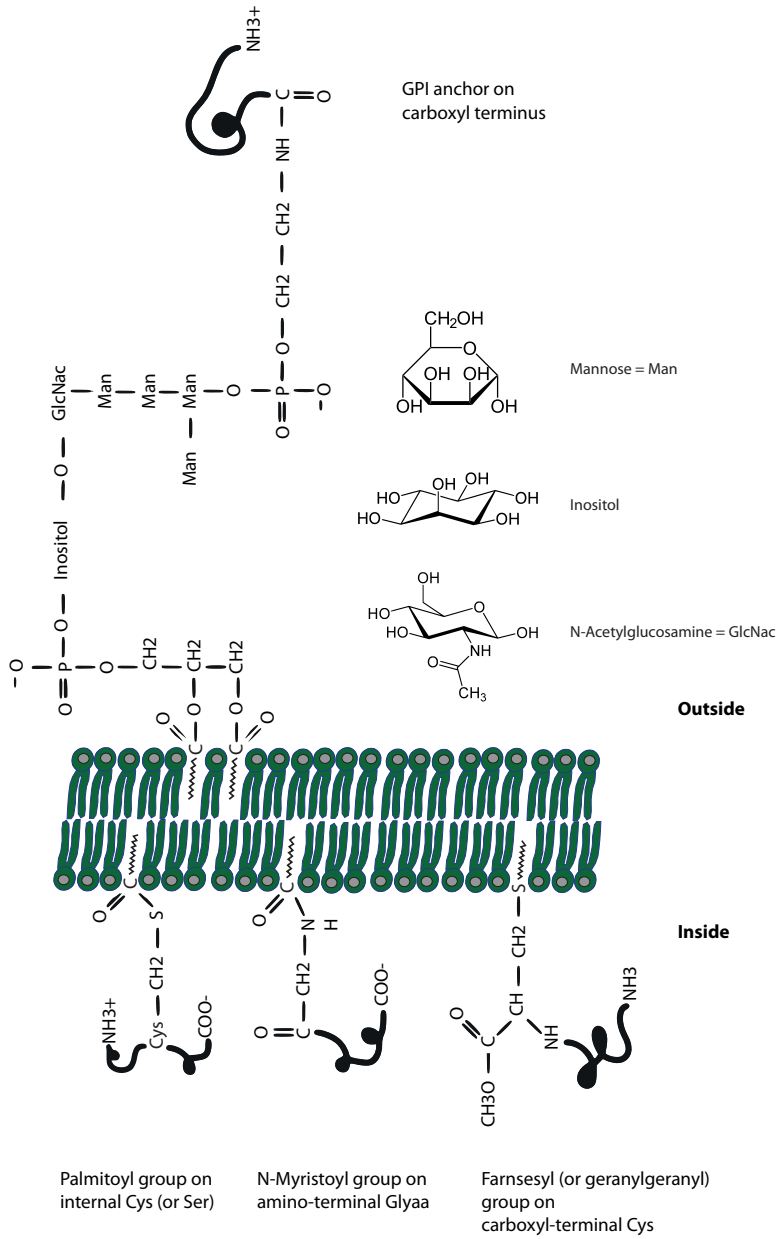

Figure 2.4: Protein lipidation. Three lipid modification exist at cytosolic proteins (Palmitoylation, myristoylation and farnesylation). GPI anchored proteins are always attached at the extracellular side of the PM. Adapted from Luckey 2008

.

Ca^{2+} ion (Lemmon, 2008). In addition to the electrostatic interactions LBD containing proteins often insert short hydrophobic helices into the membrane. Insertion of hydrophobic

amino acids into the membrane can lead to membrane curvature, as it is the case of Bin-Amphiphysin-Rvs167 (Bar) domains containing proteins (Lemmon, 2008). Currently 172 proteins containing lipid binding domains are annotated in *Saccharomyces cerevisiae* which bind to all major lipid classes. Although much research has been carried out, unfortunately *in vivo* data for lipid specificity are missing for most of the LBDs. The layer of complexity is even further increased by a combinatorial binding of LBDs to different lipids species (Gallego et al., 2010).

2.3 Protein-lipid interactions

Biological membranes are multi-component systems and it is not possible to single out individual contributions of each component, thus the PM represents a complex interplay between many different molecules. Knowledge about protein lipid interactions is important to understand plasma membrane domain formation. Hundreds of different lipid species are present within biological membranes, allowing a plethora of different interactions (Lee, 2011). Very often, the sum of many weak forces, like van der Waals interactions, electrostatics and hydrogen bonding result in very strong forces.

Generally, protein lipid interactions are difficult to study in detail but many different interactions are known, either by simple matching of charges (Galla and Sackmann, 1975; Lehtonen et al., 1996b) or by directly fitting into the shapes dictated by membrane proteins (Hite et al., 2010), the latter can even be visualised by electron crystallography (Wisedchaisri et al., 2011). These tightly bound lipids are called structural lipids which can influence the protein function dramatically, as shown for the potassium channel Kir2 (Hansen et al., 2011). This channel possess an unspecific phospholipid binding domain within the transmembrane segment (TMS) and a pocket that allows specific binding of phosphatidylinositol to the cytosolic part. PIP2 binding results in a large conformational shift of about 6Å, which leads to an opening of the channel (Hansen et al., 2011). Another interesting mechanism for protein lipid interaction is exploited by the mitochondrial protein cytochrome C. The protein binds to one the two acyl chains of a phospholipid, while the other chain remains embedded within the PM (Tuominen et al., 2002).

Lipids are highly dynamic and interact only transiently with the TMS of proteins and create a unique environment around a protein. The first layer of lipids surrounding a protein is

called annulus. Diffusion of annular lipids is slowed down, but they still exchange rapid with bulk lipids (Lee, 2011). As a result of the transient nature of this protein-lipid interaction, the local lipid environment surrounding a protein will be enriched with lipids that match the physicochemical requirements of the protein best. The size of the lipid environment surrounding a protein is determined by the coherence length and it is important for lateral PM domain formation (see section 2.1.4).

2.4 Regulation of membrane proteins

Membrane proteins are subject of tight regulation. According to the *Saccharomyces* genome database (SGD) 300 proteins are annotated to be PM proteins, but only 150 different PM proteins are present at a given time point in budding yeast (van der Rest et al., 1995). PM proteins which are not longer required are quickly removed from the PM via a process called endocytosis (see figure 2.5). Clathrin mediated and actin dependent endocytosis is the only endocytic pathway in budding yeast, although recently a second pathway for endocytosis utilising Rho1 and formins was proposed (Prosser et al., 2011).

2.4.1 Ubiquitylation of PM proteins

Prior to endocytosis the substrate is frequently phosphorylated and ubquitylated (Marchal et al., 1998; Hicke et al., 1998). Ubiquitin is a small protein of 76 amino acids, which is linked via the C-terminal glycine to the ε amino group of a lysine of the target protein (Nikko et al., 2008). This process is carried out by the sequential action of three ubiquitin ligases; first E1 ubiquitin activating, second E2 ubiquitin conjugation, and third the E3 ubiquitin-protein ligase which is required for protein recognition (Belgareh-Touze et al., 2008). The group of ubiquitin ligases is divided into two major families; RING (really interesting new protein) and HECT (homologous to E6-associated protein C-terminus). RING domain ubiquitin ligases promote the transfer of ubiquitin from E2 to the lysine of a target protein. HECT E3 domain ligases form a thioesther bond with ubiquitin and mediate the transfer to the protein of interest from E3 to the target protein without using E2 ligases (Staub and Rotin, 2006).

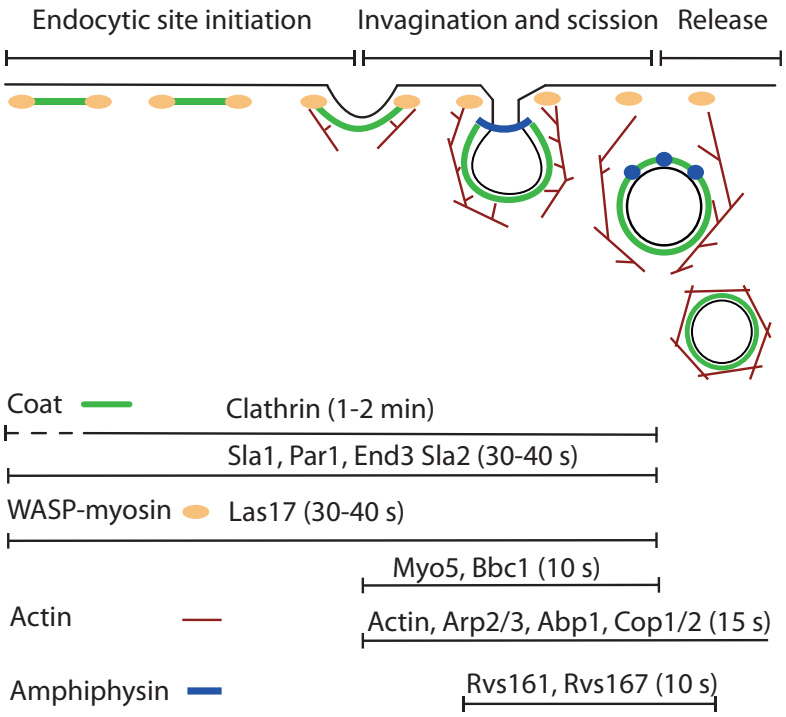

Figure 2.5: Clathrin mediated endocytosis. Endocytic proteins are organised into four modules which appear with a different timing. Early coat module proteins are required for site initiation, the actin and amphiphysin module appear at later time points at the endocytic site and are required for vesicle release and scission. Several exemplary proteins are shown. Adapted from Kaksonen et al.2006.

Ubiquitin itself contains seven lysine residues (K6, K11, K27, K29, K33, K48, and K64) which are used for chain formation (Kaliszewski and Zoadek, 2008). Ubiquitin modification represent an intercellular targeting code for PM proteins. In yeast, K-64 polyubiquitylation targets a protein towards the multivesicular body pathway, eventually resulting in degradation of the protein. Monoubiquitylation leads to internalisation of the protein and re-routing to the PM (Lauwers et al., 2010, 2009). The ubiquitylation code in mammalian cells is more complex and less well understood than the one in yeast (Mukhopadhyay and Riezman, 2007).

Rsp5, the major ubiquitin ligase in yeast and contains a HECT domain. Membrane targeting of Rsp5 is mediated via C2 domain mediated lipid binding to PS and target proteins are recognised with a WW (Trp-Trp) domain, which recognise a PY ([L/P]PxY) motif (Lauwers et al., 2010). However, most PM proteins do not contain a PY motif and the

ubiquitin ligase is recruited by an adapter protein. The first identified adapter proteins in yeast were Bul1/2 (Soetens et al., 2001; Hettema et al., 2004). The class of arrestin-related trafficking (Art) adapters is a growing class of soluble adaptors, that exclusively work on PM proteins and mediate the interaction between the E3 ligase and the target protein (Fig. 2.6) (Nikko et al., 2008; Lin et al., 2008). Proteins within this class vary greatly in terms of target specificity (Lauwers et al., 2010). Changes of environmental conditions frequently triggers a PM protein for endocytosis (Lauwers et al., 2010), which allows a allows a the constant optimisation of the yeast PM protein composition. Currently 10 different arrestins with partly overlapping substrate specificity are known to exist in *Saccharomyces cerevisiae* (Nikko and Pelham, 2009).

Amino acid transporter are often regulated in response to environmental changes, like a change in amino acid concentration. Often, if proteins are not longer required, they become ubiquitylated, endocytosed and subsequently degraded. Ubiquitylation of PM transporters require the concerted action of arrestins and Rsp5. Overlapping substrate specificities of the adaptor proteins are a frequent phenomenon. The lysine permease Lyp1 is recognised by Art1 and Art2 while the methionine permease Mup1 and the arginine permease Can1 are only recognised by Art1 (Lin et al., 2008).

2.4.2 Actin mediated endocytosis

As soon as a protein is marked for endocytosis, it is ubiquitylated, caged within a clathrin coated pit and transferred into the cell via actin mediated endocytosis. Actin mediated endocytosis is the only mechanism to remove PM proteins from the cell cortex in yeast. Although, an actin independent pathway was suggested, the existence is still under debate (Prosser et al., 2011). Actin mediated endocytosis is highly conserved between yeast and mammals and best understood in the former. It is a highly regulated and sequential process in which the interplay of almost 60 known gene products are precisely coordinated (see figure 2.5). Endocytic adaptor proteins show a defined lifetime and an order of appearance at the PM, beginning with stable and long lasting patches, followed by a slow and then a fast inward movement (Kaksonen et al., 2005). Individual endocytic proteins can be grouped into four different modules according to their appearance and dwell time at the PM. First coat–, second Wasp/Myo–, third amphiphysin– and fourth the actin module. Coat proteins assemble early at endocytic sites like the Bar domain containing proteins Ede1 and Syp1, as

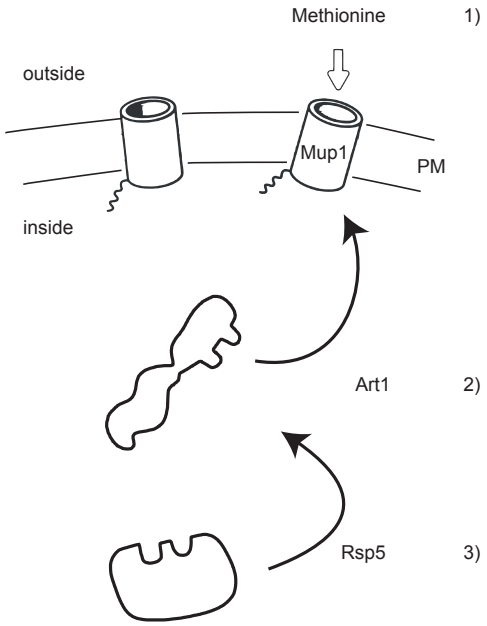

Figure 2.6: Arrestin mediated ubiquitylation. After methionine detection, Art1 binds the cargo protein Mup1 (1) and recruits the E3 ubiquitin ligase Rsp5 (2), finally Mup1 is ubiquitylated by Rsp5 (3). Adapted from Lin 2008.

well as the triscelion clathrin cage. The early coat proteins are surrounded by the WASP–Myo proteins (Las17, Pan1, Myo3), which activate the actin nucleating complex Arp2/3 complex. Abp1 and Sac6 are proteins of the actin coat complex. Finally, the actin patch is moved along actin cables into the cell. To form an endocytic vesicle, the initially flat PM has to be increasingly bent during coated pit formation, which is achieved by different Bar domain containing proteins that appear sequentially and introduce and stabilise the bending of the vesicle during maturation (Qualmann et al., 2011).

Endocytosed proteins become either re-routed to the PM or degraded within the vacuole, the fungi counterpart of the lysosome. Although much work has been carried out to dissect the sequential order of individual components of the endocytic machinery (Merrifield et al., 2002; Kaksonen et al., 2003, 2005), little is known about cargo recruitment and the spatial organisation of endocytosis (Stimpson et al., 2009)

2.5 Models of plasma membrane protein organisation

2.5.1 Lipid raft hypothesis

More than twenty years ago, evidence of protein-lipid inhomogeneities at the PM were reported. This evidence resulted from the observation that glycolipids are preferentially delivered to the apical– but not to basolateral membranes in epithelial cells (van Meer et al., 1987). Later it became clear that lipids are not only sorted towards different cell compartments, but also form microdomains within a given compartment. This discovery lead to the identification of two lipid domains, each enriched with characteristic lipids. One domain is enriched with sphingolipids and cholesterol which form a liquid ordered phase L_O and segregates from the liquid disordered domain L_D that is enriched with phospholipids. Sphingolipids, cholesterol and phospholipids segregate spontaneously into these two described domains, as demonstrated in Giant Unilamellar Vesicle (GUV) (Fig. 2.7).

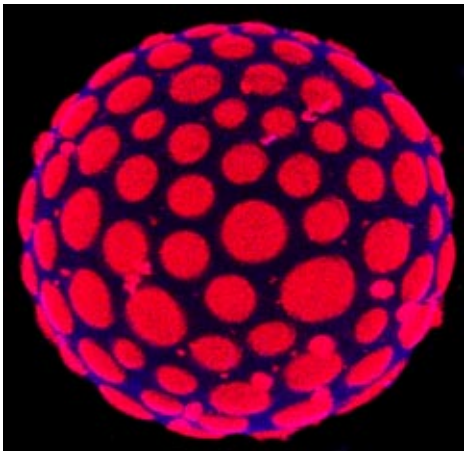

Figure 2.7: Phase sepeartion of lipids. Phase separation within a Giant unilamellar vesicle (GUV). The GUV is made of sphingomyelin, Dioleoyl-sn-glycero-phosphocholine and cholesterol. Liquid ordered (L_O) domain is labelled red and the liquid disordered (L_D) is blue. (Baumgart et. al. 2003).

This observation of spontaneous phase separation of different lipids resulted eventually in the lipid raft theory (Simons and Ikonen, 1997), which is a concept to explain lateral inhomogeneities within the PM. The validation of lipids rafts within living cells proofed to be difficult. Because of the small size and the dynamic nature, lipid rafts were biochemically defined as proteins which are resistant to the extraction with Triton X-100 at 4°C (Brown

and Rose, 1992). Proteins which were soluble under these conditions were non rafts proteins, while other proteins were defined to be raft associated. This method turned out to determine the solubility of a given protein, rather than the domain association (Tanner et al., 2011). Mutually exclusive PM protein domains in yeast appear both in the detergent resistant fraction (DRM), clearly showing the limitations of this method (Opekarova et al., 2005). Some proteins, such as the GPI-anchored placental alkaline phosphatase or the transmembrane (TM) protein haemagglutinin localise exclusively to lipid raft domains (Kahya et al., 2005; Harder and Simons, 1999; Janes et al., 1999), while other proteins are excluded from these domains. Besides the segregation of cellular proteins, raft formation was linked to virus entry into the cell (Ewers et al., 2010).

The lipid raft theory provides an elegant and relatively simple model of membrane organisation, induced by self assembly of lipids. Much research on lipid rafts and phase separation of lipids was carried out in artificial systems and results cannot be easily applied to complex biological membranes. To this end, co-clustering of integral TM proteins with L_O lipid domains have never been observed *in vivo*. It was shown that the level of lipid condensation of rafts in membranes is far below from what can be achieved in GUVs, nevertheless PM domains with a higher degree of conformational order do exist in living cells (Kaiser et al., 2009).

As mentioned above, lipid rafts are very small in size and scattered across the plane of the PM, therefore they are difficult to resolve by conventional light microscopy, unless induced via clustering with antibodies or choleratoxin (Hammond et al., 2005). Super-resolution techniques like Stimulated emission depletion (STED) microscopy, allowed to resolve raft associated proteins and were shown to form dynamic clusters of 20nm in size (Eggeling et al., 2009). Besides the question of whether or not raft like membrane domains exist, their function was not clear. Sphingolipid and sterol enriched domains proved to be important for a variety of different cellular processes, including viral entry into the cell and segregation of different proteins like different Ras isoforms and GPI proteins, or clustering of T-cell receptors within the immunological synapse (Nikolaus et al., 2010; Eisenberg et al., 2011; Jacobson et al., 2007; Scolari et al., 2009; Ewers et al., 2010; Zech et al., 2009). Live cell imaging with total internal reflection fluorescence microscopy of antigen binding to B-cell receptors clearly showed the formation of lipid raft associated microcluster (Sohn et al., 2008).

Currently, the lipid rafts concept has been revisited and the definition has become less strict. Lipid rafts are considered as transient platforms for lipid-protein complex formation and are involved in many processes like trafficking, signal transduction and cell polarisation (Coskun and Simons, 2009; Lingwood et al., 2009).

To function as signalling clusters, they have to assemble from scattered nanocluster into larger raft-like structures, by a mechanism that is not fully understood. Different models exist to explain the formation of large PM domains. The lipid shell hypothesis assumes that proteins are surrounded by static layers of lipids, which drives similar proteins into larger domains (Anderson and Jacobson, 2002). A similar but distinct model proposes that protein aggregates are surrounded or "wetted" by a thick layer of lipids and these lipids are in a different phase than the bulk lipids. This lipid or wetting film prevents proteins from domain exit and give rise to large domains (Akimov et al., 2008). The difference between the lipid shell and wetting theory is the static nature of the lipids in the former and dynamics and phase transition in the latter (Akimov et al., 2008). The lipid shell and wetting hypothesis is distinct from annular lipids, which consists of only one lipid layer around a protein, of fast exchanging lipids. Within model membranes, hydrophobic matching (see section 2.5.3) was shown to drive small peptides into raft like domains (Kaiser et al., 2011) and is suggested to be a driving force for raft like protein domain formation (Coskun and Simons, 2011). In *vivo* data shows that palmitoylation of integral PM proteins can lead to lipid raft association of PM proteins (Levental et al., 2010), suggesting that lipid rafts are a special form of hydrophobic matching, which segregates proteins depending on sphingolipids and cholesterol from proteins that require different proteins.

Although lipid raft theory was originally defined as a two domain system (L_O vs. L_D), three mutually exclusive light microscopically resolvable raft like domains were identified within living cells (Tyteca et al., 2010). In addition, by using PALM four different raft associated proteins were shown to form independent clusters of different sizes at the plane of living cells (Sengupta et al., 2011).

It is noteworthy to mention that different and often unrelated phenomena, which involve sphingolipids and cholesterol are collectively named lipid raft in the literature. Very often the size, lifetime and mobility of these "rafts" vary by orders of magnitudes.

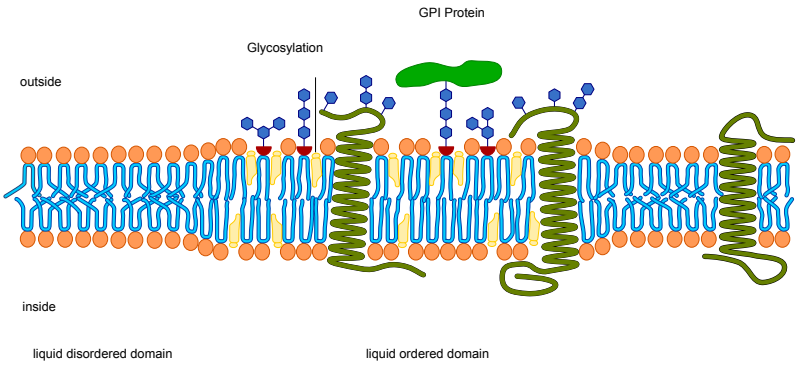

Figure 2.8: Liquid ordered and liquid disordered membrane domains. Scheme of liquid ordered L_O and liquid disordered L_D domains. L_D domains contain unsaturated phospholipids, these lipids do not allow a tight packing. lipid rafts, or lipid ordered domains contain sphingolipids and sterols. Sterols align between the saturated aliphatic lipid chains and allow a tight packing. GPI anchored proteins are associated with lipid raft domains. (Image adapted from wikipedia under GFDL license)

2.5.2 Picked fence model

Compared to artificial membranes, diffusion of lipids is much slower in living cells (5-100 times slower) and the reason for this phenomenon was unclear for decades (Swaisgood and Schindler, 1989). High-speed tracking of gold labelled lipids, (framerate of 25 μs/frame) showed a confined, rather than a processive movement of the probe. After depolymerisation of the actin cytoskeleton with LatA a linear movement of the labelled probe was recorded (Fujiwara et al., 2002). Apparently, the actin meshwork underlying the PM hinders the free diffusion of lipids. These observations lead to the formulation of a model in which actin creates a “fence” which is attached to protein “pickets" (Kusumi et al., 1993). A protein is confined within a compartment for a certain time, until it “hops” over the fence diffuses freely and eventually becomes sequestered again (Kusumi et al., 1993; Sako and Kusumi, 1994). These actin dependent membrane corrals confine not only the diffusion of lipids but also proteins and play a role in the establishment of signalling platforms (Kusumi et al., 2005; Tamkun et al., 2007).

The picket fence model was shown to be important for cell signalling, such as the CD36 receptor, which requires an actin meshwork to increase the possibility of ligand-receptor interactions (Jaqaman et al., 2011).

Additionally, it was reported that B cell receptor signalling is directly controlled by the membrane cytoskeleton (Treanor and Batista, 2010). Modulation ofdownstream signalling is achieved by restricting receptor diffusion within an actin corral (Treanor et al., 2011). MHC complexes, GPI anchored proteins (Umemura et al., 2008) as well as GPCRs (Murase et al., 2004) belong to another class of proteins which depend on the actin cytoskeleton for lateral segregation and function. Theoretical studies propose an increased receptor ligand interactions induced by the actin cytoskeleton (Chaudhuri et al., 2011) and a phase transition and subsequent micro domain formation which is also driven by the actin cytoskeleton (Machta et al., 2011). These experiments suggest that the cortical actin cytoskeleton is important for a diverse range of different cellular processes.

2.5.3 Hydrophobic matching

The hydrophobic matching theory explains the emergence of lateral heterogeneities entirely via molecular interactions between proteins and lipids. Shortly after formulation of the fluid mosaic model, the hydrophobic matching theory was introduced (Singer and Nicolson, 1972; Israelachvili, 1977), refined by Mouritsen and Bloom and is now known as the mattress model or the hydrophobic matching theory (Mouritsen and Bloom, 1984). The model assumes that hydrophobic molecules, such as the TMS of a protein has to match the thickness of the bilayer. If the hydrophobic stretch is longer than the lipid environment, hydrophobic amino acids will be exposed to interfacial water molecules. If the stretch is too small polar amino acids will be dragged into the hydrophobic core of the PM. To minimise these energetically unfavourable interactions, the hydrophobic molecule is driven into an environment that matches the length of the TM stretch.

First evidence for the validity of the hydrophobic matching model came from the observation that the lipid environment in close proximity to a protein differs from lipids being further away (Chapman, 1984). Additionally, it became clear that proteins can induce local lipid heterogeneities (Gawrisch et al., 1995). Until now, much *in vitro* and in *in vivo* data has been accumulated, showing that many proteins require a specific membrane thickness or certain lipids to function (Reichow and Gonen, 2009).

A great amount of data shows the importance of the hydrophobic matching theory for protein function. An example for hydrophobic matching on transporter function is the

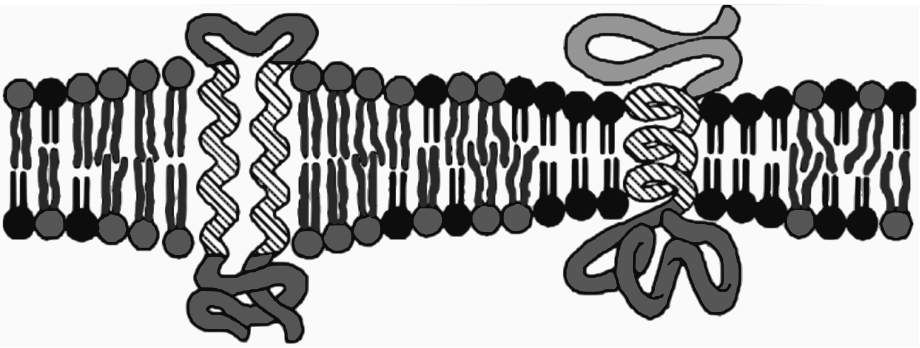

Figure 2.9: Mattress model of hydrophobic matching. The hydrophobic effect drives integral membrane proteins to match the length of the lipid bilayer. Mouritsen 1984.

Na,K-ATPase, which works best within a membrane of lipids with 22 carbon atoms acyl chains. If the membrane is less thick the protein fails to transport, but the function can be restored by adding cholesterol, which leads to thickening of the membrane (Cornelius, 2001). This finding shows elegantly that the thickness of the membrane, at least for this example is more important than the actual lipid composition. A more subtle effect of protein function in dependence of surrounding lipids was observed for the light sensitive G-protein Rhodopsin. This protein can adopt two states, M-I and M-II. The M-II is more elongated than the M-I state and thus requires a different hydrophobic matching profile of the membrane. In order to quickly adopt these two states, the protein has either to move to a different membrane compartment, or membrane curvature has to be introduced. Evidence for the latter was provided by a promotion of the M-II state after addition of PE, which has a tendency to form an inverted hexagonal phase (Jastrzebska et al., 2011; Jensen and Mouritsen, 2004). The detailed mechanism of how PE stabilises the M-II state is not clarified, but modelling of known crystal structures suggests a conformational change of a cytoplasmic loop of the protein (Huber et al., 2004).

The energy required for a protein to match the lipid bilayer can impact on the structure of the protein (Andersen and Koeppe, 2007; Jensen and Mouritsen, 2004), as it is the case for the Ca^{2+} -ATPase from the skeletal muscle sacroplasmic reticulum, which changes the whole protein structure if the lipid environment does not match the proteins requirements (Lee, 2011). In this case the cost of distorting the membrane is higher than changing the structure of the protein (Lee, 2004). The finding that the lipid bilayer changes the structure of the embedded protein acts not on beta barrel proteins (O'Keeffe et al., 2000).

Besides in organising individual proteins into matching lipid environments, the mattress model can be the driving force for phase separation and subsequent segregation of proteins in artificial membranes, creating large protein-lipid domains (Vidal and McIntosh, 2005; McIntosh et al., 2003; Kaiser et al., 2011) (see also section 2.5).

2.5.4 Caveolae

Caveolae are stable PM invaginations with a diameter of 60-80nm and first identified in mammalian cells (Parton and Simons, 2007). The major structural protein of caveolae is the polymer forming integral membrane protein caveolin. These flask shaped or sometimes branched membrane invaginations are enriched with sphingolipids (Ortegren et al., 2004) cholesterol (Fujimoto et al., 1997) and PIP2 (Fujita et al., 2009) and are connected to microtubules and the actin cytoskeleton (Mundy et al., 2002). Caveolae are involved in clathrin-independent endocytosis (Kirkham and Parton, 2005; Anderson, 1993) and contribute to mechanosensation and lipid regulation (Bastiani and Parton, 2010).

2.5.5 Protein-protein interactions and tetraspanins

Large PM protein domains can be formed via protein-protein interactions as shown in T-cells. Dependent on the membrane protein Lat, acting as a crosslinker, large heterotypic protein domains were formed (Douglass and Vale, 2005). Tetraspanins are a class of proteins that has been proposed to function in membrane organisation. These proteins contain four transmembrane domains and are known to homo- or hetero-dimerise with other tetraspanins and provide binding sites for many different membrane proteins (Charrin et al., 2009). These tetraspanin “webs" are involved in to a multitude of different cellular processes, including membrane transport and cell fusion (Rubinstein, 2011). Tetraspanins do not require cholesterol for homo-dimerisation, but for interaction with different proteins, such as integrins (Hemler, 2005). Although originally identified within mammalian cells tetraspanins were shown to exist also in fungi, in which they form large macroscopic domains (Alvarez et al., 2008; Clemente-Ramos et al., 2009).

2.5.6 Cell wall and extracellular matrix interaction

Stable PM domains can be obtained by anchoring membrane proteins to the extra cellular matrix (ECM) in mammalian cells or the cell wall in yeast. In yeast, Sur7 which localises to eisosomes (see section 2.6.2) was shown to require the cell wall to form large and stable domains (Young et al., 2002; Malinska et al., 2004). Integrin heterodimers interact with their ECM-bound ligands after activation and subsequently recruit a large number of cytosolic and peripheral membrane proteins (Kanchanawong et al., 2010). These structures are stable over minutes and connect the extracellular interaction site to the actin cytoskeleton.

2.6 *Saccharomyces cerevisiae*, a versatile model organism

2.6.1 Budding yeast, a versatile model organism

The budding yeast *Saccharomyces cerevisiae* is a unicellular organism, surrounded by a cell wall that can reproduce sexually and asexually. During asexual reproduction, the mother cell polarises towards the newly formed bud, which grows larger and eventually separates from the mother cell resulting in two cells with a haploid set of chromosomes. This whole process requires app. 2h for completion and gives rise to cells with ~5 μm in diameter. Spinning disk confocal images of a typical budding yeast cells is shown in Figure 2.10. The fast live cycle, the ease of genetic manipulation and the lack of complicated growth conditions makes *Saccharomyces cerevisiae* a versatile laboratory organism.

2.6.2 PM domains in *Saccharomyces cerevisiae*

Evidence for protein domains within the PM were found for many organisms including budding yeast. Two mutually exclusive and raft associated protein domains were identified in the yeast PM (Malinska et al., 2003; Young et al., 2002). One domain is occupied by the arginine permease Can1 (Membrane Compartment occupied by Can1, MCC) and the second domain is formed by the major ATPase Pma1 (Membrane Compartment occupied by Pma1, MCP). The MCC compartment forms stable patches, which are surrounded by a protein network, formed by Pma1 (Fig. 2.11) (Malinska et al., 2003). The static membrane

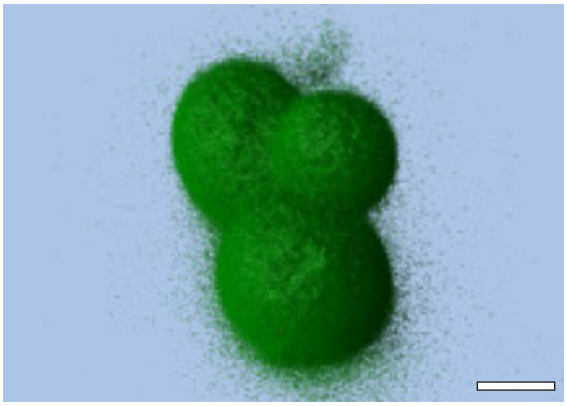

Figure 2.10: Budding yeast *Saccharomyces cerevisiae*. Spinning disk confocal images of budding yeast Pma1GFP. Scale bar: 2 μm

domain, called eisosomes co-localised entirely with the MCC compartment (Malinska et al., 2004). Although a recent study found only an enrichment of Can1 of 30% with eisosomes (Brach et al., 2011). Recently a third patch-like domain occupied by Tor1 complex 2 was identified (Membrane Compartment occupied by TorC, MCT) (Berchtold and Walther, 2009). The MCT compartment is patchy, but unlike MCC and MCP this complex does not contain any integral membrane protein and the whole patch exhibits lateral mobility. Other proteins analysed so far did not show any domain association and were said to be homogeneously distributed over the PM (Malinska et al., 2004; Stradalova et al., 2009).

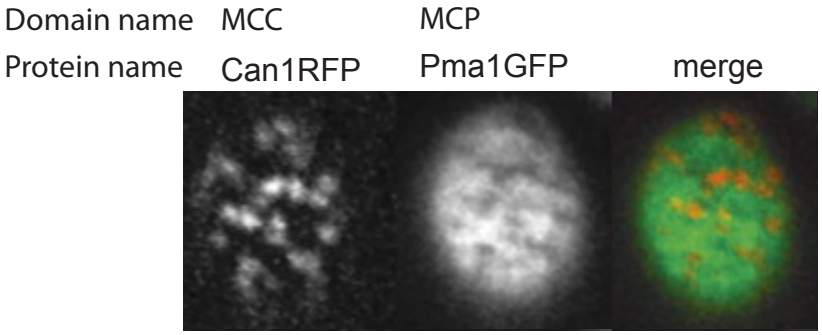

Figure 2.11: Mutual exclusive plasma membrane protein domains in yeast. The patch forming arginine permease Can1RFP (MCC or eisosomes) and the network forming major ATPase Pma1GFP (MCP) form mutually exclusive membrane compartments. Malinska 2004.

Eisosomes are static membrane invaginations, with Pil1 and Lsp1 as the core components (Walther et al., 2006). Both proteins contain Bar domains, share a high sequence homology and assemble into filaments (Ziolkowska et al., 2011; Karotki et al., 2011). Deletion of Pil1 leads to a loss of eisosomal integrity, whereas deletion of Lsp1 preserves the patchy pattern of eisosomes (Walther et al., 2006). So far, more than 20 proteins have been associated with the MCC/eisosomal compartment, of which many proteins are involved in lipid signalling and also amino acid uptake (Grossmann et al., 2008; Aguilar et al., 2010). Proteins within this complex are not evenly distributed, the two core proteins Pil1 and Lsp1 localise to the bottom of the furrow, while Sur7, a tetraspanin resides at the top (Stradalova et al., 2009). Despite tremendous effort, the functional relevance of these domains is not clear. The MCC/eisosomal domain domain is enriched with ergosterol (Grossmann et al., 2007) and functions in sphingolipid signalling (Frohlich et al., 2009). A role of eisosmes in regulating protein turnover by preventing eisosomal and associated proteins from being endocytosed was proposed. This model is based on the observation that actin patch marker proteins almost never co-localise with eisosomes and that less Can1 was detected at the PM in Δ*pil1* strains, in which eisosomes collapse into remnants (Grossmann et al., 2008). The authors claim that integral PM proteins which do not co-localise with MCC are constitutively endocytosed. This protection model divides the yeast PM into two domains with MCC/eisosomes as a domain protecting from endocytosis and the rest of the PM as permissive for endocytosis. (Fig. 2.12).

2.6.3 Lipid rafts and the yeast PM

Due to difficulties in imaging PM proteins, most studies on membrane organisation focused only on relatively few proteins, mostly signalling complexes or lipidated fluorophores. Although the tools to study membrane organisation are very diverse, including super-resolution techniques (Eggeling et al., 2009; Sengupta et al., 2011), Anisotropie measurements (Sharma et al., 2004), Forster resonance energy transfer (Fret) (Lu et al., 2008; Hess et al., 2005), single molecule tracking (Douglass and Vale, 2005) or confocal microscopy (Malinska et al., 2003; Gomez-Mouton et al., 2004), so far no super-resolution images of yeast proteins have been acquired. These above mentioned limitations of protein diversity in general and lack of high resolution imaging in yeast in special, demands a careful analysis of PM domain formation in budding yeast.

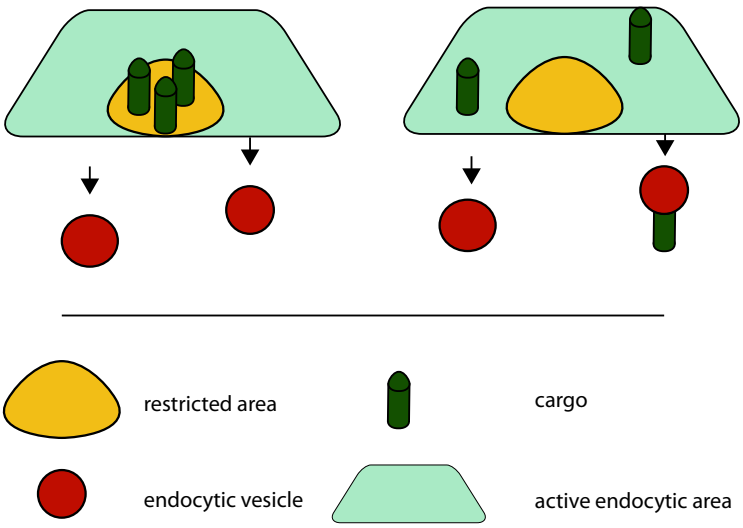

Figure 2.12: Eisosomes protect proteins from endocytosis A) Proteins within eisosomes are not endocytosed. B) Proteins not associated with eisosomes become endocytosed. Adapted from Grossmann 2008.

2.6.4 PM of *Saccharomyces cerevisiae*

Although *Saccharomyces cerevisiae* and mammalian cells are remarkably similar in basic cell morphology and function, they differ in certain aspects. Yeast and mammalian cells differ in the form of the main sterol, while it is ergosterol in yeast, it is cholesterol in mammalian cell. Ergosterol differs from cholesterol by an unsaturated C-7,8 in the ring structure and a C-22 in the side chain and by a methyl group at C-24 (Fig. 2.13).

The diffusion of proteins and lipids in yeast is at least one order of magnitude slower than in mammalian cells (10^{-6} cm^{-2}/sec yeast 10^{-7} to 10^{-8} cm^{-2}/sec mammalian cells) (Greenberg and Axelrod, 1993; Schwille et al., 1999; Valdez-Taubas and Pelham, 2003). A reason for this phenomenon is still under debate, but the high protein content of the yeast PM induces crowding effects, which will lead to a reduced diffusion coefficient (Greenberg and Axelrod, 1993). Additionally, the sterol content in yeast is much higher than in mammalian cells, which increases the rigidity of the membrane and therefore reduce the diffusion coefficient of proteins and lipids.

In contrast to mammalian cells, yeast is surrounded by a cell wall and proteins can be immobilised within this matrix. The cell wall thickness varies between 100-200nm (Dupres

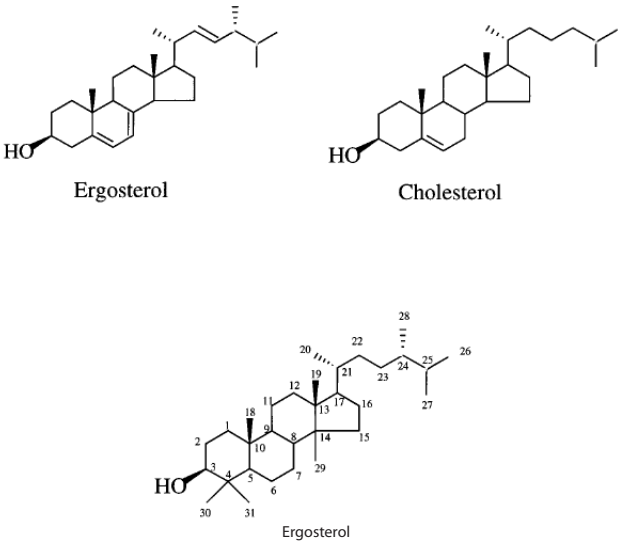

Figure 2.13: Difference between sterols Structure formulae of cholesterol and ergosterol. Ergosterol differs by an unsaturated C-7,8 in the ring structure and a C-22 in the side chain, as well as an additional methyl group at C-24.

et al., 2010), if and to which extent the cell wall organises the PM is currently not entirely clear. Actin corral mediated membrane organisation, as observed within mammalian cells (section 2.5.2), could not be verified to occur in budding yeast. Depolymerisation of the actin cytoskeleton did not lead to an increase of diffusion coefficients of PM proteins or lipids, nor to a drastic changes of PM protein organisation (Greenberg and Axelrod, 1993; Malinska et al., 2004; Valdez-Taubas and Pelham, 2003). Sphingolipid and sterol enriched domains are present in budding yeast (see section 2.6.2), but unlike the mammalian counterpart they are large and with a lifetime of hours extremely static (Malinska et al., 2004). The membrane topology of the yeast PM differs greatly from the mammalian membrane. Unlike the mammalian PM which is highly uneven, due to high turgor pressure, the yeast PM is flat and pressed against the cell wall (Aghamohammadzadeh and Ayscough, 2009; Loibl et al., 2010). The cell wall with a thickness of app. 200nm (Dupres et al., 2010), suggests that imaging of the yeast PM is impossible, but different studies report TIRFM for cell wall bearing organisms like bacteria and yeast (Yu et al., 2011; Dominguez-Escobar et al., 2011).

2.7 Advanced light microscopy

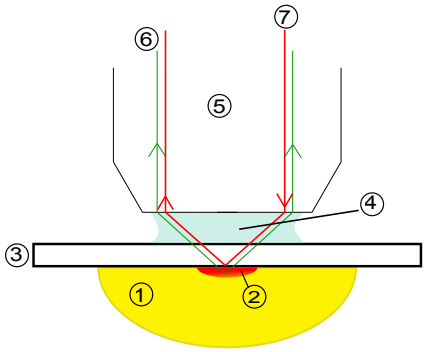

Figure 2.14: Total Internal Reflection Fluorescence Microscopy (TIRFM) Scheme showing TIRF microscopy 1. Specimen 2. Evanescent wave range 3. Cover slip 4. Immersion oil 5. Objective 6. Emission beam (signal) 7. Excitation beam (Image adapted from wikipedia under GFDL license)

Imaging cortical events is challenging, due to the small size of the organelle, weak signals and out of focus light, even if a spinning disk confocal microscope is used (axial resolution app. 600nm (Axelrod, 2001)). To acquire images of events close to– or at the PM, out of focus light has to be reduced. Total Internal Reflection Fluorescence Microscopy (TIRFM) allows the illumination of molecules close to the glass water interface, by creating an evanescent field, which decreases by the power of two and is generated when light passes from media with high to media with a low refractive index (Axelrod et al., 1983). This occurs also at the cell wall (high refractive index) PM (low refractive index) interface and can explain the successful application of this technique for cell wall bearing organisms (Uchida et al., 2010; Sparkes et al., 2011; Vizcay-Barrena et al., 2011).

Instead of passing the laser beam perpendicular into the sample, the incidental angle of the laser is tilted until a total reflection at the glass–water interface occurs. This leads to the generation of a standing evanescent wave with an exponential decay, thus exciting only molecules which are in 100-200nm distance to the glass surface (Fig. 2.14). This method has a very good signal to noise ratio and allows fast acquisition times (50ms and less) (Axelrod and Omann, 2006).

Conventional light microscopy is a powerful tool, to resolve structures within living cell, but it has its limitations if nearby structures have to be resolved. This phenomenon called diffraction limited resolution was already discovered in the 19th century (Abbe, 1873). The

minimal distance between two point sources which can be separated by conventional light microscopy is determined by the wavelength and the numerical aperture of objective.

In recent years, several microscopical techniques have been developed to break the Abbe's limit to increase the resolution below the diffractive barrier (Schermelleh et al., 2010).

Stimulated emission depletion (STED) microscopy is a technique to de-excite fluorophores which are not in the centre of the PSF of the stimulated fluorophore (Hell and Wichmann, 1994). This is achieved by generating a doughnut shaped depletion beam to induce ground state of fluorophores shifted from the centre of the donut (Schermelleh et al., 2010). Lateral resolution between 30-100nm was achieved by the use of this method (Klar and Hell, 1999).

Photoactivated Localisation Microscopy (PALM) allows the acquisition of super-resolution images by detecting the centre of mass of single non overlapping fluorophores (Betzig et al., 2006). By replacing each detected centre of mass with the point spread function of the microscope it is possible to generate pictures with increased resolution (20-40nm xy resolution) (Hess et al., 2006).

Structured Illumination Microscopy (SIM) is a super-resolution technique in which a the sample is illuminated with a series of shifted grid patterns. This leads to the generation of interference patterns, which can be combined by computational methods to a super-resolution image(Heintzmann and Cremer, 1999; Gustafsson, 2000). The spatial resolution is approximately doubled with this method compared to conventional light microscopy (Schermelleh et al., 2010).

Chapter 3

Results

3.1 Yeast plasma membrane proteins and method validation

3.1.1 Characterisation of the yeast PM proteome

We assembled a list of all PM proteins present in baker's yeast *Saccharomyces cerevisiae* to systematically investigate PM protein organisation. The complete list of 301 PM proteins (Tab. 8.1) was manually grouped by function with information obtained from the public domain, Gene Ontology, and CYGD resulting in 37 functional groups (Tab. 8.5) (Consortium, 2010a; Ruepp et al., 2004). PM proteins were further characterised by the number of TM segments or lipid anchor/binding motives. TM-HMM was used to identify TMS and lead to the identification of 217 integral TM proteins. The distribution of TMS was not even among the identified proteins; transporters with 12 TMS form the biggest group with 87 proteins followed by single spanning TM helices (Fig. 3.1).

We aimed to experimentally cover as many classes of different membrane protein as possible. Only 142 proteins showed a peripheral GFP signal, as annotated in the UCSF GFP fusion collection (Huh et al., 2003). Further GFP fusions were generated to increase the number of underrepresented classes. We used in total two different lipid binding proteins, the delta δ Domain of phospholipase C for PIP2 (Gambhir et al., 2004) and the C2 domain of Lactadherin (Lact-C2) as marker for PS (Shi et al., 2004). Ras2 (C-terminally prenylated and palmitoylated), Gpa1 and Psr1 (both N-terminally myristoylated and palmitoylated) were used as markers for lipid anchored proteins (Roth et al., 2006). For a comprehensive

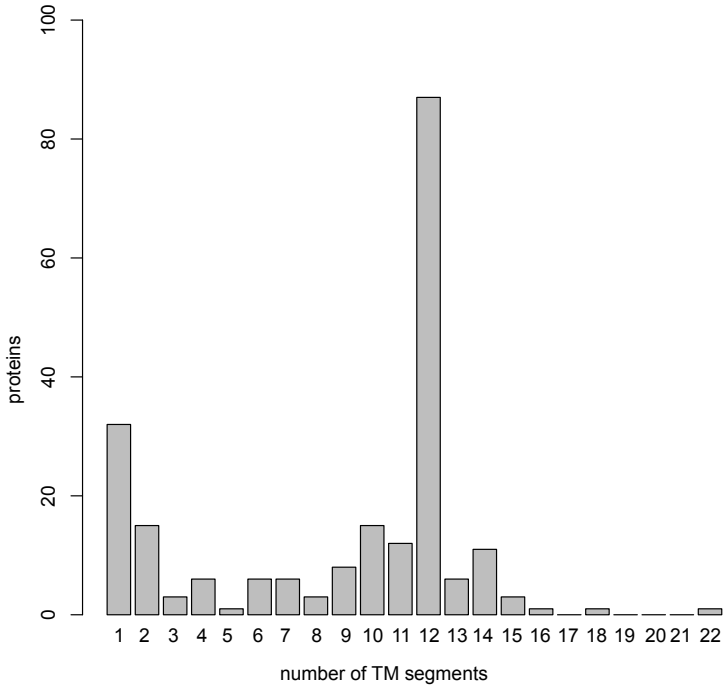

Figure 3.1: Distribution of TMS segments. Histogram showing the distribution of TMS of PM proteins in budding yeast. Transporter with 12 TMS represent the largest class.

analysis, we selected 46 representative PM proteins covering major functional groups mainly focusing on TM proteins (Fig.3.2).

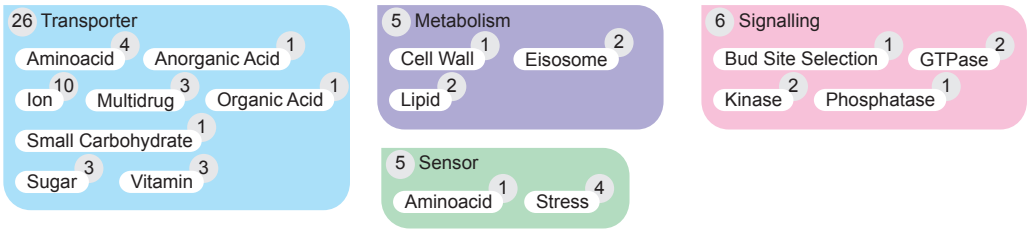

Figure 3.2: Protein classes used for the co-localisation screen. PM proteins are grouped according to their function as transporter, sensors, metabolism or signaling. Different classes are colour coded protein numbers used within this study are given for each class.

TIRF microscopy was carried out to image PM proteins (see section 2.7). The axial resolution of TIRFM is superior to confocal microscopy and the out of focus noise is negligible, making TIRF images well suited for 2D deconvolution (Sund et al., 1999). We combined TIRFM with 2D deconvolution to be able to visualise yeast PM proteins with high contrast and high temporal resolution (<100 ms) (Fig. 3.3 A). Deconvolution was applied with a maximum likelihood estimation algorithm, provided by the commercial software package Huygens (scientific Volume Imaging). For optimal deconvolution results, we experimentally determined the point spread function (PSF) of the microscope using latex microspheres for 488 and 561 laser lines. Each PSF represents an average of at least 10 independent measurements. Deconvolution of the cytosolic factor Tef1GFP did not lead to the generation of any observable structures, indicating that networks are not generated by deconvolution (Fig. 3.3 A).

2D deconvolution in combination with TIRF microscopy was further validated by comparing deconvolved with super-resolution images. TIRF- structured illumination microscopy (SIM) was used as a super-resolution technique. TIRF-SIM Images of Pma1GFP and Atto488-Sag1 showed a non-homogeneous protein distribution and a network-like pattern. The contrast was even increased if compared to deconvolved images. The patterns of PM proteins between SIM-TIRF and deconvolved TIRFM images were highly similar, indicating neither generation of new structures, nor over-restoration of deconvolved TIRFM images (Fig. 3.3 B). Comparison of Pil1 between STED and 2D deconvolution of TIRFM images revealed comparable patterns, indicating no over-restoration of TIRFM images by deconvolution (Fig. 3.4).

3.1.2 Distribution of yeast PM proteins

We visualised all 46 GFP labelled proteins of the test set and each was non-homogeneously distributed, ranging from patch to a network-like patterns (Fig.3.5 A). Patch-like proteins were defined as patterns showing discrete foci with non or very few connections between them. Network-like proteins (e.g. Pma1) contained many "track-like" elements in addition to high intensity areas (marked by asterix within the linescans, Fig. 3.5 B). Even lipid binding domains and previously as homogenous annotated proteins showed a network like appearance (Fig.3.5 C,D). However, proteins often showed intermediate states between

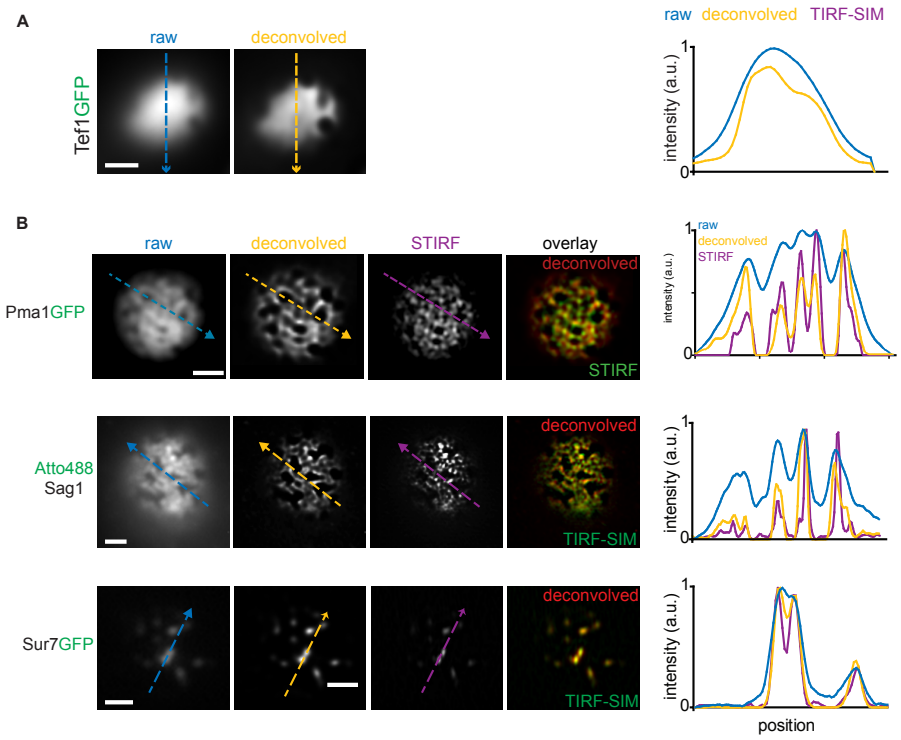

Figure 3.3: Validation of deconvolution. A) Comparison of unprocessed and deconvolved images showed comparable patterns. Cytosolic Tef1GFP was homogeneously distributed in raw and deconvolved images. Networks were not generated by deconvolution. B) Images of Pma1GFP, Atto488-Sag1 and Sur7GFP expressing cells seen by regular TIRFM (raw), TIRFM, and deconvolution and TIRF structured illumination microscopy (TIRF-SIM): The overlay demonstrated the similarity of patterns observed by STIRF and deconvolution. Linescan over raw, deconvolved and TIRF-SIM images showed an increased contrast in the deconvolved and SIM images, while maintaining the structures. Scale bar: 2 μm.

networks and patches. We defined the total surface covered by a protein as a domain. This broad definition included both patch– and network-like proteins.

We quantified the abundance of all 46 membrane proteins in our test set, by measuring the peripheral GFP signal. Equator images of all strains were acquired with high resolution (100x objective 1.45NA). To obtain comparable values the same growth conditions and acquisition times were used. Each quantification was calculated as average of >50 measurements (Tab. 8.4). Different expression levels between proteins could be well separated (Fig. 8.1 A). The measured values correlated with the TAP screen, which determined relative protein numbers by western blotting (Fig. 3.6 A) (Ghaemmaghami et al., 2003).

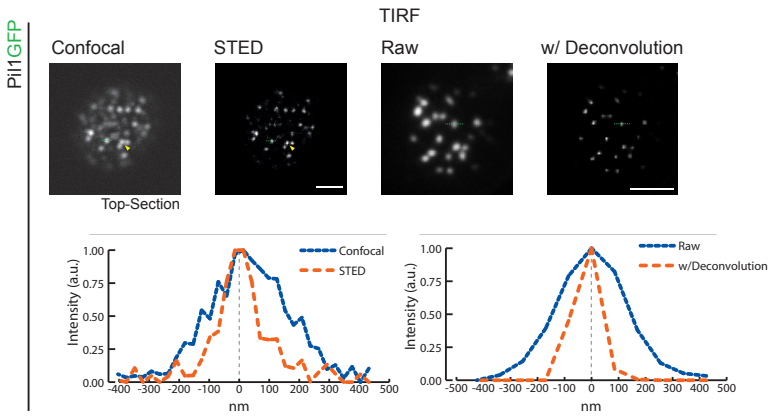

Figure 3.4: Validation of deconvolution. Confocal and STED images of Pil1GFP were compared. Diameter of Pil1GFP foci were similar for deconvolved and STED images, indicating no over restoration of images by deconvolution. Scale bar: 2 μm.

To quantitatively characterize the observed protein patterns of the test set, we developed an unsupervised histogram-based algorithm to calculate a "network-factor" for each image (Fig. 3.6 B, Tab. 8.4). Each protein had a characteristic value which could be used to distinguish intermediate patterns.

The network-factor correlated weakly with the protein expression level. Highly expressed proteins did not necessarily form networks (Bio5 and Pil1 form patches), on the other hand low expressed proteins never formed networks (Fig. 3.6 C). According to these results the minimum number of molecules to form a network ranges between 5000 and 10000 molecules per cell (numbers derived from the TAP collection).

The network-factor was calculated for the proteins shown in figure 3.5 and the protein pattern could be nicely separated by this approach, as the whole range was covered (Fig. 3.6 D, Tab. 8.4, Fig. 8.1 B). Knowledge about the network-factor and abundance for each protein can be used as a baseline to monitor the effect of drugs and mutations on both abundance and network-factor.

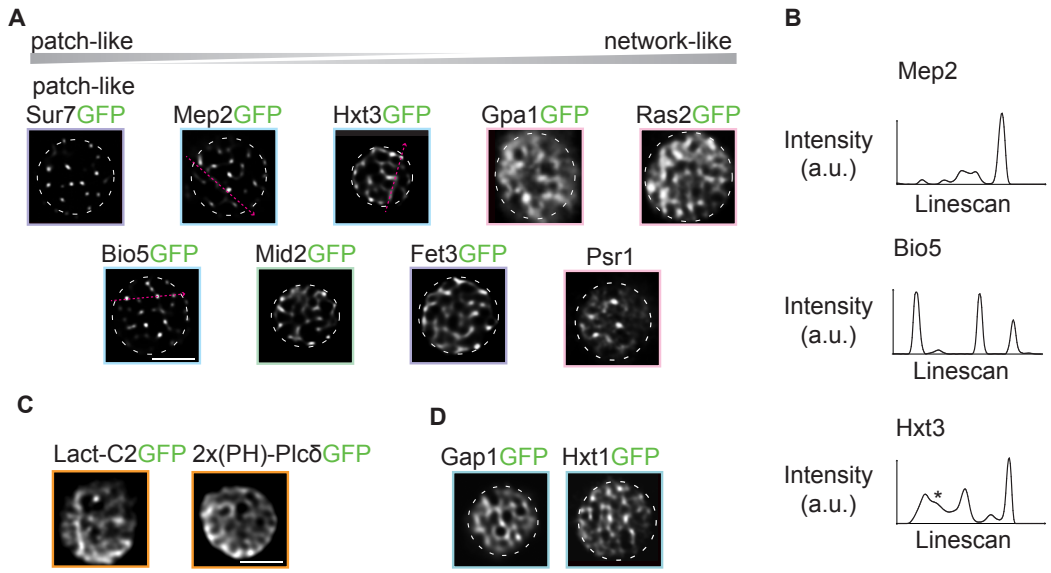

Figure 3.5: Spatial organisation of PM proteins. A) TIRFM of GFP labelled PM proteins showed two basic lateral patterns: Patch-like and network-like proteins. The transition from patch to network-like pattern is gradual. Depicted is a selection of TM proteins. Boxes around images are colour-coded by functional class. B) Linescans showed high intensity areas. Tracks are indicated by asterix. C) Lipid binding domains GFP-Lact-C2 and 2x(PH)PlcΔ were unevenly distributed. D) Previously homogeneously annotated proteins showed a network-like pattern Scale bar: 2 μm.

3.1.3 Dynamics of yeast PM proteins

To study the mobility of membrane proteins, TIRFM images of patch– and network-like proteins were performed. Frames at time zero and after 20 seconds are shown, merged images contain pseudo-coloured time frames to visualise mobility. Kymographs were taken along the lines drawn in the first frames, showing no movement for Bio5, some for Hxt3 and fast movement for Ras2 (Fig.3.7 A). Time lapse TIRFM for a subset of proteins was conducted to analyse whether lateral patterns were spatially fixed over time. We determined the correlation of the each time frame with respect to the first. The patch-like proteins Bio5 and Sur7 had spatially fixed patterns, while pattern of the network-like protein Hxt3 lost their resemblance after one minute. Interestingly, patch-like proteins (e.g. Mep2) were found to be spatially altered to the same extend as a network-like protein (e.g. Hxt3), the network pattern did not determine the mobility of PM proteins. Lipid-anchored and

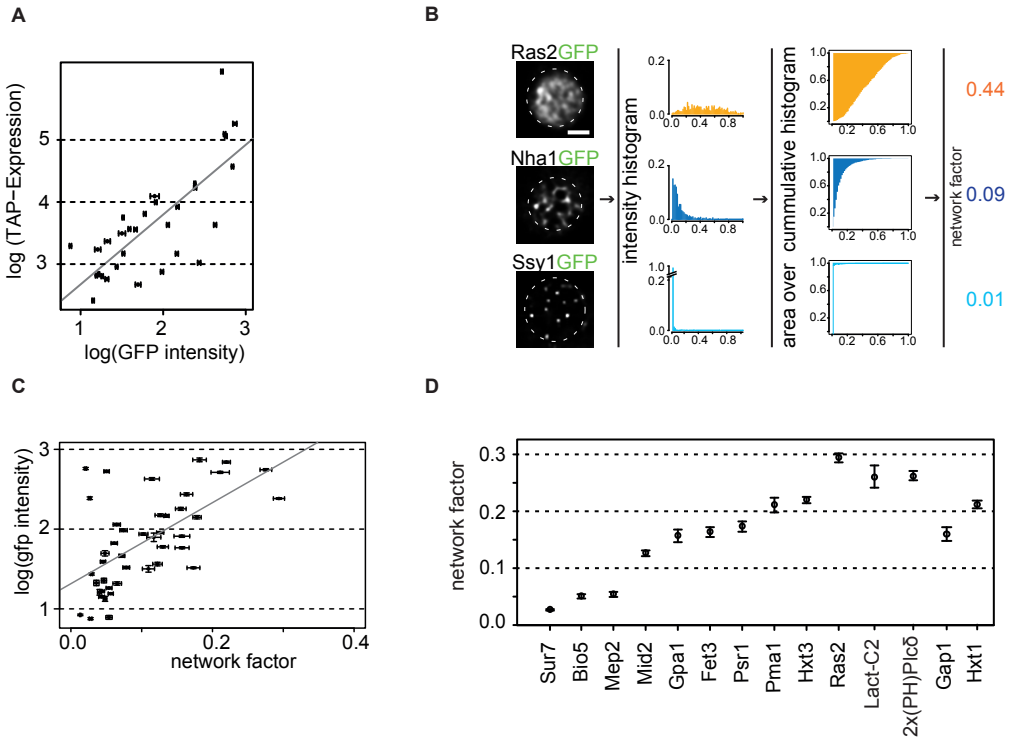

Figure 3.6: Protein abundance and network-factor determination. A)The fluorescence was determined for each protein in the test set and compared with the TAP expression screen, showing a good correlation. B) The histogram based network-factor was determined for each protein, to obtain an objective value of patch or network formation for a given protein. C) The network-factor was plotted against the protein abundance. A weak correlation was visible (R = 0.51). D) Calculated network-factors of proteins shown in figure 3.5 A. Scale bar: 2 μm.

binding proteins showed a loss of the initial pattern already after few seconds, whereas TM proteins altered the distribution remarkably slower, if at all (Fig. 3.7 B).

To screen for PM protein mobility we performed fluorescence recovery after photobleaching (FRAP) experiments on cell equators for all proteins within the test set. A small area was photobleached and subsequently the invasion of fluorescent material recorded. Some proteins showed no recovery (e.g. Nha1 or Sur7), and some showed diffusion-like recoveries (e.g. Hxt3, Pma1). Patch-like proteins showed both, a slow recovery at the same place (e.g. Fat1, Fps1) or lateral movement along the PM through the FRAP area (e.g. Ena1, Thi7). The manifold recovery patterns of the anomalous diffusion did not allow to consistently calculate recovery times. In some cases, the GFP signal was too low to record sufficient

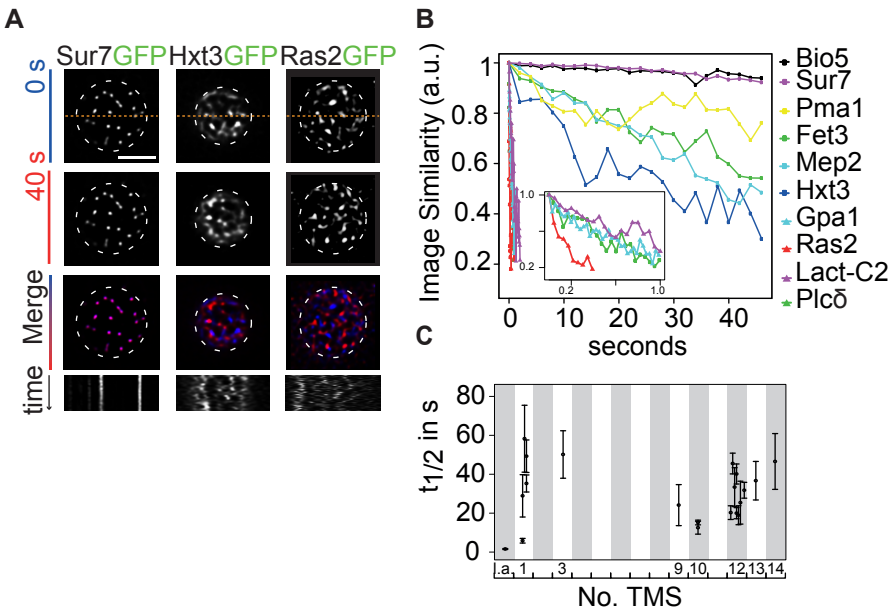

Figure 3.7: Dynamics of peripheral proteins. A) Representation of protein movement by overlay of images taken 40 s (Sur7, Hxt3) or 2 s (Ras2) apart. Kymographs were taken along the indicated dotted lines. B) Protein dynamics were analysed by a correlation analysis. The small graph is a magnification of the fast moving proteins. The proteins used for correlation analysis are shown in figure 3.5 A. C) FRAP half times of PM protein were shown as a function of TMS segments (data points: mean ± s.e.m.). l.a.: lipid anchored. Scale bar: 2 μm.

time points. FRAP experiments detected consistently low mobile fractions (MF) of 20-40% for most proteins without being determined by their spatial patterns (Tab. 8.2).

Interestingly, the number of TM segments did not correlate with the mobility or the MF (Fig.3.7 C). This experiment is consistent with published data of unusual slow diffusion of membrane protein and lipids in yeast (Greenberg and Axelrod, 1993; Valdez-Taubas and Pelham, 2003).

3.2 Plasma membrane domains

3.2.1 Method validation for the co-localisation screen

After the comprehensive protein set has been characterised, we analysed domain association of the proteins in our test set. For high-throughput imaging and analysis, we developed an

automatised pipeline including cell detection, colour-channel subpixel alignment, deconvolution, and unbiased quantification (Fig. 3.8). Manual steps were image acquisition, region of interest validation, as well as curation of all images prior analysis to sort out artefacts and wrongly cut cells.

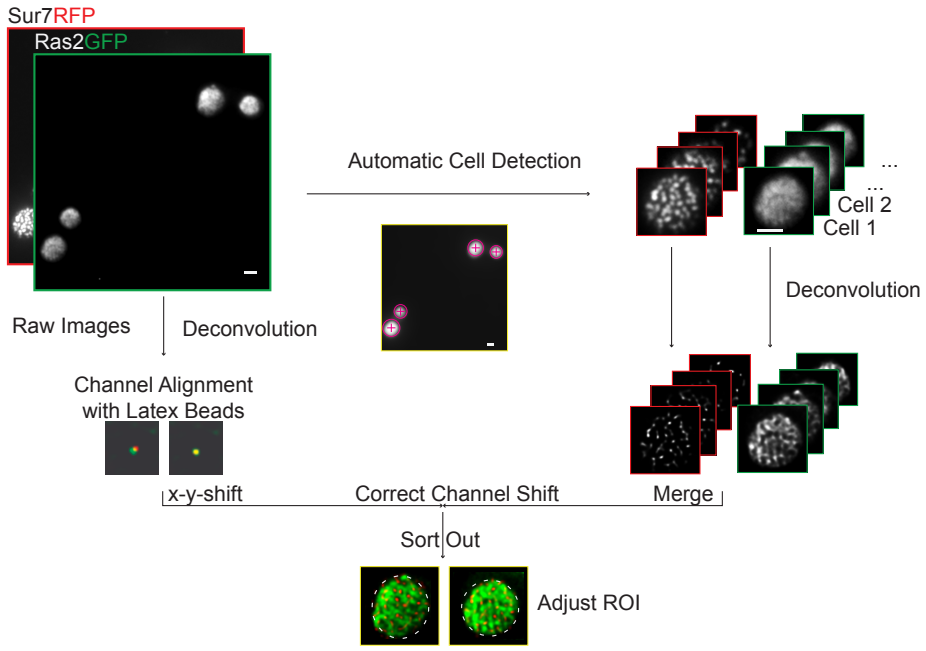

Figure 3.8: Workflow for co-localisation screen. Semi-automatic workflow of TIRF data handling, which was carried out prior analysis (Ras2GFP and Sur7RFP were used examples). All steps following image acquisition, with the exception of the last (manual selection of the region of interest (ROI) for analysis of each cell) were automated. Scale bar: 2 μm.

We implemented a linear coefficient based on the Manders overlap (Manders et al., 1993) which is a normalised coefficient based on pixel intensities responding to the ratio of intersecting to total object volume. Manders overlap coefficient was used, because it is insensitive to pixel intensity variations. The coefficient ranged from 0 to 1 for entire exclusion and total co-localisation, respectively. As positive and negative controls the mutually exclusive domain marker Sur7 and Pma1 were used (Fig. 8.3).

Sur7RFP did not show a high overlap with any proteins analysed, except the eisosomal core component Pil1. Pma1 did co-localise with PM proteins within a large range. Highest co-localisations were observed for Pmp1 (0.53 ± 0.3), the regulatory peptide of Pma1), the

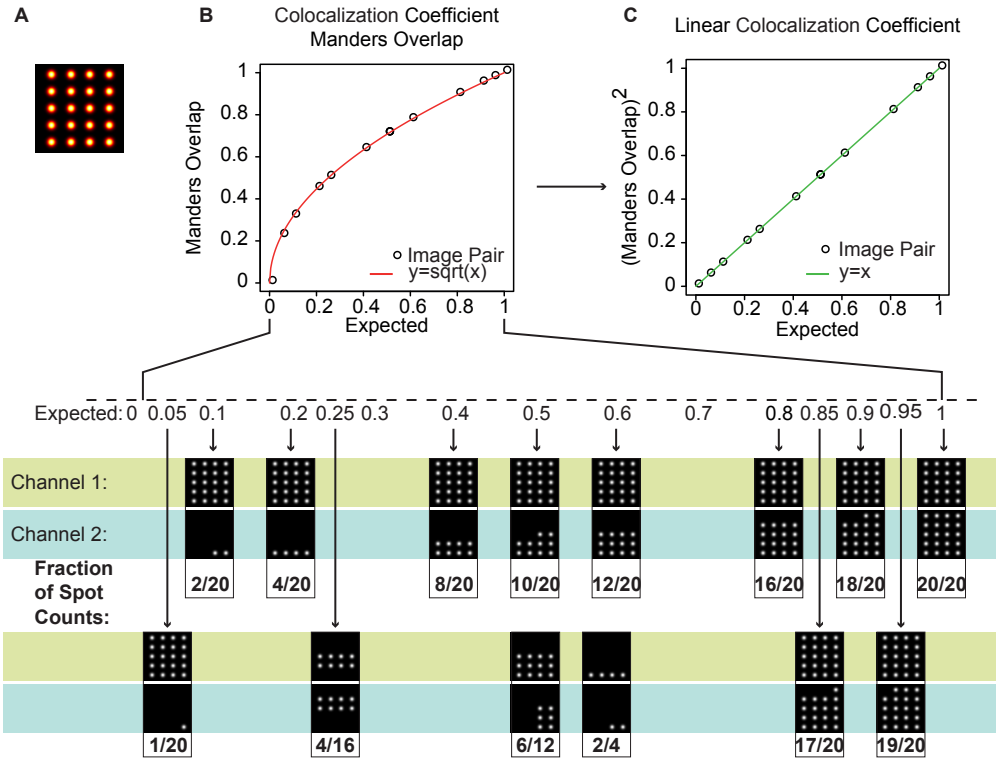

Figure 3.9: Validation of the co-localisation method. A) Synthetic images were generated to mimic patch-like patterns as visualised with false colours. Individual dots were generated with a Gaussian blur. B) To evaluate the behavior of the co-localisation overlap (according to Manders (Manders et al., 1993)), overlap of several domains were benchmarked. We defined our expected co-localisation value as the fraction of patches common to both channels. The Manders overlap was calculated for all image pairs. We found that the Manders overlap scaled as the square root of our expected co-localisation value (red fitted curve). C) A linearly scaling co-localisation coefficient was calculated by squaring the Manders overlap (green fitted curve).

small Rho-GTPase Ras2 (0.53 ± 2.2), the G-protein alpha subunit Gpa1 (0.53 ± 0.03), the ATPase Pdr5 (0.52 ± 0.03), as well as Mrh1 (0.48 ± 0.02).

Since most of the proteins examined did not co-localise with the two established yeast domains (MCC and MCP), we expanded our domain overlap comparisons. We chose four proteins that covered the range between patch (Bio5, Mep2) and network-like patterns (Hxt3, Fet3) and did not co-localise with either Pma1 or Sur7, and tested them against a smaller subset. Again, the measured pair wise domain overlaps yielded low to intermediate co-localisation co-efficients (manders between 0.2-0.5) (Fig. 3.10 B,E and Fig. 8.5 A,B;

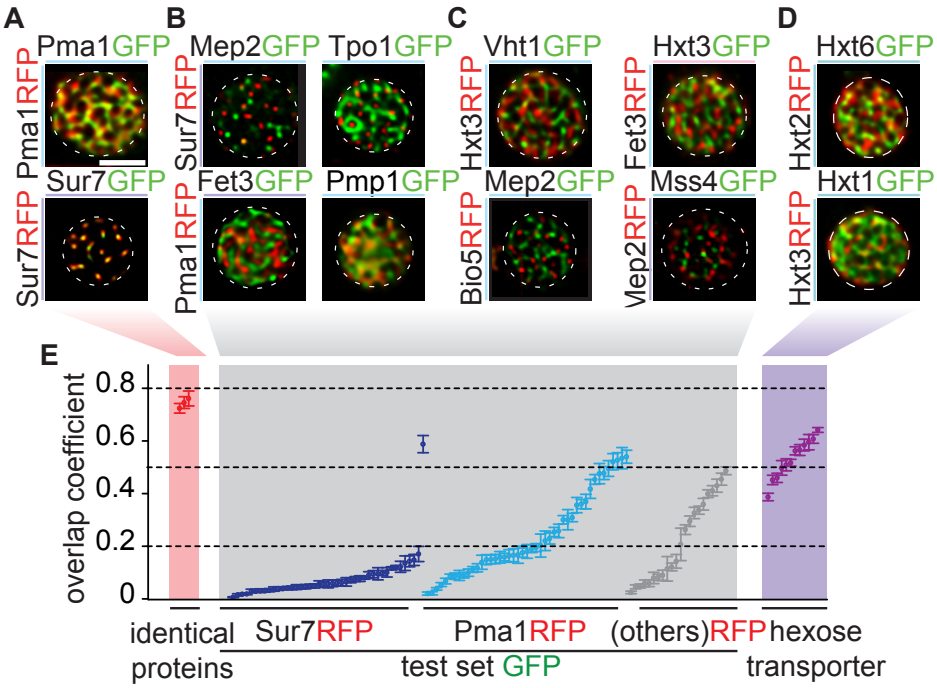

Figure 3.10: Multiple protein domains. Representative co-localisation data of TIRFM images: A) positive control, B) Co-localisation of Sur7 (patch-forming) and Pma1 (network-forming) with other patch- or network-forming proteins. C) Co-localisation of Fet3, Hxt3 (network-forming) and Bio5 or Mep2 (patch-forming) with other patch- or network-forming proteins. D) Co-localisation of different members of the hexose transporter family. E) Mean ± values of co-localisation coefficients for all proteins examined in this survey.

Tab. 8.2). In addition, the degrees of co-localisation between proteins were not correlated with protein abundance (R=0.26)(Fig. 3.11) (values derived from the TAP abundance screen (Ghaemmaghami et al., 2003)).

A reason for the generally low co-localisation values might lie in the functional diversity of our selected protein set. As shown above (Fig. 3.10), proteins with similar function showed higher co-localisation values (Pmp1 and Pma1 act together, Pma1, Pdr5 share an ATPase domain). To further test whether functional similarity facilitates co-localisation, we chose two high- (Hxt2, Hxt6) and two low-affinity (Hxt1, Hxt3) representatives among the 20 hexose transporters known in budding yeast (Ozcan and Johnston, 1999) for pairwise co-localisation experiments. All four hexose transporters were distributed in dense network patterns, and indeed exhibited higher degrees of co-localisation values than did functionally

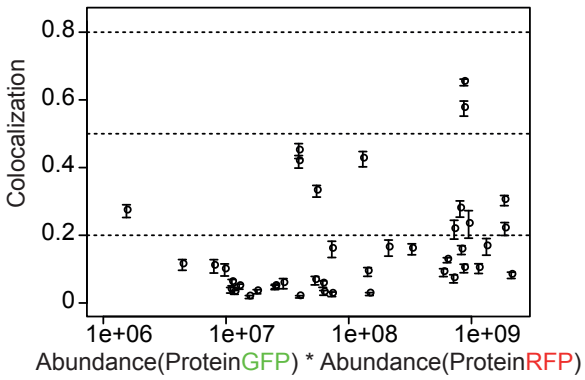

Figure 3.11: Co-localisation vs. TAP protein abundance All co-localisation coefficients measured in the course of the study are plotted against the product of the relative abundances of the protein pairs. The average co-localisation coefficient was not significantly correlated with abundance, as indicated by a Pearson correlation of 0.26.

unrelated proteins, albeit lower than those measured for GFP and RFP of the same protein (Fig. 3.10 D, E, Fig. 3.12 and Tab. 8.2).

3.2.2 Network-factor and random co-localisation

The definition of the co-localisation coefficient is dependent on the surface area covered, therefore a protein with a high network-factor is more likely to have a higher degree of co-localisation than a protein with a lower network-factor. To address the question whether the measured co-localisation coefficient is random, we first calculated the coincidental overlap for each protein pair. To calculate the expected random overlap between proteins we determined decoy values, by shuffling red and green images within a strain. Different cells were superimposed by centering and superimposing the respective regions of interest. The resulting decoy values were compared to the actual co-localisation results for the respective protein pairs (Fig. 3.13 A). Actual and decoy overlap values were highly correlated (Fig.3.13 B, $R = 0.89$, $p = 0.00$). In 70% of all tested pairs (88 of 125) co-localisation values coincided with the expected random overlap (Fig. 3.13 B, black). The remaining 30% differed significantly from their expected overlap values (t-test with $p<0.05$) and included proteins that either actively co-localised (18, magenta), or excluded each other (19, cyan) (Fig. 3.13 B, Tab. 3.1). Notably, proteins with identical or highly similar sequence (>80%)

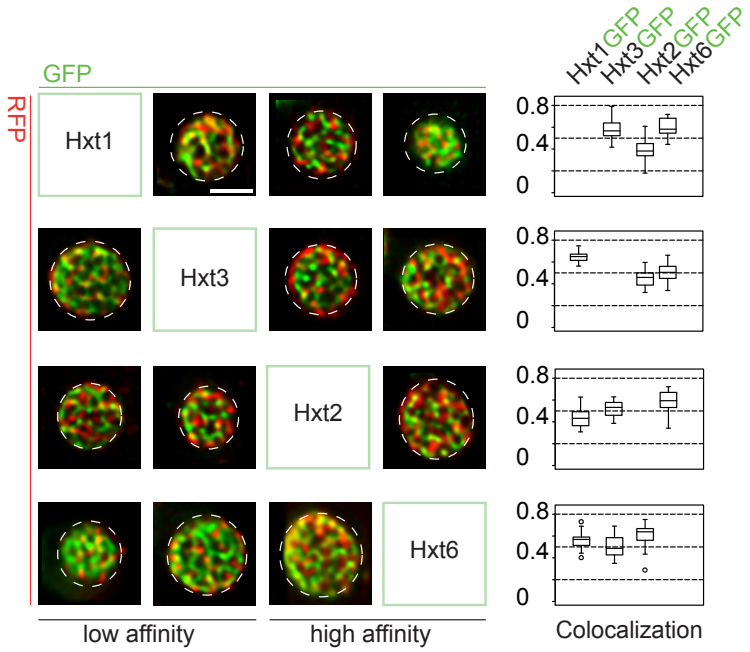

Figure 3.12: All against all co-localisation of hexose transporters. Two-colour TIRFM images of low (Hxt1/3) and high (Hxt6/2) affinity hexose transporters were shown. All proteins have >80% TMS sequence similarities. Distribution of the co-localisation values were plotted as boxplots. Scale bar: 2 μm.

consistently co-localised more often than random, while eisosomes excluded a large number of PM proteins (Tab. 3.1). Other significantly overlapping domains such, those of Sur7-Pil1, Pma1-Nha1 or Hxt3-Hnm1 have been physically or functionally linked before (Walther et al., 2006; Flegelova and Sychrova, 2005; Tarassov et al., 2008). Sur7-Bio5 also co-localised significantly better than random, although no physical link is known between these two proteins (according to SGD).

Table 3.1: Significant co-localisation values

Co-localisation Class	ProteinGFP-ProteinRFP	Co-localisation mean	p-value
better	FETPMP-PMP1	0.6288	0.00094
better	FET3-FET3	0.7613	4.6E-05
better	HXT1-HXT3	0.5654	4.6E-05
better	HXT2-HXT1	0.4598	0.00284
better	HXT2-HXT6	0.5845	0.00300
better	HXT3-FET3	0.4548	0.01242
better	HXT3-HNM1	0.4867	0.00660
better	HXT3-HXT1	0.6417	0.00022
better	HXT3-HXT2	0.4519	0.00806
better	HXT6-HXT1	0.5625	0.00364
better	HXT6-HXT2	0.6076	1.4E-05
worse	PMA1-FET3	0.1657	0.00187

Co-localisation Class	ProteinGFP-ProteinRFP	Co-localisation mean	p-value
better	PMA1-MRH1	0.478	0.00019
better	PMA1-NHA1	0.1948	0.04328
worse	PMA1-PIL1	0.0214	0.00114
better	PMA1-PMA1	0.7458	3E-06
worse	PMA1-SUR7	0.0203	0.04922
worse	PMA1-VHT1	0.0544	7.3E-05
better	PMA1-YOR1	0.1903	0.02166
better	PMP1-FET3TM	0.5125	0.00103
better	PMP1-MID2TM	0.6001	1.2E-05
better	PMP1-PMP1TM	0.7044	0
worse	SUR7-BAP2	0.0263	0.00032
better	SUR7-BIO5	0.0606	0.02173
worse	SUR7-DNF1	0.08	0.03159
worse	SUR7-FET3	0.0331	0.00072
worse	SUR7-FPS1	0.0154	0.02996
better	SUR7-FUI1	0.1219	0.04534
worse	SUR7-MID2	0.0394	0.00117
worse	SUR7-MRH1	0.0492	4.7E-05
worse	SUR7-NHA1	0.0489	0.01616
worse	SUR7-PDR5	0.0594	0.03103
better	SUR7-PIL1	0.5879	0
worse	SUR7-PMA1	0.0392	2E-06
worse	SUR7-PMP1	0.0694	0
worse	SUR7-RAS2	0.1194	1E-06
worse	SUR7-RSN1	0.0411	0.01881
worse	SUR7-SHO1	0.0182	0.01593
worse	SUR7-SSY1	0.0064	0.01364
better	SUR7-SUR7	0.7241	0
worse	SUR7-TCB3	0.0191	0.00033
worse	SUR7-TPO1	0.0455	1.5E-05

We next wanted to identify parameters affecting domain overlap. We found a highly significant correlation between co-localisation and the joint network-factors (Fig. 3.13 C) R = 0.71, p = 0.0) but only weak correlation with protein abundance (Fig. 3.13 D and Fig. 8.1 B). Protein abundance represents the peripheral GFP signal, determined for each protein by measuring the GFP signal of the equator (see section 3.1.2, Fig. 8.1 A and Tab. 8.3). To test the influence of network-factors on protein co-localisation in more detail, we generated decoy cells using images from different strains but with similar network-factors. We then gradually increased the divergence between the reference network-factors and those used for decoy calculations. As expected, correlation between decoy and actual overlap values decreased with increasing divergence in network-factors (Fig. 3.14 A-C). In summary, correlation analyses clearly demonstrated a strong influence of the network-factor on co-localisation with other proteins.

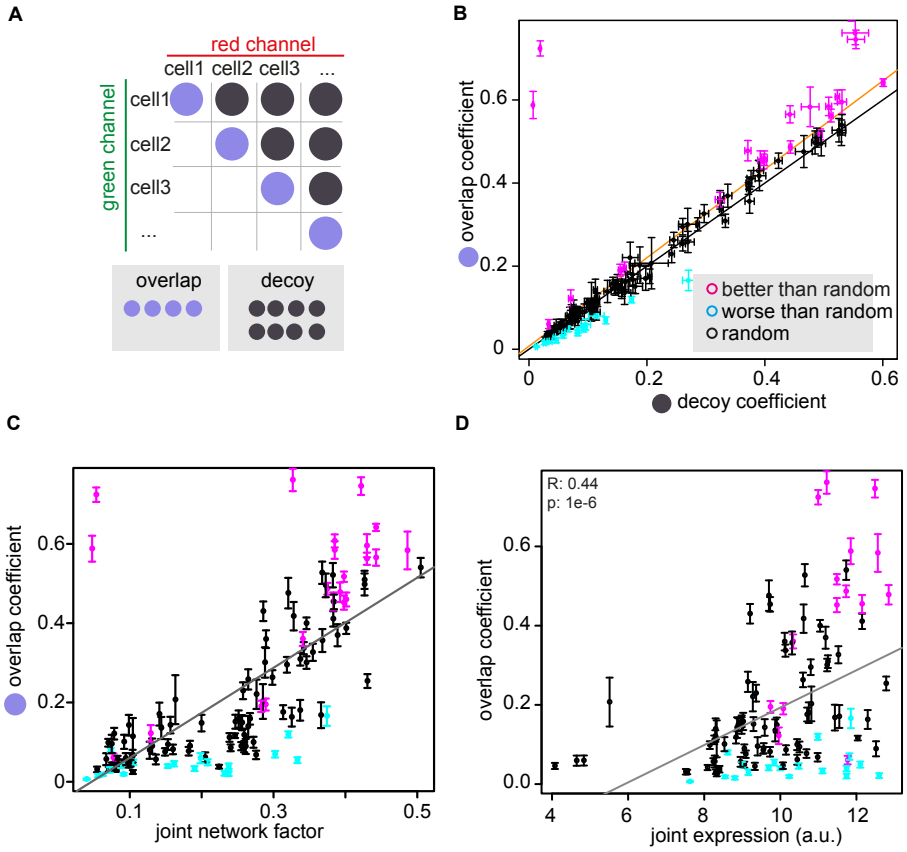

Figure 3.13: Factors influencing co-localisation. A) Schematic representation of the selection procedure for calculation of real (red and green channels from the same cell) and decoy (red and green channels from different cells of the same strain) overlap values are shown. B) Correlation between real and decoy overlap coefficients (termed overlap coefficient and decoy coefficient, respectively) are shown. The values were highly correlated with a Pearson coefficient of R=0.89 (orange line, p-value=0.0). Data points were shown as mean <s.e.m. in both directions. The black line indicates identity. Protein pairs co-localising significantly ($p<0.05$) better or worse than expected from decoy values, are shown in magenta and cyan, respectively. C) Correlation between overlap coefficient and joint network-factor (sum of network-factors) are shown. R=0.71, p-value=0.0, grey line. Colour code as in (B). D) Weak correlation of overlap coefficients and joint expression levels.

3.2.3 Factors affecting PM domains

After identification of the network-factor and thus the spatial pattern of a protein as a force influencing co-localisation, we aimed to identify factors influencing the pattern formation. Two previously proposed mechanisms are the association of membrane proteins with stable

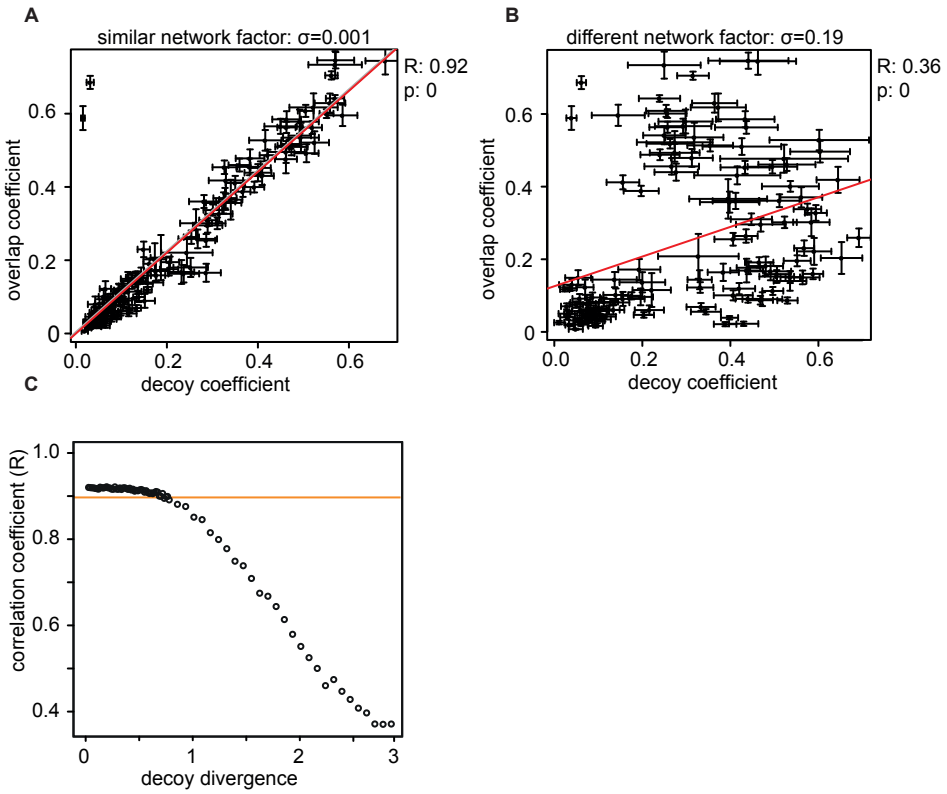

Figure 3.14: network-factor and co-localisation. A,B) Correlation plots between decoy and real overlap coefficients for decoy values were calculated from cells with similar or divergent network-factors. The divergence is indicated as σ. R and p values for correlations are shown. C) The decoy values were calculated by using cells with defined network-factors. The correlation (R) between decoy and real overlap values is lost with increasing divergence between network-factors of the original images and those of the selected decoy cells. Divergence is plotted as z-score.

or dynamic scaffolds, such as the extracellular matrix (Galla and Sackmann, 1975) or cortical actin cytoskeleton (Kusumi et al., 1993). In addition, the lipid composition was reported to greatly influence PM protein domain formation (Simons and Ikonen, 1997; Bagatolli et al., 2010a). We tested the influence of these factors, by introducing mutants or using drugs, using the network-factor as readout. Enzymatic degradation of the cell wall with zymolyase, led to clear changes in most PM protein distributions (Fig. 3.15 C). Many distributed protein domains collapsed into larger aggregates or elongated substructures (Fig. 3.15 C). These effects were difficult to interpret, as zymolyase caused unspecific aggregate formation of PM proteins. Because of these unspecific and pleiotropic effects, we

focused on more subtle changes, such as the removal of the actin cytoskeleton or influencing the lipid composition of the PM. Depolymerisation of actin with Latrunculin B had only minor influence on the network-factor (Fig. 3.15 A).

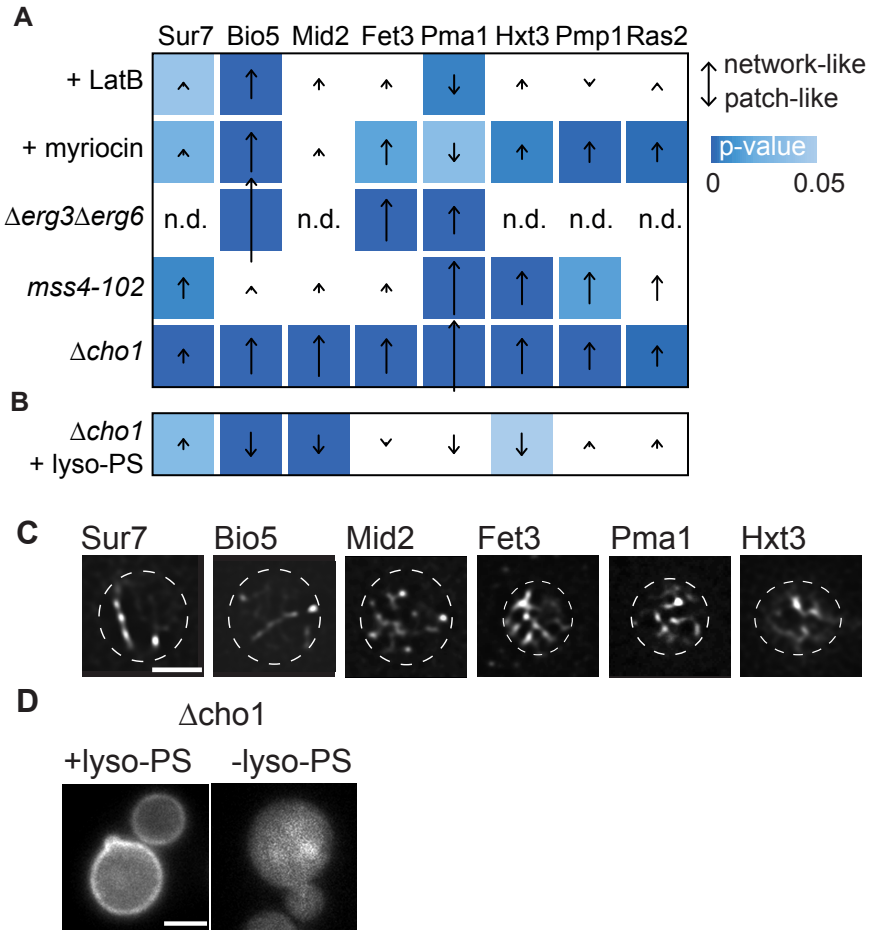

Figure 3.15: Determinants affecting the network-factor. A) Matrix showing the effects of perturbations of the actin cytoskeleton (LatB) or lipid composition on network-factors of selected proteins. Arrows indicate the direction and extent of change compared to control cells. Colours indicate level of significance with white being not significant. B) Reversibility of Δ*cho1* effects on network-factors after supplementing media with lyso-PS. Distribution of some proteins (e.g. Bio5) reverts back to control patterns. C) Effect of cell wall depletion on a selection of proteins. Clusters of proteins and elongated structures were observed. D) GFP-Lact-C2 in Δ*cho1* background. With addition of lyso-PS GFP-Lact-C2 localises to the PM, without it locates to the cytosol. n.d.: not determined, strain could not be generated. Scale bar: 2 μm.

Finally, we tested the influence of lipids on the formation of PM protein domains, by blocking different lipid biosynthesis pathways. We used several approaches to perturb the lipid composition of the PM. The drug myriocin inhibits the serine palmitoyl transferase, which is the first step of sphingosine biosynthesis, which resulted in a depletion of sphingolipids. Deletion of CHO1 blocks the canonical pathway of phospholipid synthesis. If the medium is supplemented with choline the level of PS is greatly reduced (Hikiji et al., 1988; Fairn et al., 2011). Successful depletion of PS was confirmed by using GFP-Lact-C2 localisation as a marker; if PS is successfully depleted GFP-Lact-C2 localises to the cytosol (Fig. 3.15 D). Deletions of single genes of the sterol biosynthesis pathway can be well compensated by *Saccharomyces cerevisiae*, but sterol composition were strongly altered in $\Delta erg3\Delta erg6$ strains (Guan et al., 2009). Finally, use of the temperature-sensitive allele of the phosphatidylinositol kinase *mss4-103* (Davierwala et al., 2005) allowed the reduction of PIP2 levels. All lipid perturbations had strong but selective effects on network-factors but differed in their target range (Fig. 3.15 A). Nearly all perturbations increased the calculated network-factors, i.e. reduction in lipid complexity was associated with reduced protein segregation. While depletion of sphingolipids by myriocin and PIP2 level reduction by *mss4-103* only affected a subset of proteins. The deletion of CHO1 and the depletion of ergosterol affected the network-factors of all tested proteins (Fig. 3.15 A).

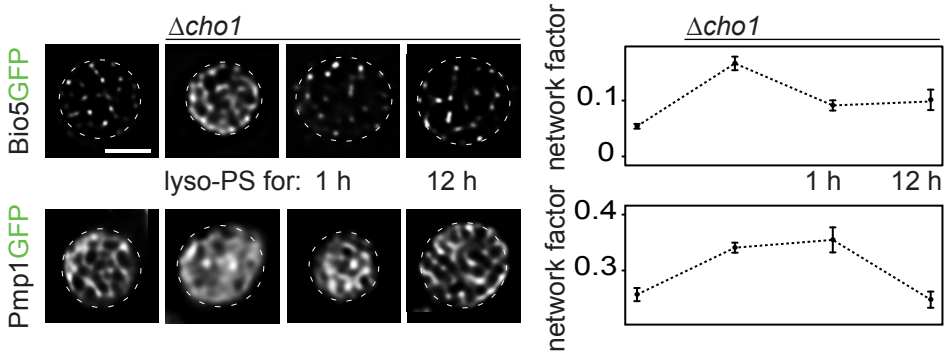

Figure 3.16: Phosphatidylserine influence the network-factor. The distribution patterns of Pmp1GFP and Bio5GFP in $\Delta cho1$ strains supplemented with lyso-PS for different time periods were shown. Bio5GFP network factors already recovered after 1 h while Pmp1 was only affected after 12 h. Scale bar: 2 μm.

We supplemented $\Delta cho1$ cells with lyso-PS to to validate a specific effect of PS depletion on PM protein organisation. Successful incorporation of PS into the PM was monitored

with GFP-Lact-C2 (Fig. 3.15 D). Remarkably, within 1 h after lyso-PS addition, network factors for some proteins, such as Bio5, were restored to wild-type levels (Fig. 3.16). Lack of, or incomplete recovery of other tested proteins could be explained by long-lasting defects in secretion in Δ*cho1* strains. Indeed, culturing Δ*cho1* cells overnight in medium supplemented with lyso-PS, led to a recovery of the network-factor of Pmp1 to wild-type levels (Fig. 3.16). Our results thus indicate that lipid composition differentially influences lateral protein segregation in the yeast PM.

3.2.4 Transmembrane sequences and domain formation

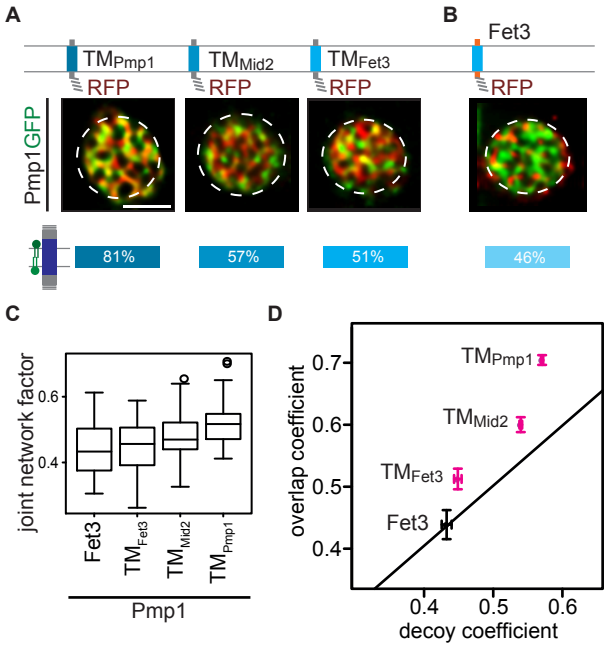

Figure 3.17: TM sequence determines protein co-localisation. A) Localisation patterns of synthetic TMS-RFP fusion constructs were shown. TMS of the single-spanning TM proteins Pmp1, Mid2 and Fet3 were co-localised with full length Pmp1GFP. Sequence identities between TMS including flanking amino acids regions are indicated in percent. B) Co-localisation and TMS sequence identity between Fet3 and Pmp1 were shown. C) Similar joint network-factors for protein pairs in (A) and (B). D) Correlation between real and decoy overlap values for indicated TMS constructs with Pmp1. All pairs with sequence identity above random values co-localised significantly (random overlap: black line, magenta: increased overlap, $p<0.05$), while Fet3 and Pmp1 had random TMS similarity and co-localised also with random levels. Scale bar: 2 μm.

A role for lipid composition in lateral protein segregation implies lipid-protein interactions, which would be expected to occur via TMS or lipid anchors. To experimentally validate this potential link, we generated minimal constructs containing only a single TMS. We fused the TMS of the single-span proteins Fet3, Mid2, and Pmp1 to RFP and measured the degree to which each minimal construct co-localised with the full-length Pmp1GFP protein as a reference domain marker. All three TMS constructs localised to the PM and formed comparable network-like patterns (Fig. 3.17 A, C). Moreover, we found a clear correlation between overlap coefficients and TMS sequence similarities. While the Pmp1 TMS (TM_{Pmp1}) showed the expected strong overlap with the full-length protein; TM_{Mid2} and TM_{Fet3} constructs showed less co-localisation with Pmp1, which reflects their divergence from the TM_{Pmp1} sequence (Fig. 3.17 A). All three constructs had a similar network-factor, which is important for comparison of co-localisation values (Fig. 3.17 C). Although different co-localisations were observed, all three constructs still co-localised significantly (Fig. 3.17 D), but in accordance to their respective sequence similarity. However, Fet3GFP full length protein which has the least sequence similarity of the used constructs, co-localised randomly with Pmp1GFP (Fig. 3.17 B, D).

To test whether the TMS could re-localise a whole protein to a different domain, we ectopically expressed a chimera generated of Fet3 and the TMS of Pmp1 (Fet_{Pmp}). Note that Fet3 co-localised strongly with itself but only weakly with Pmp1 (Fig. 3.18). Importantly, since Fet3 is a monomeric protein (Pozdnyakova and Wittung-Stafshede, 2010), it is unlikely that the co-localisation of Fet3 with itself was due to simple oligomerisation. Similarly, the Fet_{Pmp} chimera was unlikely to bind directly to endogenous Fet3. According to our expectations, the Fet_{Pmp} chimera did not co-localise with Fet3 but with Pmp1 instead (Fig. 3.18). In other words, a TMS of only 22 amino acids was sufficient to redirect a 600-amino acid protein to a different PM domain. Our results therefore indicate that TMS can act as instructive cues for lateral segregation of proteins in biological membranes.

3.2.5 Functional relevance of domain association

To test whether protein re-localisation altered protein function, we assayed for the protein function of the Fet3 WT and the Fet_{Pmp} chimera. The Ferro-O2-oxireductase Fet3 is important for iron uptake (Eide et al., 1992). If Fet3 is re-localised to a different domain, the cell should be impaired in iron uptake. Fet3 mediated iron uptake is only required when

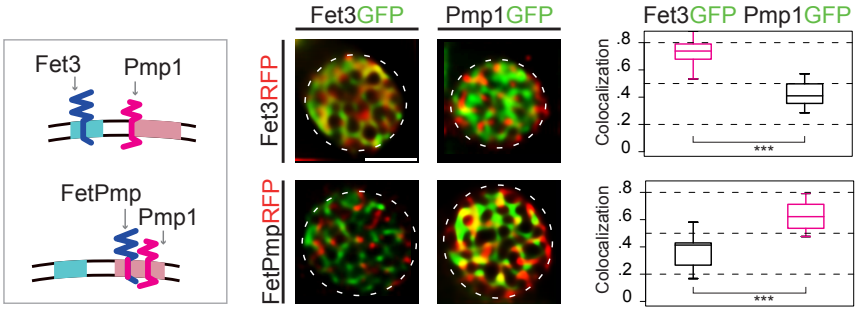

Figure 3.18: Protein function depends on domain association. Fet_{Pmp} is a chimeric construct in which the Fet3 TMS was replaced by the TMS of Pmp1. Note that the change resulted in the re-location of Fet_{Pmp} to the Pmp1 domain. Box plots showing co-localisation coefficients. The cartoon illustrates the co-localisation of the chimera with Pmp1. Scale bar: 2 μm.

grown on iron limiting media. By adding bathophenanthroline disulphonate (BPS) to the media it was possible to sequester even trace amounts of iron. Cells show drastic growth defects in Δ*fet3* background strains. Fet3 introduced on a plasmid to Δ*fet3* background strain rescued the growth defect; as expected Fet_{Pmp} showed growth defects (Fig. 3.19).

To conclude, the TM segment swap did not only successfully segregate Fet_{Pmp} to the Pmp1 domain, but also affected iron uptake of cells. Since it cannot be ruled out that the swap of the TMS of Fet3 impaired function of the enzymatic domain, we further tested protein function after changing domain association of the arginine permease Can1.

We altered the domain association of the arginine transporter Can1, which mediates uptake of the toxic arginine analogue canavanine. Functional Can1 leads to canavanine uptake and therefore canavanine incorporation into proteins, causing cell death; Impairment of Can1 function confers resistance to canavanine (Fig. 3.20 B). To alter Can1 localisation we used a variant of the recently described anchor-away system (Haruki et al., 2008). By this approach, GFP-tagged proteins were recruited to a target protein fused to a monomeric anti GFP antibody, called a GFP-Binder (GB). Co-expressing Pma1GB and Can1GFP, led to a successful displacement of Can1GFP from eisosomes and re-localisation to the Pma1 domain (Figure 3.20 A). The control Δ*can1* strain was able to grow on canavanine containing medium, whereas Can1GFP and Pma1GB alone did not impair Can1 uptake (Fig. 3.20 B).

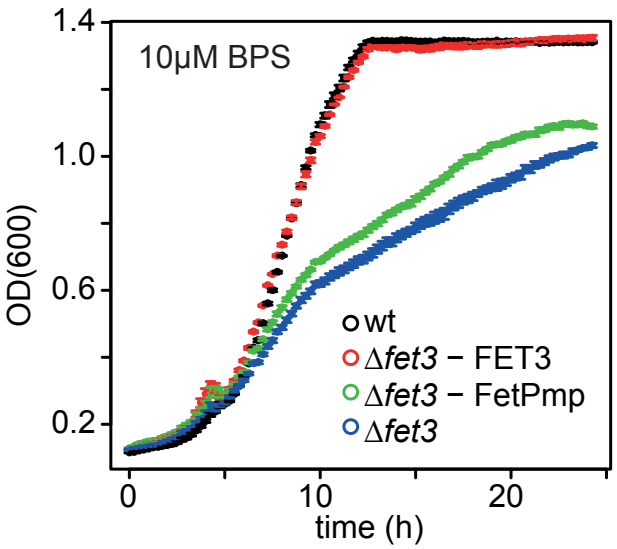

Figure 3.19: Protein function depends on domain association. Growth curves of the indicated strains in iron-depleted medium after BPS addition were shown. The Fet_{Pmp} chimera was unable to growth in iron depleted media.

3.3 PM domains and endocytosis

3.3.1 Cargo mediated endocytosis

So far, we examined the PM organisation and identified a large number of different, partly overlapping PM protein domains. The next important question is how PM proteins are spatio-temporal regulated. More precisely, how is it possible to selectively remove a single PM protein domain. In order to understand PM organisation it is important to study delivery and removal of PM proteins to and from the PM. Actin mediated endocytosis is the main pathway for PM protein turnover in yeast. Currently, the knowledge of the connection between endocytosis and PM domains is limited and two concurrent models exist. Both models divide the yeast PM into two domains (MCC and MCP). One model suggest that proteins within MCC are protected from endocytosis, while the other suggest an increased endocytosis via MCC (Grossmann et al., 2008). Our study revealed the existence of many partially overlapping protein domains (see section 3.2). We therefore aimed to determine, the functional significance of PM domains and endocytosis.

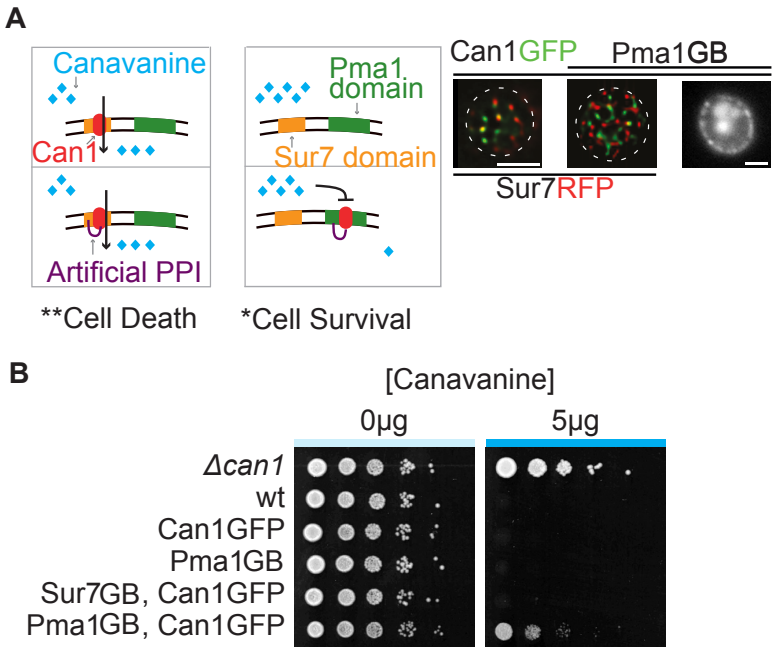

Figure 3.20: Can1 function depends on domain association. A) Schematic representation of the re-localisation of Can1GFP to the Pma1 domain. Two colour TIRFM images showing the displacement of Can1GFP from MCC. The equatorial image shows no internalisation of Can1 after canavanine addition. B) Growth assays of Can1GFP on plates with (5 μg) and without canavanine. Ectopic re-localisation of Can1 to the Pma1 domain by Pma1GB results in loss of Can1 function, as indicated by increased resistance to canavanine. Scale bar: 2 μm.

To monitor endocytosis of PM domains, we analysed co-localisation of the late endocytic marker Abp1RFP with different integral PM protein fused to GFP. Abp1 binds to the actin cage of the endocytic patch at the internalisation step and is therefore, as a late endocytic marker suitable to monitor the final step of endocytosis. A subset of 8 integral PM proteins covering the full range between low and high network-factors was chosen for the co-localisation with Abp1RFP (Fig. 3.21 Tab. 3.2). Both channels (GFP and RFP) were recorded over a time course of two minutes. Abp1RFP patches were automatically tracked using the Imagej software package particle tracker and a custom made Matlab program. We observed low co-localisation between tested proteins and Abp1RFP (Fig. 3.21 Tab. 3.2). This finding reflects the low turnover of many PM proteins; Pma1 for example was reported to have a turnover of 11h (Benito et al., 1991).

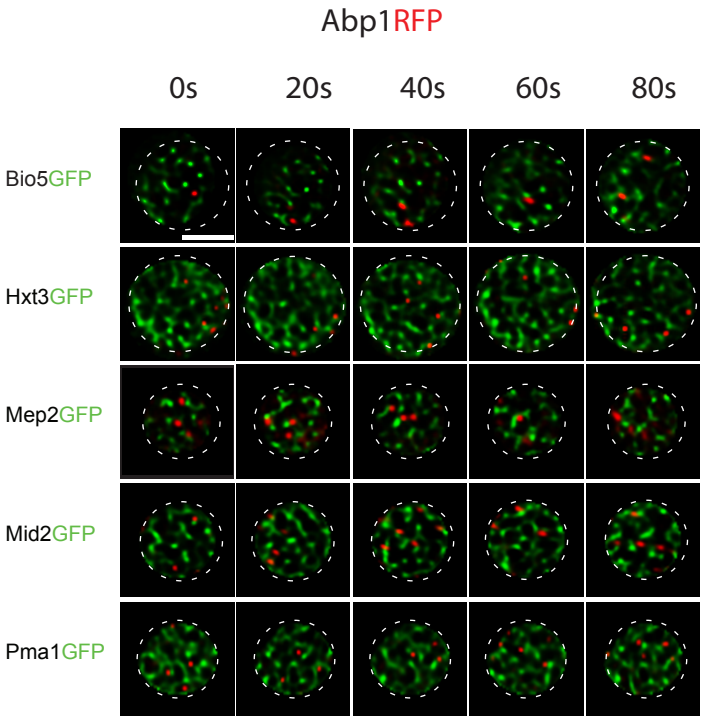

Figure 3.21: PM domains and endocytosis. A) Co-localisation of different PM marker proteins for patch and network-like domains with the actin patch marker Abp1RFP. Time series of images showing little overlap between domains and the actin patch marker Abp1RFP. Tracking of actin patches and subsequent co-localisation was automated. Scale bar: 2 μm.

3.3.2 Mup1 – a marker for endocytosis

We had to resort an inducible marker system to monitor endocytosis of cargo proteins, because of the low co-localisation of PM proteins with actin patches. Sufficient amounts of substrate induce internalisation and degradation of many amino acid transporters. Mup1 was reported to be internalised quickly after methionine addition to the media (Lin et al., 2008) and becomes ubiquitylated by the E3 ligase Rsp5 which in turn is recruited by the arrestin ligase Art1 (section 2.4). After ubiquitylation, Mup1 is internalised and degraded in the vacuole within 60 minutes (Lin et al., 2008). We tested whether Mup1 would also localise to the MCC patch-like compartment, as many amino acid permeases are known to localise to the MCC compartment (Stradalova et al., 2009; Grossmann et al., 2008). Co-localisation of Mup1GFP with the MCC marker Sur7RFP showed a high degree of

Table 3.2: Co-localisation of Abp1RFP patches with PM domains

PM protein	(%) Co-localisation	Number of patches	Patch–Network
Ena2	0	348	patch
Bio5	2.6	710	patch
Fet4	0	53	patch
Hxt3	8.3	460	network
Pma1	3	634	network
Sho1	1.8	243	patch
Tpo1	2.3	292	network
Mid2	6.2	368	network

co-localisation (Fig. 3.22 A). Endocytosis of Mup1 was triggered by supplementing the medium with methionine. Shortly after methionine addition (<10min) Mup1 lost the patchy pattern and formed a dense network, which did not co-localise with Sur7RFP (Fig. 3.22 A). The patch-like appearance of MCC depends on the presence of to core and scaffold protein complex termed eisosomes; deletion of the core eisosomal component Pil1 was shown

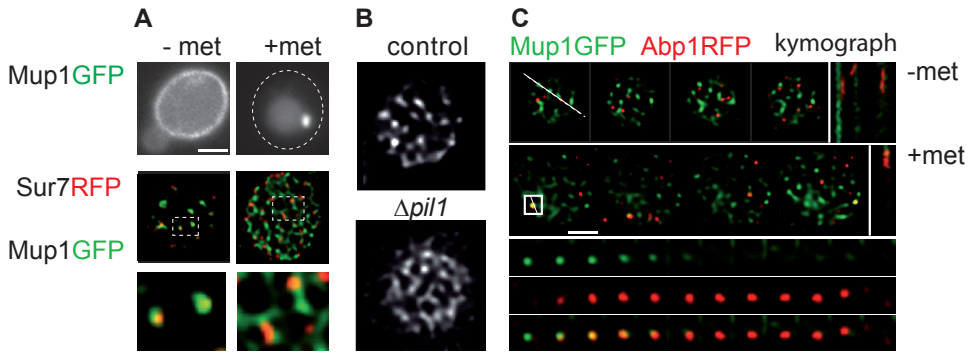

Figure 3.22: Mup1 an inducible cargo for endocytosis. A) Mup1 was present at the cell cortex in media lacking methionine (-met) and degraded within 60min after methionine addition (+met). TRIRFM images of Mup1GFP appeared patchy without– and network-like after the addition of methionine (image acquired 5 min after methionine addition). Mup1GFP co-localised with Sur7RFP. After the addition of methionine the co-localisation was lost (image acquired 5min after methionine addition). B) In Δ*pil1* background the patchy pattern of Mup1 was lost and the protein formed a network. C) Montage of time series of Mup1GFP and Abp1RFP with and without methionine. Without methionine Mup1GFP and Abp1RFP did not co-localise, after methionine addition Mup1GFP co-localised with Abp1RFP. Kymograph of Mup1GFP with Abp1RFP is shown for +met and -met conditions. Scale bar: 2 μm.

to disrupt MCC organisation(Grossmann et al., 2007). Consistently, Mup1 lost its patchy pattern upon PIL1 deletion and instead was distributed in a network (Fig. 3.22 B).

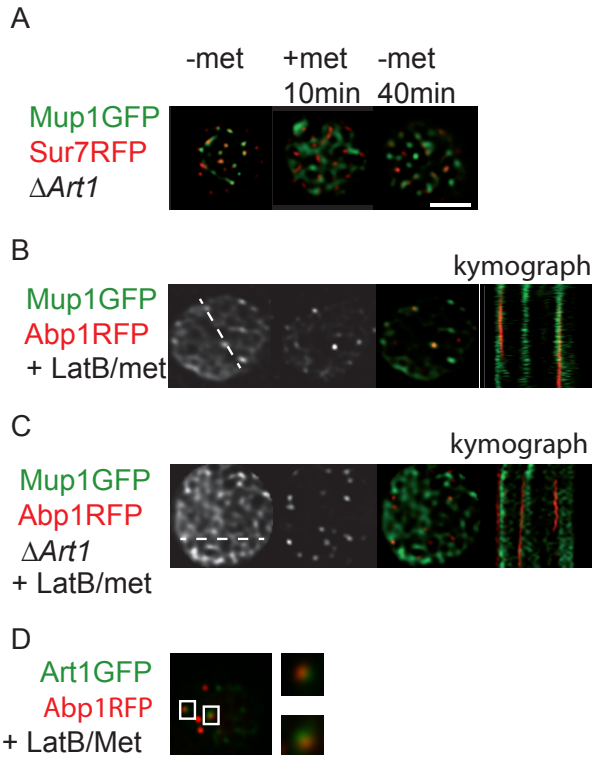

Figure 3.23: Mup1 and endocytosis. A) Pulse chase experiment to monitor endocytic uptake of Mup1GFP in Δ*art1* background. Depicted are images of Mup1GFP without methionine, 10min after methionine addition and after 40min of methionine washout. Mup1GFP was not endocytosed, but could move in and out of eisosomes. B) Mup1GFP was stabilised at endocytic sites after methionine addition and additional actin patch stabilisation by addition of LatB. C) Mup1GFP was not stabilised any longer at actin patches after actin cable depolymerisation and methionine addition in Δ*art1* background strains. D) Art1GFP co-localised with the stabilised actin patch marker Abp1RFP. Kymograph of Mup1GFP and Abp1RFP is shown with (B, C) methionine. Scale bar: 2 μm.

To further characterise early steps of endocytosis of Mup1, we co-expressed Mup1GFP with Abp1RFP and measured the co-localisation in presence and absence of methionine (Fig. 3.22 C). In presence of methionine Abp1RFP did not co-localise with Mup1GFP; after methionine addition Mup1GFP was released from eisosomes, accumulated into foci and disappeared together with Abp1RFP (Fig. 3.22 C).

The mechanism leading to domain exit of Mup1 is currently unknown. To test whether binding of Art1 and therefore ubiquitylation was required for MCC exit of Mup1; we co-expressed Mup1GFP and Sur7RFP in ART1 deletion strain. Upon methionine addition Mup1GFP lost the MCC association and distributed into a dense network which was not endocytosed and remained stable on the PM (Fig. 3.23 A). Methionine washout re-introduced Mup1 MCC association within 40min (Fig. 3.23 A).

These results strongly support ubiquitylation independent MCC exit of Mup1. In order to test ubiquitin requirements to concentrate Mup1 at the site of endocytosis, we stabilised actin patches at the cell cortex by depolymerisation of actin cables by adding a low concentration of the actin monomer sequestering drug LatB (5 μM LatB) (Carlsson et al., 2002). By triggering endocytosis of Mup1GFP in Δ*art1* background and control strains by methionine supplementation, we were able to show that Mup1GFP was only stabilised at endocytic sites if Art1 was present (Fig. 3.23 B,C). Interestingly, ubiquitylation of Mup1GFP occurred at least partly at the endocytic site as shown by co-localisation of Art1GFP with Abp1RFP after LatB addition (Fig. 3.23 D).

We next wanted to identify the signal sequence within Mup1 leading to domain exit. We focused on the C-terminal part of Mup1 because domain exit of Mup1 did not depend on ubiquitylation, as shown in the previous experiment and the ubiquitylation site was mapped to the cytoplasmic N-terminal tail (Lin et al., 2008). By comparison of the C-termini of different yeast amino acid permeases, we identified three distinct sequence domains (Fig. 3.24). The first domain showed relatively little conservation between permeases. The second domain contained conserved sequences (marked with asterix) enriched in charged amino acids (Fig. 3.24). The third domain contained two predicted casein kinase II phosphorylation sites at serine at position 57 and 60 (Mup1 C-terminus, modified serines are marked SEQEKSL). Yeast Phospho web interface was used for phosphorylation site prediction (Ingrell and Blom, 2007). We generated three yeast strains containing truncations of the Mup1 C-terminus at indicated positions T1, T2, T3 (Fig. 3.24) and tested whether Mup1 was endocytosed after methionine addition. Truncations of T2 and T3 did not have any observable effect on Mup1 endocytosis, but the truncated version T1, in which the whole C-terminus is removed remained associated with MCC (Fig. 3.25 A). We did not observe endocytosis of Mup1-T1. TIRFM image of Mup1 with truncation T1 (whole C-terminus)

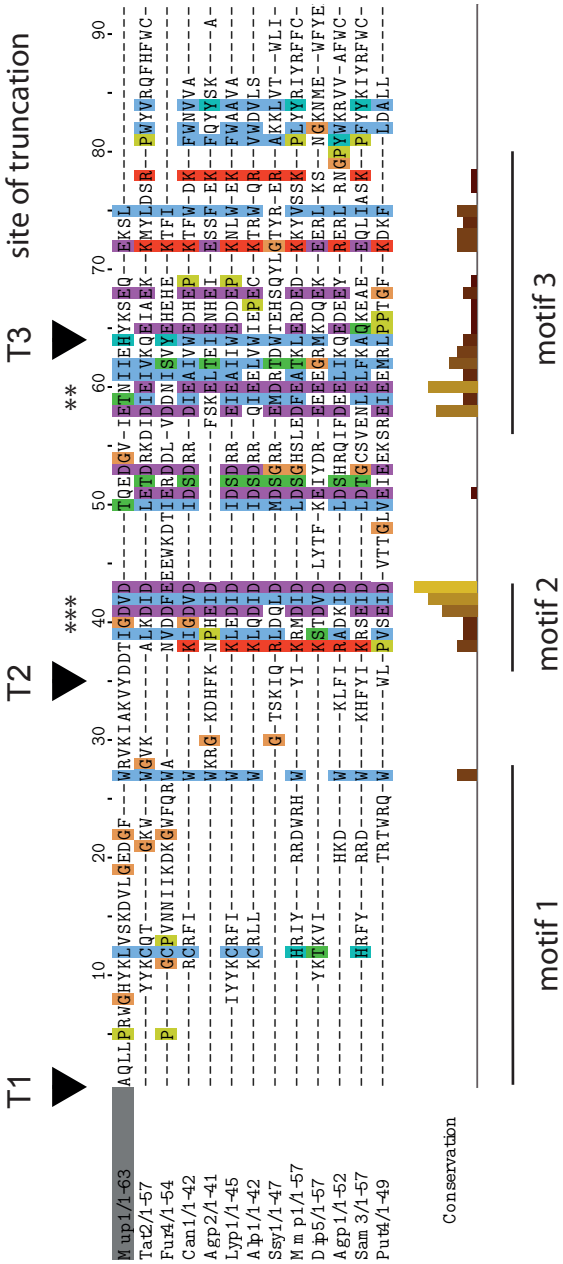

Figure 3.24: Alignment of C-termini of amino acid transporter from budding yeast. Sequence alignment of the C-termini of amino acid permeases from *Saccharomyces cerevisiae*, highly conserved amino acids are highlighted in purple and blue. Three motifs were identified and labelled motif 1,2,3. Motif1 is not conserved except a W residue, motif2 exhibits a conserved DVD stretch. Motif3 includes a putative casein kinase II phosphorylation site at serine 57 and 60. T1,T2,T3 indicate sites at which Mup1 was truncated.

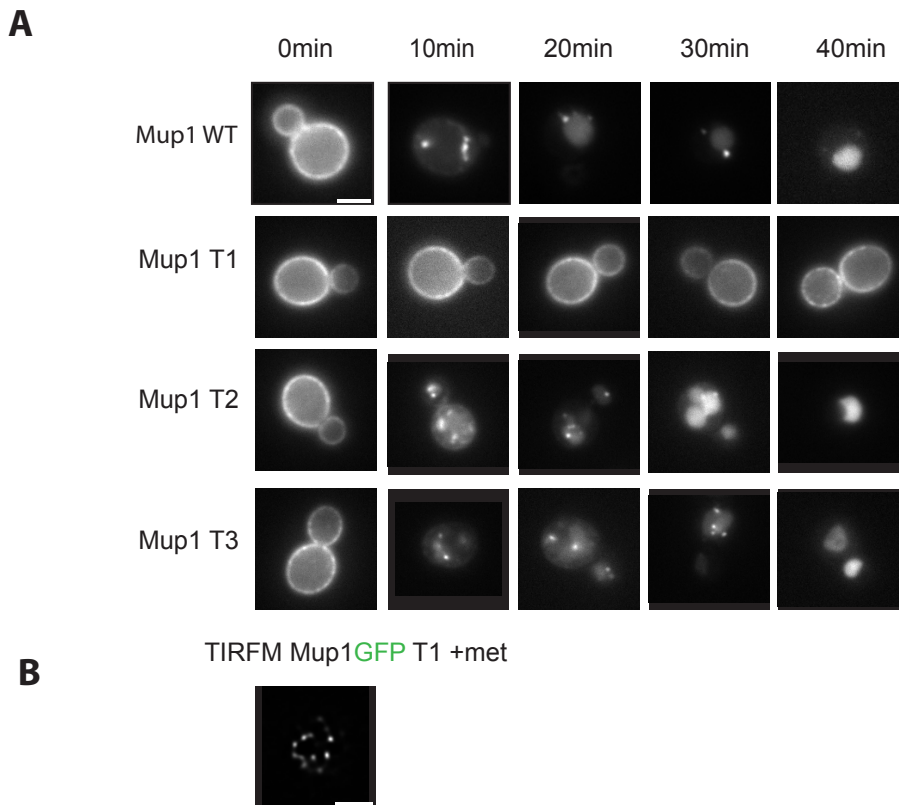

Figure 3.25: Endocytosis of Mup1 with truncated C-termini. A) Equator Epi fluorescence images series of WT and truncations of Mup1GFP, methionine was added at t0 and imaged every 10 minutes to 40 minutes total. Truncations T2 and T3 lead to endocytosis of Mup1GFP, while truncation T1(whole C-terminus) resulted in Mup1GFP being unable to be endocytosed. B) TIRFM image of Mup1GFP with truncation T1 showing a patchy pattern, indicating continued MCC domain association. Scale bar: 2 μm.

showed a patchy pattern even after addition of methionine, indicating a continued MCC domain association (Fig. 3.25 B).

Previous experiments conducted within this study showed the necessity of Mup1GFP to move to the site of endocytosis, to become ubiquitylated and internalised. In summary, cargo can most likely not recruit the endocytic machinery, but has to move to the site of endocytosis.

We next addressed the question whether cargo is able to induce actin patch assembly. To test whether Mup1 can induce actin patch assembly, we artificially tethered full length Mup1 protein to the MCC compartment by co-expressing Mup1GFP, Sur7GB and Pil1RFP

(Fig. 3.26 A, B). Mup1GFP tethered to Sur7GB was unable to exit eisosomes after addition of methionine and actin patches did not form at MCC/eisosomal compartment (Fig. 3.26 C). Conclusively Mup1 was not able to recruit the endocytic machinery.

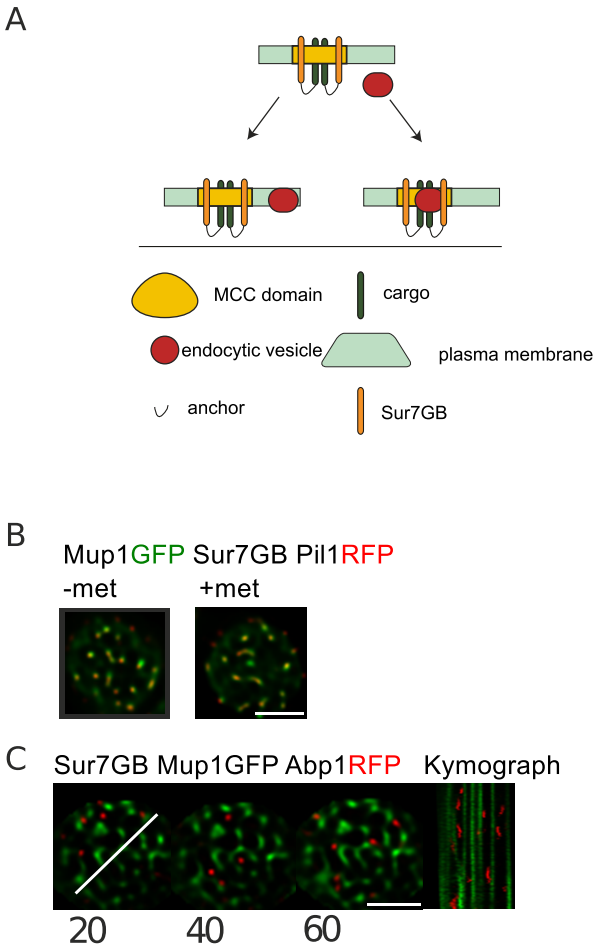

Figure 3.26: Endocytic machinery recruitment. A) Scheme showing tethering of Mup1 to eisosomes. Cargo (green) was tethered to a domain (yellow/orange), endocytic patches were coloured red. B) Mup1GFP tethered to Sur7GB co-localised with Pil1RFP and was not released from eisosomes after methionine addition (+met). C) Actin patches did not co-localise with Mup1GFP after methionine addition (Different time points are shown). Kymograph was drawn along the dotted line. Scale bar: 2 μm.

Table 3.3: Endocytic adaptors screened for ectopic endocytic site initiation (NPF = nucleation promoting factors)

Endocytic modules and adaptor proteins				
Early coat	Late coat	NPF	Ampiphysin	other
Apl2	End3	Bzz1	Rvs161	Dnf1
Apl4	Lsb3	Las17	Rvs167	Inp52
Clc1	Pan1	Vrp1		Scd5
Ede1	Sla1			Sep7
Ent1	Sla2			
Syp1				
Yap1801				

3.3.3 Endocytic site initiation

After Identification that cargo is unable to recruit the endocytic machinery we aimed to identify proteins that can serve as landmarks for endocytosis. We co-expressed Sur7GB together with in frame GFP fusions of early endocytic adaptor proteins to systematically re-localise these adaptor proteins to MCC, to test for proteins with the capacity of endocytic site initiation.

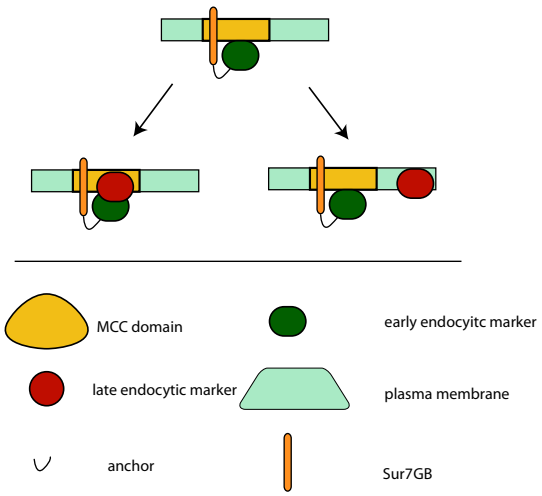

Figure 3.27: Endocytic landmark screen. Scheme showing early endocytic marker (green) tethered to eisosomal domain (yellow/orange). The late endocytic marker protein Abp1RFP was monitored to detect ectopic actin patch formation(red).

The MCC compartment was reported to be entirely devoid of actin patch assembly and it was proposed that proteins within this domain are protected from endocytosis (Brach et al., 2011; Grossmann et al., 2008). We used the late endocytic marker Abp1RFP as a readout for endocytic site initiation. Co-localisation of Abp1RFP with immobilised adaptor proteins indicated ectopic endocytic site formation at the MCC. The scheme of this experiment is given in figure 3.27 and early endocytic marker proteins are listed in table 3.3.

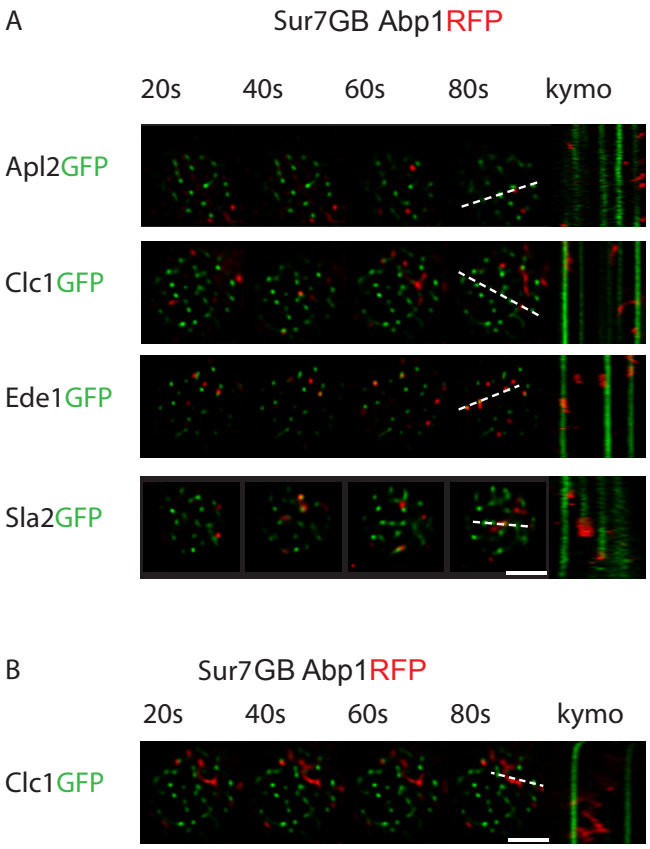

Figure 3.28: Endocytic landmark screen. A) Montage showing cells expressing early endocytic marker proteins (GFP), Sur7GB and Abp1RFP. Co-localisation of Ede1GFP with Abp1RFP indicated an ectopic actin patch assembly. Little or no co-localisation was observed for most other endocytic marker proteins. Time points of every 20s are shown. Kymograph was drawn along the indicated line. B) Clc1GFP anchored to eisosomes showed CLC1 deletion phenotype (Abp1RFP comet tails). Scale bar: 2 μm.

Table 3.4: List of endocytic regulatory proteins and early endocytic adaptor proteins which were artificially anchored to MCC; Ectopic actin cage formation was monitored by co-localisation with Abp1RFP.

Protein name	# of Abp1RFP patches	# Co-localisation of Abp1RFP with MCC	(%) Co-localisation of actin patches with MCC
Vrp1	81	10	20
Ent1	89	23	25
Apl2	174	9	5
Apl4	288	17	6
Yap1801	157	24	15
Inp52	218	5	2
Clc1	56	10	18
Scd5	37	2	5
Ede1	108	52	59
Syp1	83	13	16
Lsb3	103	16	16
Dfu1	81	13	16
las17	55	3	5
Sep7	16	3	19
Sla1	37	6	16
Sla2	43	13	30
Bzz1	132	9	7
End3	54	6	11
Pan1	325	63	20

Successful re-localisation of endocytic marker proteins was indicated by a static patch-like appearance of the early endocytic marker, which implies binding to the static MCC domain. Re-localisation of Ede1 to MCC was sufficient for assembly and internalisation of actin patches at MCC (60% of patches co-localised with MCC). Sla2 did also re-direct endocytosis to MCC, but with a reduced efficiency if compared to Ede1GFP (30% of patches co-localised with MCC) (Fig. 3.28 A, Tab. 3.4). Interestingly, anchoring of Clc1 to MCC resembled the knockout phenotype Clc1, in which Abp1 was reported to show large comet tails (Fig. 3.28 B).

Chapter 4

Discussion

4.1 Plasma membrane protein domains

4.1.1 Patchwork model of membrane organisation

According to our findings we propose a model for the self-organisation of biological membranes into numerous domains. In the resulting "patchwork" membrane, co-existing domains overlap with each other to various degrees depending on the similarity of their constituent proteins and lipids (Fig. 4.1). This model is based on the following observations.
First, we identified many partly overlapping, but discrete PM protein domains. The localisation of most of the proteins was random, although not for all proteins.
Second, proteins which had a high TMS sequence similarity co-localised to a greater extend than unrelated proteins (see hexose transporter co-localisation in Fig. 3.12). We could identify the TMS as a driving force for lateral segregation of peptides and proteins (see Fig. 3.17 and Fig. 3.18).
Third, domain formation was greatly influenced by the lipid composition of the PM. We altered lipid composition of the PM by blocking lipid biosynthesis pathways. Each lipid had a distinct and large influence on PM domain organisation of the examined proteins (Fig. 3.15 and Fig. 3.16). Interestingly, PS depletion showed the most drastic effect on PM protein localisation pattern and influenced all proteins which can be explained by the high abundance (30%) and the high negative net charge. Indeed PS was shown to be essential for polarisation in yeast (Saito et al., 2007) and acts as a signalling platform for numerous membrane proteins (Fairn et al., 2011).

Taken together these results strongly support a patchwork model of membrane organisation, which depends on the TMS of a protein and the surrounding lipid environment (Fig. 4.1). This model does not rule out other possibilities of membrane organisation, like lipid anchors, special lipid binding domains, and anchorage of proteins to the cell wall (see section 2.5).

4.1.2 Mechanisms driving patchwork membrane formation

The patchwork model of membrane organisation extends far beyond current understanding of membrane organisation. Only few different PM domains have been identified within living cells and only three mutual exclusive domains within budding yeast have been described (Stradalova et al., 2009). Biological membranes represent the sum of many weak interactions between proteins and lipids, hence the patchwork model of membrane organisation cannot be explained by a single theory, but by an interplay between existing models and concepts.

Theories explaining lateral inhomogeneities within biological membranes are the lipid raft concept (see section 2.5.1), the picked fence model (see section 2.5.2), and the hydrophobic matching theory (see section 2.5.3).

While the picked fence model was shown to not occur within budding yeast (Valdez-Taubas and Pelham, 2003), lipid rafts can only explain the emergence of a few domains (L_O vs. L_D). The hydrophobic matching theory on the other hand has the capacity to explain many PM protein domains. Limitations of the hydrophobic matching theory are the exclusive focus on the TMS length and membrane thickness, therefore neglecting contributions of further protein-lipid interactions. Protein-lipid interactions have been described for a long time on different levels. Annular lipids were already proposed in the second half of the last century (Lee, 1977) and interact only transiently with proteins. In addition selective interaction with proteins by geometric matching the shape or charge of proteins was shown in many cases (Galla and Sackmann, 1975; Lehtonen et al., 1996a; Hite et al., 2010). These tight protein-lipid interactions were reported to be important for correct protein function (Huber et al., 2004; Lee, 2004; Bagatolli et al., 2010a). Raft formation and phase separation was recently reported to be induced by hydrophobic matching (Kaiser et al., 2011; McIntosh et al., 2003; Vidal and McIntosh, 2005). Phase separation is the rational of the lipid raft

concept, explaining lateral segregation of lipid and proteins into mutual exclusive domains (Simons and Ikonen, 1997). Indeed, the hydrophobic matching theory was shown to provide the mechanistic basis for lipid raft formation in artificial membranes (Coskun and Simons, 2011; Lingwood and Simons, 2010).

Lipid raft as a domain formed via hydrophobic matching re-classifies rafts as a membrane compartment among others. Within our patchwork model lipid rafts would represent a PM domain which requires sphingolipids and sterols. Slight variations of sphingolipid requirements for certain proteins would predict different raft like domains, which were indeed recently reported within living cells (Tyteca et al., 2010; Sengupta et al., 2011). The hydrophobic matching theory, in combination with protein-lipid interactions explains the domain plurality within the patchwork model of membrane organisation.

Formation of large PM protein domains, as those which have been described within this study can be explained by the "wetting" model, originally introduced to provide the theoretical basis for lipid raft formation (Akimov et al., 2008). Small protein-lipid clusters of the same or similar proteins, will recruit matching lipids, either as annular lipids or by tight protein-lipid interactions. This will result in an enrichment of certain lipids around growing protein clusters. Depending on the coherence length, more proteins and lipids will be recruited (see section 2.1.4), eventually resulting in the formation of large microscopically resolvable PM protein domains. Proteins which differ in their protein environment will therefore segregate into different domains, while similar proteins are expected to show an overlap with others.

Large network like domains like the ones identified within this study, were never observed in mammalian cells. Several reasons can explain these observations. First, systematic studies of a comprehensive set of PM proteins with high spatial and temporal resolution are currently missing. Second, the diffusion of proteins and lipids is much higher in mammalian cells compared to yeast (Greenberg and Axelrod, 1993; Valdez-Taubas and Pelham, 2003) (Fig. 3.7, Tab. 8.2). The coherence length is larger if protein and lipid diffusion is slow and this will lead to the formation of large protein domains. Additionally proteins can induce a phase separation as a result of surrounding lipids, creating an environment of several nanometers around the whole domain (Akimov et al., 2008). This "wetting" environment, which differs in phase from the bulk lipids will prevent proteins from domain exit. Indeed, large protein and lipid domains were observed in artificial membranes (Kaiser et al., 2011;

de la Serna et al., 2009) and were predicted by molecular dynamic calculations (Wallace et al., 2006).

These examples indicated domain formation purely based on protein-lipid interactions. The idea of a multi domain organisation of PM proteins in yeast was already proposed by a study based on FRAP experiments (Abankwa et al., 2008).

Pure protein-lipid driven PM protein domain formation cannot entirely explain protein domain formation. In addition to protein-lipid based interactions, protein-cytoskeleton, or protein-cell wall interactions are likely to contribute to lateral segregation of PM proteins.

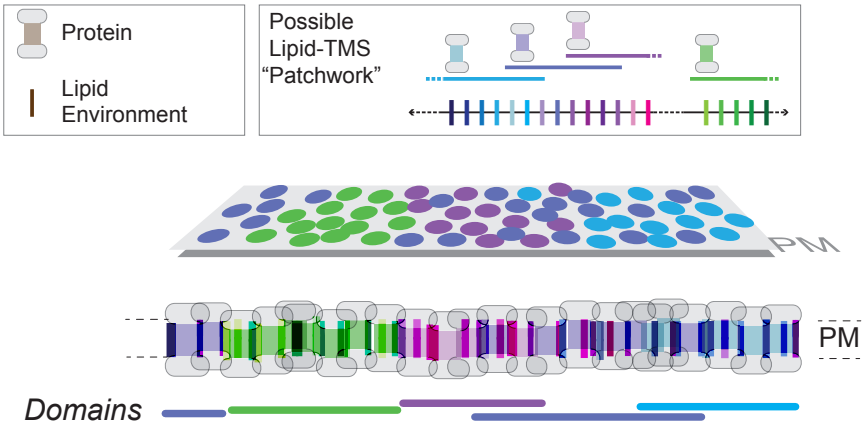

Figure 4.1: Patchwork model of membrane organisation. Biological membranes contain multiple lipid species (rods) and differ in the TMS of proteins (cylinders). Compatibility of components is indicated by similar colours. Every TMS interacts with a range of different lipids, resulting in a range of possible overlaps, as indicated by mixing of rods and cylinders. Entirely different TMS and lipids will segregate into different domains, shown with green lipids and TMS. The large number of domains can be explained by domain overlap.

Until now, we have performed the most comprehensive and detailed analysis of PM organisation and domain formation within living cells. The resulting patchwork model of membrane organisation describes the PM as a highly organised and compartmentalised organelle for the first time. These results introduce a new level of complexity to the research field of membrane organisation, which allows to test for protein function depending on PM domain association.

4.1.3 Factors influencing membrane domains in yeast and functional importance

So far, only three different PM domains were described in yeast and most of the PM proteins were thought to be homogeneously distributed. We in contrast observed a heterogeneous distribution of PM proteins. All tested membrane proteins segregated into patch or network like domains. The pattern was characteristic for each protein and strongly influenced by the lipid composition of the PM (Fig. 3.15, 3.17). Interestingly, PM protein domain formation was influenced by lipids on several levels. The patchy protein Bio5 collapsed into a network after PS depletion and the patchy pattern of Bio5 was re-established after supplementation of Lyso-PS. In strains depleted of PS, Pmp1 required several hours to re-establish WT pattern after Lyso-PS addition. This result can be explained with secretion defects of Pmp1 in the $\Delta cho1$ background strain. It is known that proteins require certain lipids during synthesis. Pma1 requires sphingolipids, in contrast Can1 needs PE and ergosterol for correct insertion into the PM (Opekarova et al., 2005).

The observation of impaired Can1 function after transfer to MCP can be explained by a specific lipid environment which is required for correct protein function (Fig. 3.20). In liposomes Can1 was shown to require ergosterol and PE to mediate arginine uptake (Opekarova and Tanner, 1994). This ergosterol PE dependence implicates a role of eisosomes in creating a special lipid environment which promotes PM protein function. Many amino acid permeases co-segregate to eisosomes (Fur4, Tat2, Lyp1, Mup1, Can1, Hup1), which implies a role for eisosomes in maintaining an environment for amino acid transporter to function. A connection between domain association and protein function was already shown for several "raft" associated proteins, including amino acid permeases (Lauwers and Andre, 2006; Stradalova et al., 2009). The validity of this concept was further demonstrated by our work on Can1 function.

4.1.4 Spatially separated two step mechanism of endocytosis

The dynamic behaviour of the PM cannot solely be understood in terms of lateral segregation of proteins. Additionally the delivery and removal of membrane proteins has to be taken into account. After the formulation of the patchwork model of membrane organisation, we focussed on the connection of PM domains and endocytosis. Currently the

only PM domain which was analysed within the context of endocytosis is the MCC. Two contradicting theories were reported for this compartment, on one hand to be the site of endocytosis (Walther et al., 2006) and on the other hand to be devoid of endocytosis (Grossmann et al., 2008; Brach et al., 2011).

We observed a low overlap between PM proteins and actin patches by performing co-localisation studies, indicating a low level of endocytosis for PM proteins in general (see section 3.3.1).

We studied endocytic cargo recruitment using Mup1 as marker for MCC. Mup1 is only present at the PM if methionine is lacking in the medium and is quickly removed after addition of this amino acid (Lin et al., 2008). On basis of our findings, we propose two spatially separated events as a prerequisite for endocytosis of Mup1. First, upon methionine addition Mup1 becomes triggered for endocytosis and exits the MCC (Fig. 4.2 A,B). The signal for domain exit is likely to be a phosphorylation as was shown for several PM proteins (Nikko et al., 2008; Toshima et al., 2009). In a second spatially separated step, the protein becomes ubiquitylated, accumulates at endocytic sites and is subsequently removed from the cell surface (Fig. 4.2 C,D). Ubiquitylation was a prerequisite for the cargo to be captured within the endocytic site, because knockout of Art1 prevented Mup1 from accumulation at the endocytic site (Fig. 3.23). Furthermore Art1 co-localised with the endocytic patch marker protein Abp1 and not with the MCC. Further evidence that cargo has to move to the site of endocytosis comes from the experiment in which Mup1 was not internalized after artificially anchored to MCC. Lastly, we showed that the C-terminus of Mup1 was important for MCC exit. Truncated Mup1 was not removed from the PM, thus indicating that cargo cannot recruit the endocytic machinery and has to move to the site of endocytosis. We therefore propose that the cargo has physically move to the site of endocytosis.

This two step model of endocytosis allows the fine grained regulation of cell surface proteins and gathering proteins from different domains into the same endocytic patch. Although the diffusion of cell surface proteins is very slow (Greenberg and Axelrod, 1993), mobility is sufficient to allow proteins to move to sites of endocytosis. Validity of this model for a broad range of different PM transporters needs yet to be tested.

On basis of our results, with a low level of endocytosis for every protein unless actively marked for endocytosis, we extend the MCC protection model as a general mechanism regulating protein turnover.

4.1.5 Landmark proteins for endocytosis

As described in section 4.1.4 the cargo Mup1 was not able to recruit the endocytic machinery and so far, landmark proteins or cues for endocytic site initiation are still under debate (Weinberg and Drubin, 2012). Early proteins are known to bind to PIP2 but whether PIP2 or early arriving proteins define the endocytic site remains still elusive (Weinberg and Drubin, 2012).

We identified proteins with the capacity of ectopic endocytic site initiation, by ectopically anchoring a number of early endocytic marker proteins to the MCC/eisosomal domain.

The protein with the greatest capacity for ectopic endocytic site initiation was the early endocytic landmark protein Ede1 (Gagny et al., 2000). Ectopic localisation of Ede1 to eisosomes was sufficient to re-localise 60% of actin patches to eisosomes. Interestingly, the second early arriving protein Syp1 did not initiate an ectopic endocytic event. This finding is consistent with slight differences in function of Syp1 and Ede1. During asexual reproduction, yeast cells are polarised to the place of bud formation. Ede1 was shown to be important for vesicle formation within the mother cell, while Syp1 is required for polarised endocytosis (Stimpson et al., 2009).

Sla2, which arrives at the step of coat formation was also capable to initiate an ectopic endocytic site. Although Sla2 is not an early adaptor protein, re-localisation to eisosomes was sufficient to mediate endocytic coat formation and internalisation.

Unfortunately, it cannot be ruled out that anchoring of endocytic adaptor proteins to the eisosomal compartment will destroy protein folding and therefore function. A negative result cannot be interpreted as a lack of endocytic site initiation. This is illustrated by clathrin light chain, which when anchored to the eisosomal compartment mimics the clathrin knockout phenotype (see section 3.28 B), with large actin comet tails. This result clearly shows the limitations of this method.

In summary, we developed a method to screen for proteins involved in endocytic site initiation and were able to identify major regulators for endocytosis. Application of this method allows us to re-direct endocytosis to desired places.

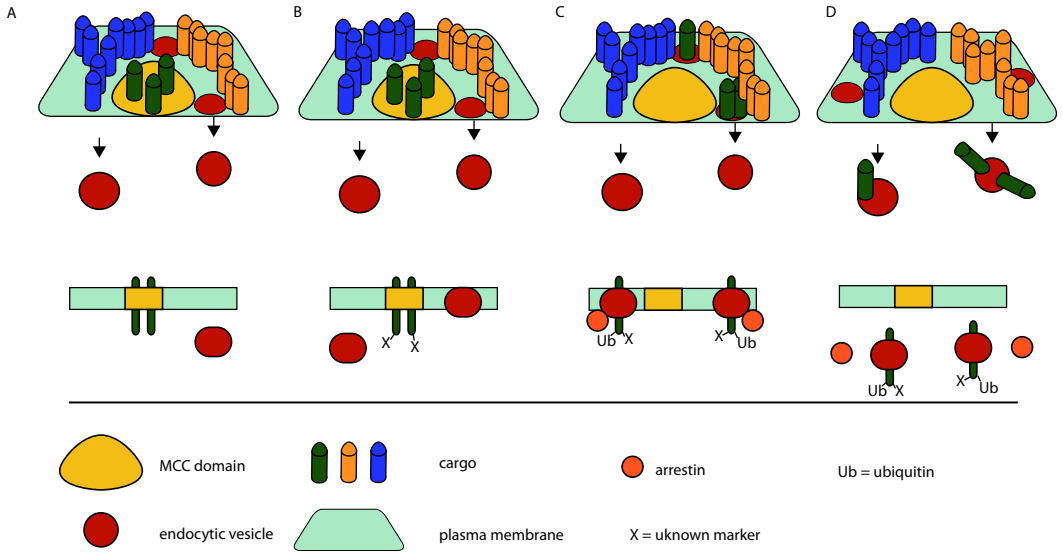

Figure 4.2: Spatial organisation of endocytosis. A) Under steady-state conditions PM proteins are not subject of endocytosis. B) After stimulus the protein becomes postranslationally modified and exits the domain. C) At the endocytic site, the protein becomes ubiquitylated and stabilised. D) The protein is removed from the cell cortex

Chapter 5

Outlook

We carried out the so far largest and most comprehensive screen on plasma membrane protein organisation. The patchwork model of membrane organisation incorporates existing models, like hydrophobic matching and scaffolding into a unified model. We identified factors influencing the membrane organisation (lipids, TMS) and developed a tool to monitor subtle changes of PM protein appearance (network factor). Furthermore we dissected the relationship between PM domains and endocytosis. This study opens a new field of membrane research, as the developed tools can be used to screen for drugs altering membrane organisation. Many physiological defects arise from wrongly segregated proteins. For example the function of a transporter depends on the correct domain association and hence a suitable lipid environment. It will be of general interest to apply these findings acquired in yeast to higher organsims. The understanding of the relationship of human diseases and membrane organisation defects can be benefitial for the development of novel therapeutics. Low efficiency of iron uptake, for example, is a known problem for many females and for large parts of humans in the third world. A better understanding of domains, lipids and transporter function, resulting in a more efficient iron uptake may be of great benefit for the society. The experiments conducted in this study shows that iron uptake depends on correct domain association. Further studies need to identify the molecular details which drive protein segregation, to obtain a better understanding of PM protein organisation.

Chapter 6

Material

All standards, enzymes and other reagents used in this study are listed below (Tab.6.1, 6.3, 6.4, 6.6). Chemicals were obtained at highest purity when not stated otherwise. All materials were stored according to the manufacturer. Oligonucleotides were synthesised by metabion International AG.

6.0.6 Consumables

Table 6.1: Chemicals

Manufacturer	Name
Becton, Dickinson and Company	Difco Bacto Agar
	Difco Bacto Pepton
	Difco Trypton
	Difco Yeast Extract
	Yeast Nitrogen Base w/o amino-acetate
Carl Roth GmbH	Ampicillin
	Bromphenol Blue
	Ethidium bromide solution (1%)
	EDTA
	Glycerol
	HCl
	Triton X-100

Manufacturer	Name
Invitrogen	DNA-agarose
Merck KGaA	D(+)-Glucose
	Isopropanol
	Boric Acid
	$MnCl_2$ x $2H_2O$
	RbCl
New England BioLabs GmbH	dNTP mix
PAA Laboratories GmbH	Geneticin
Sigma-Aldrich Chemie GmbH	Ethanol
	NaOH
	Tris Base
Werner BioAgents	CloNAT
Alfa	AesarBPS
Sigma	Myriocin
Sigma	LatB
Sigma	100T-zymolyase
Avanti	Lyso-PS

Table 6.2: Antibodies and fluorophores

Manufacturer	Name
Sigma	Atto647N anti mouse (50185)
Roche	GFP antibody mouse (11814460001)
NEB	ACP surface starter kit

Table 6.3: Biochemicals

Manufacturer	Name
Chromotek	GFP-Trap_A
	RFP-Trap_A
Eppendorf AG	Sheared Salmon Sperm DNA

Manufacturer	Name
Finnzymes	Phusion high-fidelity DNA-polymerase
New England Biolabs GmbH	T4 DNA ligase
	Taq DNA polymerase
	Restriction enzymes

Table 6.4: Standards

Manufacturer	Name
Fermentas GmBH	GeneRuler^{TM}DNA Ladder Mix
Fermentas GmBH	PageRuler^{TM}Prestained Protein Ladder

6.0.7 Tool for microscopy

Table 6.5: Tools for microscopy

Tools for microscopy	Name
MatTek	Glass Bottom Culture Dishes
Ibidi	Sticky-Slide 8 well (80828)
Vitlab	Glass container
Thomas Scientific	Ceramic staining rack
Menzel Glaser	Coverslips 1 (18 x 18 mm)
Menzel Glaser	Microscope Slides
Zeiss	Immersion Oil
Invitrogen	FluoSpheres

6.0.8 Oligonucleotides

Table 6.6: Oligonucleotides

Name		Sequence
RWS672	5' Erg6 test	ctatcctctgctgctctc
RWS673	3' Erg6 test	gtaaaggcatcggacagtc
RWS674	5' Erg6 test	cgatttagttctcgacgttg
RWS675	3' Erg6 test	gcgatctttctatgttcagg
RWS1658	5' Erg3 test	cataatgatatgcgtatc
RWS1659	3' Erg3 test	ccgtagaccagatgactc
RWS1189	3' Rsp5 Prom SacI	tccggatttttttctttttttctttcctttctgttac
RWS1190	5' Rsp5 Prom BspEI	gagctcgggaggggcttctatctcgac
RWS1173	5'Art1 test	ggcggaagcttcaagac
RWS1174	5'Art2 test	ctcatcgagctgtagtg
RWS1684	Erg6 S1	cataatttaaaaaaacaagaataaaataataatatagtaggcagcataagcgtacgctgcaggtcgac
RWS1685	Erg6 S2	ggtatatatcgtgcgctttatttgaatcttattgatctagtgaatttaatcgatgaattcgagctcg
RWS1328	Fet3 3'TM	gatcccatcataccataaattgcaattgtgataataccaagaataccggcaaagcaggagaatgtcatggcaataataccagtcatctgca
RWS1327	Fet3 5'TM	gatgactggtattattgccatgacattctctgctttgccggtattcttggtattatcacaattgcaatttatggtatgatgg
RWS1399	Fet3 flanking 3'	ggatccgaagaaccgtttggctttag
RWS1400	Fet3 flanking 5'	ctgcagatgactaacgctttgctctctatagc
RWS1398	Fet3 Mid2 TM 3'	cggtcgcatcttccatatacaattaaagccagtatcaccag
RWS1397	Fet3 Mid2 TM 5'	accggttttaccaaaaaaatcgtcattggttgtgtggttgg
RWS1396	Fet3 Pmp1 TM wo poly 3'	cggtcgcatcttccatatcgaatctttgcaatcctctttgtctag
RWS1394	Fet3 Pmp1TM 5'	accggttttaccaaaaaattaccaggtggtgttattttag
RWS1395	Fet3 Pmp1TM poly 3'	cggtcgcatcttccatatcgataatggtagcaataatggc
RWS1417	Fet3 Seq 1051	ggtgtgaattacgccttc
RWS1418	Fet3 Seq 1516	ccaagatgctcattctc
RWS1416	Fet3 Seq 550	gctgagcccatcccacag
RWS1328	Fet3 TM 3'	gatcccatcataccataaattgcaattgtgataataccaagaataccggcaaagcaggagaatgtcatggcaataataccagtcatctgca
RWS1327	Fet3 TM 5'	gatgactggtattattgccatgacattctctgctttgccggtattcttggtattatcacaattgcaatttatggtatgatgg
RWS1501	Fet3 TM recombination 3'	cagggtccacgtgcaagtctcgaataacctttcggtcgcatcttccatatc
RWS1502	Fet3 TM recombination 5'	gatttaactggtgaaaatgttcagcatgccttcattcctaccggttttaccaaaaaa
RWS1549	Fet3 utr 3'	gcattattgaatttgaaacgtgg
RWS1550	Fet3 utr 5'	ccttcgagggagtatgcc
RWS1303	Hxt6 test	cttctattggcaacatc
RWS1298	Mid2 TM 3'	gatccaattaaagccagtatcaccagaatcagtggtacaccaataccaaccacacaaccaatgacgatagtcatctgca
RWS1297	Mid2 TM 5'	gatgactatcgtcattggttgtgtggttggtattggtgtaccactgattctggtgatactggctttaattg
RWS1651	Mup1 cterm BHI 3'	ggatcccagcgatttttcttgttcac
RWS1651	Mup1 cterm BHI 3'	ggatcccagcgatttttcttgttcac
RWS1650	Mup1 cterm SalI 5'	gtcgacgcccaattattgccaagatgg
RWS1650	Mup1 cterm SalI 5'	gtcgacgcccaattattgccaagatgg
RWS1178	pADH 3'	gatcctcgaggcggccagcttggagttg
RWS1535	pFet3 3'	ctgcagctagttctaatttttttgctactc

Name		Sequence
RWS1534	pFet3 5’	ctcgaggctgccttctttgcgataatg
RWS1175	pGal 3’	gatcctgcagatccggggttttttctcc
RWS1176	pGPD 3’	gatcctgcagatccgtcgaaactaagttc
RWS782	Pma1 3’	ggatccttaggtttccttttcgtgttg
RWS781	Pma1 5’	ctgcagatgactgatacatcatcctcttc
RWS1300	PmpI TM 3’	gatccgataatggtagcaataatggcaatacaagccaaaccgaccaaaatgaaaactaaaataacaccacctggtaaagtcatctgca
RWS1299	PmpI TM 5’	gatgactttaccaggtggtgttatttttagttttcattttggtcggtttggcttgtattgccattattgctaccattatcg
RWS783	pPma1 5’	ctcgagcaattatgaccggtgacgaaac
RWS784	pPma1 5’	ctgcagattgatattgtttgataattaaatc
RWS548	Ras2 3’Primer KpnI	ggtaccttaacttataatacaacagccac
RWS550	Ras2 3’Prom BHI	ggatccttttttttctgtatatctcctttc
RWS549	Ras2 5’Primer XhoI	ctcgagatgcctttgaacaagtcgaac
RWS551	Ras2 5’Prom XbaI	tctagaggaaacaaggttcacatcag
RWS1581	Ssy1 test 3’	gcgtaaagcagtgtcaatatttag
RWS1582	Ssy1 test 5’	cagcatatggtggcctg
RWS429	Abp1 S2	gtatttttttacgtaagaataatataatagcatgacgctgacgtgtgattCTAatcgatgaattcgagctcg
RWS428	Abp1 S3	gacggctcaaaaggtctcttccccagcaattatgtgtctttgggcaaccgtacgctgcaggtcgac
RWS1059	Art1 S2	ctaagataaaaatatatggtaaatacctttaacgaatattataaaatTTAatcgatgaattcgagctcg
RWS1060	Art1 S3	gaatacaaaactttttccgattttctagattccaatagaataacccagcgtacgctgcaggtcgac
RWS1257	Bio5 S2	gtatcgacctaggaatttataaggactgtttttctttcaacagcatcttaatcgatgaattcgagctcg
RWS1256	Bio5 S3	gtatgcagtagttttctgcattatcagcatcgttgttttccctacatgcatccgtacgctgcaggtcgac
RWS613	Can1 S3	ggaagatcatgaaccaaagacttttttgggacaaattttggaatgttgtagcacgtacgctgcaggtcgac
RWS612	Can1S2	gaatgcgaaatggcgtggaaatgtgatcaaaggtaataaaacgtcatatctaatcgatgaattcgagctcg
RWS1185	Clc1 S2	ccttctcttccttagttcattatggttcttattattcatcatcatttaatcgatgaattcgagctcg
RWS1186	Clc1 S3	gcttaaagaaattcttttgagattgaaaggtaacgcgaaggctcccggtgctcgtacgctgcaggtcgac
RWS1613	Ede1 S2	cgaggaagaagtacaaaaagaagacgaaatggtccattacagactaatcgatgaattcgagctcg
RWS1612	Ede1 S3	gcaactgggatctagaagccgccactaacttttttgttggatagtgctcgtacgctgcaggtcgacc
RWS920	Fet3 S2	ccgaaaaaaaaaaaaacaggttaaccgcaaaatacatgatcttcctttattaatcgatgaattcgagctcg
RWS919	Fet3 S3	cattccactgaaaagcatcaatttttaactaaagccaaacggttcttccgtacgctgcaggtcgac
RWS1551	Ftr1 S2	caacagaaaataggtggaaaactcccaccctgtgctagacttcattcaatcgatgaattcgagctcg
RWS1552	Ftr1 S2	cgtcgccacagacaaggaagtcctccacgttaaagccgactctcttcgtacgctgcaggtcgac
RWS1061	Hxt1 S2	gaaattaaatactgtataagtcattaaaatatgcatattgagcttgtttagtttaatcgatgaattcgagctcg
RWS1062	Hxt1 S3	cctaatgcatgatgaccaaccattttacaagagtttgtttagcaggaaacgtacgctgcaggtcgac
RWS1063	Hxt3 S2	gaatcttaaaatacactattattcagcactacggtttagcgtgaaattaatcgatgaattcgagctcg
RWS1064	Hxt3 S3	gatgcatgatgaccagccattctacaagaaaatgttcggcaagaaacgtacgctgcaggtcgac
RWS1302	Hxt6 S2	gcatttcaaatgcacaaattagagcgtgatcatgaattaataaaaatgttcgcaaattaatcgatgaattcgagctcg
RWS1301	Hxt6 S3	cgctgaagaaatggctcacgatgataagccattgtacaagagaatgttcagcaccaaacgtacgctgcaggtcgac
RWS1255	Mep2 S2	gttacataaagattaaacataaaatcatagtctgcttgagtatatcattaatcgatgaattcgagctcg
RWS1254	Mep2 S3	ctacgccttccgacgcttcttctactaagaacactgaccatatagtacgtacgctgcaggtcgac
RWS1258	Pdr10 S2	gttaactaattttgcatatacaatgaatgtagccagtaatatttaattatcgatgaattcgagctcg
RWS1259	Pdr10 S3	caatatttttatactggctggtgcgggttccaaagaaaagcaaaaaattaaagaaacgtacgctgcaggtcgac
RWS1611	Pil1 S2	ctgctggtttttttttttttgtttctaatagattgttgatttattttgattaatcgatgaattcgagctcg
RWS1610	Pil1 S3	caagtcggacaccagcaaagtgagtctcttccccaacaaacaacagctcgtacgctgcaggtcgac
RWS701	Pma1 S2	caagttgattaaaatgtgacaaaattatgattaaatgctacttcaacaggattaatcgatgaattcgagctcg

Name		Sequence
RWS700	Pma1 S3	cgaagacttcatggctgctatgcaaagagtctctactcaacacgaaaaggaaacccgtacgctgcaggtcgac
RWS1554	Pmp1 S2	caaagatgaaggggacaggaaataaaatggctcgctccgccctttttaatcgatgaattcgagctcg
RWS1553	Pmp1 S3	ccattatctacagaaaatggcaagctagacaaagaggattgcaaagattccgtacgctgcaggtcgac
RWS1187	Rsp5 S1	gcttgggtattatatttaaagtaacagaaaggaaagaaaaaagaaaaaaaATGcgtacgctgcaggtcgac
RWS1188	Rsp5 S4	cctcttatataatgactctgcagccactaacttgacggatatggatgaaggcatcgatgaattctctgtcg
RWS1652	S2 Can1 trunc	ggaatcgatgtcgacatctccaatcttccaaataaatctgcatctttaatcgatgaattcgagctcg
RWS1654	S2 Lyp1	cgtctatttttttatttttttctattttgaaggcatgcaagaggttctgtgactaatcgatgaattcgagctcg
RWS1653	S2 Lyp1 trunc	gatgtcaatatcttctagcttccaaataaatctgcatttgtagtatatttaatcgatgaattcgagctcg
RWS1655	S3 Lyp1	cgacgagcctaagaatttatgggagaaattctgggctgctgttgcacgtacgctgcaggtcgac
RWS1253	Ssy1 S2	taataataataataatactaacaataataatactaataatagtacatataaccctatcgatgaattcgagctcg
RWS1252	Ssy1 S3	gggaacaatatagggaaagagcgaagaagttggttacctggctgattcgtacgctgcaggtcgac
RWS703	Sur7 S2	gagagaagaaaggggtataaatatatattacaaagcggaaaacttgcgccatttaatcgatgaattcgagctcg
RWS702	Sur7 S3	cttcttcactataagaaaatcacacgagcgcccggacgatgtctctgttcgtacgctgcaggtcgac
RWS1496	Mup1 S2	gaatgttcatacgtgattataagaatcgagatgagatggtaagtacctttttggttaatcgatgaattcgagctcg
RWS1497	Mup1 S3	cgttattgaaacgaatataatcgaacattacaaaagtgaacaagaaaaatcgctgcgtacgctgcaggtcgac
RWS1498	Mup1 S3 trun	cttctttggtggtgtttactacgttgtttgggcccaattattgccaagatggggccgtacgctgcaggtcgac
RWS1621	Mup1 S3-1629	cttggtgaagatgggttctggagagtcaaaattgccaaagtttatcgtacgctgcaggtcgac
RWS1622	Mup1 S3-1695	gatacacaagaagacggcgttattgaaacgaatataatcgaacatcgtacgctgcaggtcgac

6.0.9 Devices and commercial kits

Devices

Table 6.7: Devices

Manufacturer	Name
Beko	Freezer
Heraeus Sepatech	Pico 17
	Fresco 17
	Biofuge primoR
Liebherr	Refridgerator
Syngene	GebeFlash
Thermo Electron Corporation	PXE0.2 Thermocycler
	Gensys 10uv
VWR International GmbH	VV3 Vortex

Commercial kits

The following Kits were used in this study (Tab.6.8).

Table 6.8: Commercial Kits

Manufacturer	Name
Promega	Wizard®SV Gel and PCR Clean-Up System
Omega bio-tek	E.Z.N.A.®Plasmid Mini Kit I

6.0.10 Strains

The listed bacterial strain was used for plasmid selection and amplification (Tab.6.9).

Table 6.9: Bacterial strains

Name	Genotype
E.coli DH5α	fhuA2 Δ(argF-lacZ)U169 phoA glnV44 Φ80 Δ(lacZ)M15 gyrA96 recA1 relA1 endA1 thi-1 hsdR17

Table 6.10: Yeast strains

Name Number Strain	Strain Number Genotype	Genotype
FSS001	BY4741	HXT1-GFP::KANR his3 leu2 lys2 met15 ura3
FSS002	BY4741	HXT1-RFP::NATR Hxt2-GFP::HIS3 leu2 lys2 met15 ura3
FSS003	BY4741	HXT1-RFP::NATR Hxt3-GFP::HIS3 leu2 lys2 met15 ura3
FSS004	BY4741	HXT1-RFP::NATR Hxt6-GFP::HIS3 leu2 lys2 met15 ura3
FSS005	BY4741	HXT1-GFP::KANR Hxt2-RFP::NATR leu2 lys2 met15 ura3
FSS006	BY4741	HXT2-RFP::NATR Hxt3-GFP::HIS3 leu2 lys2 met15 ura3
FSS007	BY4741	HXT2-RFP::NATR Hxt6-GFP::HIS3 leu2 lys2 met15 ura3
FSS008	BY4741	HXT1-GFP::KANR Hxt3-RFP::NATR leu2 lys2 met15 ura3
FSS009	BY4741	HXT3-RFP::NATR Hxt2-GFP::HIS3 leu2 lys2 met15 ura3
FSS010	BY4741	HXT3-RFP::NATR Hxt6-GFP::HIS3 leu2 lys2 met15 ura3
FSS011	BY4741	HXT1-GFP::KANR Hxt6-RFP::NATR leu2 lys2 met15 ura3
FSS012	BY4741	HXT6-RFP::NATR Hxt2-GFP::HIS3 leu2 lys2 met15 ura3
FSS013	BY4741	HXT6-RFP::NATR Hxt3-GFP::HIS3 leu2 lys2 met15 ura3
FSS014	BY4741	GAS1GFP::URA3 his3 leu2 lys2 met15
FSS015	BY4741	RAS2GFP::URA3 his3 leu2 lys2 met15
FSS016	BY4741	pFet3-Fet3GFP CEN URA his3 leu2 lys2 met15 ura3
FSS017	BY4741	pFet3-Fet3RFP CEN LEU his3 leu2 lys2 met15 ura3
FSS018	BY4741	pPma1-PMA1-RFP CEN LEU his3 leu2 lys2 met15 ura3
FSS019	BY4741	pGPD-PMA1-GFP CEN URA his3 leu2 lys2 met15 ura3
FSS020	BY4741	pSUR7-SUR7-RFP CEN LEU his3 leu2 lys2 met15 ura3
FSS021	BY4741	SUR7-GFP::HIS3 leu2 lys2 met15 ura3
FSS022	BY4741	pSUR7-SUR7-GB CEN LEU his3 leu2 lys2 met15 ura3
FSS023	BY4741	Pma1-GB::NATR his3 leu2 lys2 met15 ura3
FSS024	BY4741	Can1-GFP::HIS3 pSUR7-SUR7-GB CEN LEU leu2 lys2 met15 ura3
FSS025	BY4741	Can1-GFP::HIS3 Pma1-GB::NATR leu2 lys2 met15 ura3
FSS026	BY4741	*fet3*::KANR pFet3-Fet3GFP CEN URA his3 leu2 lys2 met15 ura3
FSS027	BY4741	*fet3*::KANR pFet3-Fet3GFP CEN URA pFet3-Fet3RFP CEN LEU his3 leu2 lys2 met15 ura3
FSS028	BY4741	*fet3*::KANR pFet3-Fet3-GFP CEN URA pFet3-Fet3Chimera-RFP CEN LEU his3 leu2 lys2 met15 ura3
FSS029	BY4741	*fet3*::KANR Pmp1-GFP::his3 leu2 lys2 met15 ura3
FSS030	BY4741	*fet3*::KANR Pmp1-GFP::his3 pFet3-Fet3RFP CEN LEU leu2 lys2 met15 ura3
FSS031	BY4741	*fet3*::KANR Pmp1-GFP::his3 pFet3-Fet3Chimera-RFP CEN LEU
FSS032	BY4741	Pmp1-GFP::his3 pPma1-Pmp1TM-RFP CEN LEU leu2 lys2 met15 ura3
FSS033	BY4741	Pmp1-GFP::his3 pPma1-Mid2TM-RFP CEN LEU leu2 lys2 met15 ura3
FSS034	BY4741	Pmp1-GFP::his3 pPma1-Fet3TM-RFP CEN LEU leu2 lys2 met15 ura3
FSS035	BY4741	ATR1-GFP::HIS3 pSUR7-SUR7-RFP CEN LEU leu2 lys2 met15 ura3
FSS036	BY4741	BAP2-GFP::HIS3 pSUR7-SUR7-RFP CEN LEU leu2 lys2 met15 ura3
FSS037	BY4741	BIO5-GFP::HIS3 pSUR7-SUR7-RFP CEN LEU leu2 lys2 met15 ura3

Name	Strain	Genotype
FSS038	BY4741	BIT61-GFP::HIS3 pSUR7-SUR7-RFP CEN LEU leu2 lys2 met15 ura3
FSS039	BY4741	DNF1-GFP::HIS3 pSUR7-SUR7-RFP CEN LEU leu2 lys2 met15 ura3
FSS040	BY4741	ENA1-GFP::HIS3 pSUR7-SUR7-RFP CEN LEU leu2 lys2 met15 ura3
FSS041	BY4741	ENA2-GFP::HIS3 pSUR7-SUR7-RFP CEN LEU leu2 lys2 met15 ura3
FSS042	BY4741	FAA3-GFP::HIS3 pSUR7-SUR7-RFP CEN LEU leu2 lys2 met15 ura3
FSS043	BY4741	FET3-GFP::HIS3 pSUR7-SUR7-RFP CEN LEU leu2 lys2 met15 ura3
FSS044	BY4741	FET4-GFP::HIS3 pSUR7-SUR7-RFP CEN LEU leu2 lys2 met15 ura3
FSS045	BY4741	FLC1-GFP::HIS3 pSUR7-SUR7-RFP CEN LEU leu2 lys2 met15 ura3
FSS046	BY4741	FPS1-GFP::HIS3 pSUR7-SUR7-RFP CEN LEU leu2 lys2 met15 ura3
FSS047	BY4741	FTR1-GFP::HIS3 pSUR7-SUR7-RFP CEN LEU leu2 lys2 met15 ura3
FSS048	BY4741	FUI1-GFP::HIS3 pSUR7-SUR7-RFP CEN LEU leu2 lys2 met15 ura3
FSS049	BY4741	GAP1-GFP::HIS3 pSUR7-SUR7-RFP CEN LEU leu2 lys2 met15 ura3
FSS050	BY4741	GAS1-GFP:URA pSUR7-SUR7-RFP CEN LEU leu2 lys2 met15 ura3
FSS051	BY4741	GPA1-GFP::HIS3 pSUR7-SUR7-RFP CEN LEU leu2 lys2 met15 ura3
FSS052	BY4741	HNM1-GFP::HIS3 pSUR7-SUR7-RFP CEN LEU leu2 lys2 met15 ura3
FSS053	BY4741	HXT2-GFP::HIS3 pSUR7-SUR7-RFP CEN LEU leu2 lys2 met15 ura3
FSS054	BY4741	HXT3-GFP::HIS3 pSUR7-SUR7-RFP CEN LEU leu2 lys2 met15 ura3
FSS055	BY4741	ITR2-GFP::HIS3 pSUR7-SUR7-RFP CEN LEU leu2 lys2 met15 ura3
FSS056	BY4741	MEP2-GFP::HIS3 pSUR7-SUR7-RFP CEN LEU leu2 lys2 met15 ura3
FSS057	BY4741	MID2-GFP::HIS3 pSUR7-SUR7-RFP CEN LEU leu2 lys2 met15 ura3
FSS058	BY4741	MNR2-GFP::HIS3 pSUR7-SUR7-RFP CEN LEU leu2 lys2 met15 ura3
FSS059	BY4741	MRH1-GFP::HIS3 pSUR7-SUR7-RFP CEN LEU leu2 lys2 met15 ura3
FSS060	BY4741	MSS4-GFP::HIS3 pSUR7-SUR7-RFP CEN LEU leu2 lys2 met15 ura3
FSS061	BY4741	NHA1-GFP::HIS3 pSUR7-SUR7-RFP CEN LEU leu2 lys2 met15 ura3
FSS062	BY4741	PDR12-GFP::HIS3 pSUR7-SUR7-RFP CEN LEU leu2 lys2 met15 ura3
FSS063	BY4741	PDR5-GFP::HIS3 pSUR7-SUR7-RFP CEN LEU leu2 lys2 met15 ura3
FSS064	BY4741	PIL1-GFP::HIS3 pSUR7-SUR7-RFP CEN LEU leu2 lys2 met15 ura3
FSS065	BY4741	PMA1-GFP::HIS3 pSUR7-SUR7-RFP CEN LEU leu2 lys2 met15 ura3
FSS066	BY4741	PMP1-GFP::HIS3 pSUR7-SUR7-RFP CEN LEU leu2 lys2 met15 ura3
FSS067	BY4741	PSR1-GFP::HIS3 pSUR7-SUR7-RFP CEN LEU leu2 lys2 met15 ura3
FSS068	BY4741	RAS2-GFP::HIS3 pSUR7-SUR7-RFP CEN LEU leu2 lys2 met15 ura3
FSS069	BY4741	RAX2-GFP::HIS3 pSUR7-SUR7-RFP CEN LEU leu2 lys2 met15 ura3
FSS070	BY4741	RSN1-GFP::HIS3 pSUR7-SUR7-RFP CEN LEU leu2 lys2 met15 ura3
FSS071	BY4741	SHO1-GFP::HIS3 pSUR7-SUR7-RFP CEN LEU leu2 lys2 met15 ura3
FSS072	BY4741	SLN1-GFP::HIS3 pSUR7-SUR7-RFP CEN LEU leu2 lys2 met15 ura3
FSS073	BY4741	SSY1-GFP::HIS3 pSUR7-SUR7-RFP CEN LEU leu2 lys2 met15 ura3
FSS074	BY4741	SUR7-GFP::HIS3 pSUR7-SUR7-RFP CEN LEU leu2 lys2 met15 ura3
FSS075	BY4741	TCB3-GFP::HIS3 pSUR7-SUR7-RFP CEN LEU leu2 lys2 met15 ura3
FSS076	BY4741	THI7-GFP::HIS3 pSUR7-SUR7-RFP CEN LEU leu2 lys2 met15 ura3
FSS077	BY4741	TPO1-GFP::HIS3 pSUR7-SUR7-RFP CEN LEU leu2 lys2 met15 ura3
FSS078	BY4741	VHT1-GFP::HIS3 pSUR7-SUR7-RFP CEN LEU leu2 lys2 met15 ura3
FSS079	BY4741	YLR413W-GFP::HIS3 pSUR7-SUR7-RFP CEN LEU leu2 lys2 met15 ura3
FSS080	BY4741	YOR1-GFP::HIS3 pSUR7-SUR7-RFP CEN LEU leu2 lys2 met15 ura3
FSS081	BY4741	ATR1-GFP::HIS3 PMA1-RFP CEN LEU leu2 lys2 met15 ura3

Name	Strain	Genotype
FSS082	BY4741	BAP2-GFP::HIS3 PMA1-RFP CEN LEU leu2 lys2 met15 ura3
FSS083	BY4741	BIO5-GFP::HIS3 PMA1-RFP CEN LEU leu2 lys2 met15 ura3
FSS084	BY4741	BIT61-GFP::HIS3 PMA1-RFP CEN LEU leu2 lys2 met15 ura3
FSS085	BY4741	DNF1-GFP::HIS3 PMA1-RFP CEN LEU leu2 lys2 met15 ura3
FSS086	BY4741	ENA1-GFP::HIS3 PMA1-RFP CEN LEU leu2 lys2 met15 ura3
FSS087	BY4741	ENA2-GFP::HIS3 PMA1-RFP CEN LEU leu2 lys2 met15 ura3
FSS088	BY4741	FAA3-GFP::HIS3 PMA1-RFP CEN LEU leu2 lys2 met15 ura3
FSS089	BY4741	FET3-GFP::HIS3 PMA1-RFP CEN LEU leu2 lys2 met15 ura3
FSS090	BY4741	FET4-GFP::HIS3 PMA1-RFP CEN LEU leu2 lys2 met15 ura3
FSS091	BY4741	FLC1-GFP::HIS3 PMA1-RFP CEN LEU leu2 lys2 met15 ura3
FSS092	BY4741	FPS1-GFP::HIS3 PMA1-RFP CEN LEU leu2 lys2 met15 ura3
FSS093	BY4741	FTR1-GFP::HIS3 PMA1-RFP CEN LEU leu2 lys2 met15 ura3
FSS094	BY4741	FUI1-GFP::HIS3 PMA1-RFP CEN LEU leu2 lys2 met15 ura3
FSS095	BY4741	GAP1-GFP::HIS3 PMA1-RFP CEN LEU leu2 lys2 met15 ura3
FSS096	BY4741	GAS1-GFP:URA PMA1-RFP CEN LEU leu2 lys2 met15 ura3
FSS097	BY4741	GPA1-GFP::HIS3 PMA1-RFP CEN LEU leu2 lys2 met15 ura3
FSS098	BY4741	HNM1-GFP::HIS3 PMA1-RFP CEN LEU leu2 lys2 met15 ura3
FSS099	BY4741	HXT2-GFP::HIS3 PMA1-RFP CEN LEU leu2 lys2 met15 ura3
FSS100	BY4741	HXT3-GFP::HIS3 PMA1-RFP CEN LEU leu2 lys2 met15 ura3
FSS101	BY4741	ITR2-GFP::HIS3 PMA1-RFP CEN LEU leu2 lys2 met15 ura3
FSS102	BY4741	MEP2-GFP::HIS3 PMA1-RFP CEN LEU leu2 lys2 met15 ura3
FSS103	BY4741	MID2-GFP::HIS3 PMA1-RFP CEN LEU leu2 lys2 met15 ura3
FSS104	BY4741	MNR2-GFP::HIS3 PMA1-RFP CEN LEU leu2 lys2 met15 ura3
FSS105	BY4741	MRH1-GFP::HIS3 PMA1-RFP CEN LEU leu2 lys2 met15 ura3
FSS106	BY4741	MSS4-GFP::HIS3 PMA1-RFP CEN LEU leu2 lys2 met15 ura3
FSS107	BY4741	NHA1-GFP::HIS3 PMA1-RFP CEN LEU leu2 lys2 met15 ura3
FSS108	BY4741	PDR12-GFP::HIS3 PMA1-RFP CEN LEU leu2 lys2 met15 ura3
FSS109	BY4741	PDR5-GFP::HIS3 PMA1-RFP CEN LEU leu2 lys2 met15 ura3
FSS110	BY4741	PIL1-GFP::HIS3 PMA1-RFP CEN LEU leu2 lys2 met15 ura3
FSS111	BY4741	PMA1-GFP::HIS3 PMA1-RFP CEN LEU leu2 lys2 met15 ura3
FSS112	BY4741	PMP1-GFP::HIS3 PMA1-RFP CEN LEU leu2 lys2 met15 ura3
FSS113	BY4741	PSR1-GFP::HIS3 PMA1-RFP CEN LEU leu2 lys2 met15 ura3
FSS114	BY4741	RAS2-GFP::HIS3 PMA1-RFP CEN LEU leu2 lys2 met15 ura3
FSS115	BY4741	RAX2-GFP::HIS3 PMA1-RFP CEN LEU leu2 lys2 met15 ura3
FSS116	BY4741	RSN1-GFP::HIS3 PMA1-RFP CEN LEU leu2 lys2 met15 ura3
FSS117	BY4741	SHO1-GFP::HIS3 PMA1-RFP CEN LEU leu2 lys2 met15 ura3
FSS118	BY4741	SLN1-GFP::HIS3 PMA1-RFP CEN LEU leu2 lys2 met15 ura3
FSS119	BY4741	SSY1-GFP::HIS3 PMA1-RFP CEN LEU leu2 lys2 met15 ura3
FSS120	BY4741	SUR7-GFP::HIS3 PMA1-RFP CEN LEU leu2 lys2 met15 ura3
FSS121	BY4741	TCB3-GFP::HIS3 PMA1-RFP CEN LEU leu2 lys2 met15 ura3
FSS122	BY4741	THI7-GFP::HIS3 PMA1-RFP CEN LEU leu2 lys2 met15 ura3
FSS123	BY4741	TPO1-GFP::HIS3 PMA1-RFP CEN LEU leu2 lys2 met15 ura3
FSS124	BY4741	VHT1-GFP::HIS3 PMA1-RFP CEN LEU leu2 lys2 met15 ura3
FSS125	BY4741	YLR413W-GFP::HIS3 PMA1-RFP CEN LEU leu2 lys2 met15 ura3

Name	Strain	Genotype
FSS126	BY4741	YOR1-GFP::HIS3 PMA1-RFP CEN LEU leu2 lys2 met15 ura3
FSS127	BY4741	BIO5-GFP::HIS3 MEP2-RFP::NATR leu2 lys2 met15 ura3
FSS128	BY4741	MSS4-GFP::HIS3 MEP2-RFP::NATR leu2 lys2 met15 ura3
FSS129	BY4741	Thi7-GFP::HIS3 MEP2-RFP::NATR leu2 lys2 met15 ura3
FSS130	BY4741	Atr1-GFP::HIS3 MEP2-RFP::NATR leu2 lys2 met15 ura3
FSS131	BY4741	Bit61-GFP::HIS3 MEP2-RFP::NATR leu2 lys2 met15 ura3
FSS132	BY4741	MEP2-GFP::HIS3 BIO5-RFP::NATR leu2 lys2 met15 ura3
FSS133	BY4741	MSS4-GFP::HIS3 BIO5-RFP::NATR leu2 lys2 met15 ura3
FSS134	BY4741	THI7-GFP::HIS3 BIO5-RFP::NATR leu2 lys2 met15 ura3
FSS135	BY4741	ATR1-GFP::HIS3 BIO5-RFP::NATR leu2 lys2 met15 ura3
FSS136	BY4741	BIT61-GFP::HIS3 BIO5-RFP::NATR leu2 lys2 met15 ura3
FSS137	BY4741	HNM1-GFP::HIS3 Fet3-RFP::NATR leu2 lys2 met15 ura3
FSS138	BY4741	HXT3-GFP::HIS3 Fet3-RFP::NATR leu2 lys2 met15 ura3
FSS139	BY4741	MId2-GFP::HIS3 Fet3-RFP::NATR leu2 lys2 met15 ura3
FSS140	BY4741	TPO1-GFP::HIS3 Fet3-RFP::NATR leu2 lys2 met15 ura3
FSS141	BY4741	VHT1-GFP::HIS3 Fet3-RFP::NATR leu2 lys2 met15 ura3
FSS142	BY4741	HNM1-GFP::HIS3 Hxt3-RFP::NATR leu2 lys2 met15 ura3
FSS143	BY4741	FET3-GFP::HIS3 Hxt3-RFP::NATR leu2 lys2 met15 ura3
FSS144	BY4741	MId2-GFP::HIS3 Hxt3-RFP::NATR leu2 lys2 met15 ura3
FSS145	BY4741	TPO1-GFP::HIS3 Hxt3-RFP::NATR leu2 lys2 met15 ura3
FSS146	BY4741	VHT1-GFP::HIS3 Hxt3-RFP::NATR leu2 lys2 met15 ura3
FSS147	BY4741	SSY1-GFP::HIS3 leu2 lys2 met15 ura3
FSS148	BY4741	GFP-PHx2::URA leu2 lys2 met15 his3
FSS149	BY4741	LACT-C2-GFP::URA leu2 lys2 met15 his3
FSS150	BY4741	ACP-Sag1::KANR leu2 lys2 met15 his3 ura3
FSS151	BY4741	*cho1*::NATR leu2 lys2 met15 ura3
FSS152	BY4741	*cho1*::NATR Pmp1-GFP::HIS3 leu2 lys2 met15 ura3
FSS153	BY4741	*cho1*::NATR SUR7-GFP::HIS3 leu2 lys2 met15 ura3
FSS154	BY4741	*cho1*::NATR Fet3-GFP::HIS3 leu2 lys2 met15 ura3
FSS155	BY4741	*cho1*::NATR Hxt3-GFP::HIS3 leu2 lys2 met15 ura3
FSS156	BY4741	*cho1*::NATR Mid2-GFP::HIS3 leu2 lys2 met15 ura3
FSS157	BY4741	*cho1*::NATR BIO5-GFP::HIS3 leu2 lys2 met15 ura3
FSS158	BY4741	*cho1*::NATR RAS2-GFP::URA leu2 lys2 met15 his3
FSS159	BY4741	*Mss-102*::KANR Pmp1-GFP::HIS3 leu2 lys2 met15 ura3
FSS160	BY4741	*Mss-102*::KANR SUR7-GFP::HIS3 leu2 lys2 met15 ura3
FSS161	BY4741	*Mss-102*::KANR Fet3-GFP::HIS3 leu2 lys2 met15 ura3
FSS162	BY4741	*Mss-102*::KANR Hxt3-GFP::HIS3 leu2 lys2 met15 ura3
FSS163	BY4741	*Mss-102*::KANR Mid2-GFP::HIS3 leu2 lys2 met15 ura3
FSS164	BY4741	*Mss-102*::KANR BIO5-GFP::HIS3 leu2 lys2 met15 ura3
FSS165	BY4741	*Mss-102*::KANR RAS2-GFP::URA leu2 lys2 met15 his3
FSS166	BY4741	*erg3*::KANR *erg6*::HIS3 Pma1-GFP::NAT leu2 lys2 met15 ura3
FSS167	BY4741	*erg3*::KANR *erg6*::HIS3 Pma1-GFP::NAT leu2 lys2 met15 ura3
FSS168	BY4741	*erg3*::KANR *erg6*::HIS3 Pma1-GFP::NAT leu2 lys2 met15 ura3
FSS169	BY4741	SUR7-GFP::HIS3 PMA1-RFP CEN LEU leu2 lys2 met15 ura3

Name	Strain	Genotype
FSS170	BY4741	APL2-GFP::HIS3 SUR7-GB CEN LEU ABP1-RFP::NATR lys2 met15 ura3
FSS171	BY4741	APL4-GFP::HIS3 SUR7-GB CEN LEU ABP1-RFP::NATR lys2 met15 ura3
FSS172	BY4741	CLC1-GFP::HIS3 SUR7-GB CEN LEU ABP1-RFP::NATR lys2 met15 ura3
FSS173	BY4741	EDE1-GFP::HIS3 SUR7-GB CEN LEU ABP1-RFP::NATR lys2 met15 ura3
FSS174	BY4741	ENT1-GFP::HIS3 SUR7-GB CEN LEU ABP1-RFP::NATR lys2 met15 ura3
FSS175	BY4741	SYP1-GFP::HIS3 SUR7-GB CEN LEU ABP1-RFP::NATR lys2 met15 ura3
FSS176	BY4741	YAP1801-GFP::HIS3 SUR7-GB CEN LEU ABP1-RFP::NATR lys2 met15 ura3
FSS177	BY4741	END3-GFP::HIS3 SUR7-GB CEN LEU ABP1-RFP::NATR lys2 met15 ura3
FSS178	BY4741	LSB3-GFP::HIS3 SUR7-GB CEN LEU ABP1-RFP::NATR lys2 met15 ura3
FSS179	BY4741	PAN1-GFP::HIS3 SUR7-GB CEN LEU ABP1-RFP::NATR lys2 met15 ura3
FSS180	BY4741	SLA1-GFP::HIS3 SUR7-GB CEN LEU ABP1-RFP::NATR lys2 met15 ura3
FSS181	BY4741	SLA2-GFP::HIS3 SUR7-GB CEN LEU ABP1-RFP::NATR lys2 met15 ura3
FSS182	BY4741	BZZ1-GFP::HIS3 SUR7-GB CEN LEU ABP1-RFP::NATR lys2 met15 ura3
FSS183	BY4741	LAS17-GFP::HIS3 SUR7-GB CEN LEU ABP1-RFP::NATR lys2 met15 ura3
FSS184	BY4741	VRP1-GFP::HIS3 SUR7-GB CEN LEU ABP1-RFP::NATR lys2 met15 ura3
FSS185	BY4741	RVS161-GFP::HIS3 SUR7-GB CEN LEU ABP1-RFP::NATR lys2 met15 ura3
FSS185	BY4741	RVS167-GFP::HIS3 SUR7-GB CEN LEU ABP1-RFP::NATR lys2 met15 ura3
FSS186	BY4741	DNF1-GFP::HIS3 SUR7-GB CEN LEU ABP1-RFP::NATR lys2 met15 ura3
FSS187	BY4741	INP52-GFP::HIS3 SUR7-GB CEN LEU ABP1-RFP::NATR lys2 met15 ura3
FSS188	BY4741	SCD5-GFP::HIS3 SUR7-GB CEN LEU ABP1-RFP::NATR lys2 met15 ura3
FSS189	BY4741	ENA2-GFP::HIS3 ABP1-RFP::NATR leu2 lys2 met15 ura3
FSS190	BY4741	BIO5-GFP::HIS3 ABP1-RFP::NATR leu2 lys2 met15 ura3
FSS191	BY4741	FET4-GFP::HIS3 ABP1-RFP::NATR leu2 lys2 met15 ura3
FSS192	BY4741	HXT3-GFP::HIS3 ABP1-RFP::NATR leu2 lys2 met15 ura3
FSS193	BY4741	PMA1-GFP::HIS3 ABP1-RFP::NATR leu2 lys2 met15 ura3
FSS194	BY4741	SHO1-GFP::HIS3 ABP1-RFP::NATR leu2 lys2 met15 ura3
FSS195	BY4741	TPO1-GFP::HIS3 ABP1-RFP::NATR leu2 lys2 met15 ura3
FSS196	BY4741	MID2-GFP::HIS3 ABP1-RFP::NATR leu2 lys2 met15 ura3
FSS197	BY4741	MUP1-GFP::HIS3 SUR7-RFP CEN LEU lys2 met15 ura3
FSS198	BY4741	MUP1-GFP::HIS3 ABP1-RFP::NATR leu2 lys2 met15 ura3
FSS199	BY4741	MUP1-GFP::HIS3 leu2 lys2 met15 ura3
FSS199	BY4741	*pil1*::KANR MUP1-GFP::NATR leu2 lys2 met15 ura3
FSS200	BY4741	*art1*::KANR MUP1-GFP::NATR leu2 lys2 met15 ura3
FSS201	BY4741	*art1*::KANR MUP1-GFP::NATR SUR7-RFP CEN LEU lys2 met15 ura3
FSS202	BY4741	*rsp5-1*::KANR MUP1-GFP::NATR SUR7-RFP CEN LEU lys2 met15 ura3
FSS203	BY4741	*rsp5-1*::KANR MUP1-GFP::NATR ABP1-RFP::HIS3 lys2 met15 ura3
FSS203	BY4741	ART1-GFP::KANR ABP1-RFP::NATR his3 lys2 met15 ura3
FSS204	BY4741	MUP1-GFP::NATR ABP1-RFP::KANR SUR7-GB CEN LEU lys2 met15 ura3 his3
FSS205	BY4741	*mup1-1695*::NatR his3 leu2 lys2 met15 ura3
FSS206	BY4741	*mup1-1629*::NatR his3 leu2 lys2 met15 ura3
FSS207	BY4741	*mup1-1439*::NatR his3 leu2 lys2 met15 ura3

6.0.11 Buffers

Table 6.11: Buffer

Name	Content
TE Buffer	10 mM Tris-HCl pH8.0, 1 mM EDTA, sterile filtered
10x TBE Buffer	440 mM Tris, 440 mM Boric Acid, 10 mM EDTA
6x Loading Dye	1.5 g/L Bromphenol Blue, 50% (v/v) Glycerol
RF1 Buffer	100 mM RbCl, 50 mM $MnCl_2$+x $2H_2O$, 30 mM Potassium acetate, 10 mM $CaCl_2$x $2H_2O$, 15% (v/v) Glycerol, ad pH 5.8 Acetic acid, sterile filtered, storage at 4°C
RF2 Buffer	10 mM MOPS, 10 mM $RbCl_2$, 75 mM $CaCl_2$ x 2 H_2O, 15% (v/v) Glycerol, ad pH 5.8, sterile filtered
SORB Acetic acid, sterile filtered	100 mM LiOAc,10 mM Tris, 1 mM EDTA/NaOH, 1 M Sorbitol, ad pH 8.0
PEG-Mix 1 mM EDTA/NaOH, 40% PEG 3350, ad pH 8.0, sterile filtered, stored at 4°C	100 mM LiOAc, 10 mM Tris,
ACP-Label Sphero	50 mM Tris-Cl pH 8.8, 100 mM NaCl,10 mM MgCl2 1 M Sorbitol 10 mM,Tris pH7.6

Media

YT medium was used for bacteria cultures. For selection purposes 100 μg/mL Ampicillin were added. YPD rich medium and SCD synthetic medium were used for yeast cultures. For selection SCD-Depletion medium or SCD/YPD medium with CloNat at 300 μg/ml was used.

Table 6.12: Media

Name	Content
YT-medium	0.8% (w/v) Bacto-trypton, 0.5% (w/v) Bacto-yeast extract, 0.5% (w/v) NaCl
YT-plates	YT-medium, 1.5% (w/v) Agar
Iron-depletion-medium	SC-ALL, 10 mM BPS
YPD-medium	2% (w/v) Bacto-peptone, 1% (w/v) Bacto-yeast extract, 2% (w/v) Glucose
SCD-medium	6.7% (w/v) Bacto-yeast nitrogene base (for selection w/o amino acids)
SCD-plates	SC-medium, 2% (w/v) agar
Canavanine Plates	SC-Arg, 5 μM Canavanine

Computational software

Table 6.13: Software

Company	Name
Adobe	Creative Suite 5 Premium
Canonical Ltd	Ubuntu Desktop 10.04 32 Bit
Molecular Devices	Metamorph
M. Wayne Davis	ApE A Plasmid Editor
R Foundation for Statistical Computing	R: A Language and Environment for Statistical Computing
The MathWorks	Matlab R20010a
Wayne Rasband	ImageJ 1.43U

6.0.12 Microscopy

Epifluorescence microscope

Table 6.14: Epifluorescence microscope setup

Component	Supplier	Description
Microscope	Zeiss	Zeiss Imager A1
Objective	Olympus	Olympus 1.3 NA 100x
Camera	Andor Technology	iXon EM+ DU-897ECS
Lamp	Xcite	Xenon lamp
Shutter Control	Uniblitz VCM-1	Vincent Associates
Motor	Visitron MS-2000 Nanodrive	Visitron Systems GmBH
Table	Applied Precision	xy-motorized table
Software	Metamorph 7.0	Molecular Devices

TIRF microscope

Table 6.15: TIRF Setup

Component	Supplier	Description
Microscope	Till-Photonics	IMIC standing unit
Objective	Olympus	Olympus 1.45 NA 100x
Control Unit	Till-Photonics	ICU
Camera	Andor Technology	iXon EM+ DU-897ECS
Tirf angle control	Till-Photonics	Galvanometer-drive 2-axis scan head
Laser 1	Coherent Saphire	DPSS laser with 75 mW at 488 nm
Laser 2	Cobolt Jive	DPSS laser with 75mW at 561 nm
DIC light source	Till-Photonics	LED lamp
Epifluorescence light source	Till-Photonics	Polychrome unit
Laser selection and regulation	Till-Photonics	AOTF
Climate control	MPIB workshop custom build	Temperature control unit with heating block
Software	Till-Photonics	Live-Aquisition

Chapter 7

Methods

7.1 Computational methods

7.1.1 Imageprocessing

TIRFM images were restored by deconvolution using the Classical Maximum Likelihood Estimation algorithm in Huygens Professional 3.4 Software (Scientific Volume Imaging b.v.). With TIRFM, green and red fluorescent latex beads were imaged separately to experimentally determine the point spread functions (PSF) for each channel and experimental setting. Roughly 20 beads were averaged to distill the PSF, which were then used as input for deconvolution. With this supervised image restoration technique no artefacts were generated (Fig. 3.3 A): For visualisation purposes, image resolutions were projected to 300dpi in all figures. Analysis and quantifications were always performed on non-projected deconvolved images.

7.1.2 FRAP analysis

For equatorial FRAP experiments a single spot was bleached. A kymograph was obtained along the membrane of the entire cell, normalised to background intensities and corrected for photobleaching using a region opposite of the FRAP spot. Recovery was fitted with a simple exponential fit $y = a(1 - exp(-xb)$. Half-times $t1/2 = -log(0.5)/b$ and mobile fractions (Mf = a) are only given for FRAP experiments that could be reliably fitted. For proteins Faa3, Gpa1, Psr1 and Ras2 FRAP was recorded over fifteen seconds. All other

recoveries were observed over a period of 5 min. FRAP evaluations were carried out with customised Matlab routines (Matlab 2010a, The MathWorks). In all FRAP movies five frames were imaged as reference prior to the FRAP event. Autocorrelation analysis Individual cells were cut and a subregion manually selected. Calculation of the autocorrelation in relation the selected region.

7.1.3 Particle tracking

Individual cells were automatically cut and deconvolved. Endocytic patches were tracked using the imageJ plugin particle tracker (Sbalzarini and Koumoutsakos, 2005). Subsequent analysis steps were carried out on a custom made Matlab code (mathworks). All steps were automised.

7.1.4 Co-localisation pipeline

An automated data analysis pipeline was established to avoid any unnecessary bias (Waters, 2009). First, cells were automatically detected and extracted from the image data. Since TIRFM visualises only the top section of a cell, standard cell detection algorithms could not be applied. Instead, maximum projections of red and green channels were blurred (Gaussian blur) and filtered for noise (median filter) in order to smooth out the spatial patterns to the expected cell boundary. This made cells easily detectable by iteratively searching for high intensity peaks in the image before detecting the cell boundaries by derivations in x and y directions. Second, the extracted images containing just one cell were separately deconvolved in each channel. In addition the beads were also deconvolved. Third, sub pixel alignment of deconvolved bead images was used to determine the x-y shift of the two filter sets for each image. After shifting the red channel with respect to the beads, each image contained one cell recorded with two independent channels. Finally, the co-localisation was quantified with a linear coefficient. All algorithms and evaluations were implemented in Java and Matlab. Co-localisation between proteins was quantified using a squared Manders overlap coefficient (Manders et al., 1993; Zinchuk and Grossenbacher-Zinchuk, 2009) with $M=(\sum R_i G_i)^2)/\sum R_i^2 \sum G_i^2$. Thresholding procedures were not reliable or reproducible enough to quantify the variable network-like patterns, but the contrast in our images was sufficiently high after deconvolution to allow us to obtain reproducible co-localisation values

without the need for thresholding. To minimize contributions from remaining background fluorescence (due to optical blurring), regions of interest were restricted to within cells.The Manders overlap is sensitive to background signals and unequal intensities in the two channels. Both of these issues are addressed in the following. Intensity values in each channel were scaled to the entire 8bit range for simplified handling of images during subsequent analyses. A Java package was implemented (using the ImageJ Application Programming Interface (API) rsbweb.nih.gov/ij and classes from www.uhnres.utoronto.ca /facilities/wcif) to quantify the co-localisation of red and green channels. The intensity values inside each ROI per channel was scaled to the entire 8bit range for equal weighting of both channels (identical intensity range).

We evaluated the performance of the Manders overlap with synthetic images (Fig. 3.9) and found that it scaled with the square root of the expected value. We therefore defined a linear co-localisation coefficient by using the squared Manders overlap. This modified Manders coefficient was used throughout the study and is referred to as the overlap coefficient. To obtain decoy or random overlap values, red and green channels were shuffled either between cells from a particular strain (Fig. 3.13 A) or between cells with a particular network factor (Fig. 3.14 A). Regions for overlap calculation were cropped and aligned to fully enclose spatial patterns in both channels.

7.1.5 Autocorrelation analyses

For image autocorrelation analyses, a region of interest on the cell surface was manually selected and pixel intensities I within this region were correlated over time. We calculated the Pearson correlation coefficient by comparing intensities at each time-point (t=i) with those in the first frame (t=0), thus evaluating the variation between intensity values P(It=0,It=i).

7.1.6 *In silico* colocalisation coefficient

Similarities of TMS were calculated by pairwise global alignments with a Java implementation of the Needlemann-Wunsch algorithm. The JAligner API (jaligner.sourceforge.net) for local alignments was adjusted to calculate global alignments using MCLA matrices (McLachlan, 1972) of chemical aa similarity. Gap open and gap extend parameters were

set to 5 and 0.5, respectively, to avoid long gaps within the short sequences. TMS similarities were determined from pair-wise alignments. Similarity values scale between 0 and 1, while the alignment score has no defined maxima. To determine the range of similarities between randomly generated TMS we shuffled amino acids across all TMS while preserving TMS length and calculated all-against-all pair wise alignments for the decoy TMS set. The median random similarity was 43 % with an interquartile range from 38-48 %. Therefore the 46 similarity between TMS of Fet3 and Pmp1 was considered random.

7.1.7 Plasma membrane proteome

To systematically investigate the lateral organisation of PM proteins we assembled a list of all proteins associated with the PM in the yeast *Saccharomyces cerevisiae*. The set of 279 PM-associated proteins was manually classified with respect to biological function and type of membrane anchor (Tab. 8.1). From this we selected a representative set of 46 proteins that included examples of all major functional categories (transporters, sensors, signalling and metabolism) on the PM. Protein sequences were obtained from uniprot V.18.may2010 (Consortium, 2010b). Transmembrane (TM) segments (TMS) have been experimentally defined for only two of the 279 proteins. Thus, a consensus prediction tool for TMS was utilised: We implemented Java packages to assist reading MetaTM (Klammer et al., 2009) TMS predictions for all PM proteins from the Java DAS client library (Dasobert, www.spice-3d.org/dasobert). Information on lipid anchors was obtained from the Uniprot sequence annotations as well as prediction tools (Maurer-Stroh et al., 2002; Ren et al., 2008). Protein abundance values were obtained from quantifications of TAP-tagged proteins (Ghaemmaghami et al., 2003). Proteins for which no reliable abundance data was available (not visualised, low signal or technical problem) were not included in the calculation.

7.1.8 Statistical analysis

Statistical analyses were performed with R Version 2.8.1 (www.r-project.org). We applied two-sided two sample t-test (α=0.05) with Bonferroni correction. Common significance levels are indicated as follows: *** $p < 0.01$, n.s. = not significant.

Data distributions are shown with box plots or with average ± s.e.m (standard error mean). Box plots depict the median and upper and lower quartiles of the data distribution as a box. Solid lines indicate the sample minimum and maximum. Outliers are individually marked with (o).

To determine the correlation of scattered datasets, the Pearson correlation coefficient was calculated with R. The coefficient measures the linear dependency of two datasets. +1 and -1 indicate positive and negative dependencies, respectively. Values near 0 indicate random dependency, thus, no correlation.

Phosphorylation site prediction was carried out with the online yeast phosphorylation site prediction tool NetPhosYeast 1.0 Server (http://www.cbs.dtu.dk/services/NetPhosYeast/) .

7.2 Yeast methods

S. cerevisiae strain BY4741 (Euroscarf, Frankfurt, Germany) was used throughout. Unless otherwise indicated, GFP fusions from the UCSF GFP fusion collection (Huh et al., 2003) were used. Cells were grown aerobically in synthetic media at 30°C . At OD 0.2-0.6, cells were used for microscopic analysis. Hxt2/Hxt6 were grown in medium containing 0.5 % glucose, Bio5 in medium lacking biotin and Gap1 in minimal medium (Jacobs et al., 1980).

7.2.1 Cell wall digest

Cells were grown ON and diluted 1:10 the next morning and let grow for 2-4h. Cells were harvested and resuspendet in 100 μl spherobuffer (1 M Sorbitol 10 mM Tris pH7.6), 5 μl 100T zymolyase was added and incubated for 1h at 30°C . Suspension was washed 3x with spherobuffer prior imaging.

7.2.2 Sphingolipid depletion

To deplete sphingolipids, logarithmically growing yeast cells were incubated for 1h with 5 μM of myriocin (sigma) in synthetic media at 30°C and used directly for microscopy.

7.2.3 Latrunculin treatment

Logarithmically growing yeast cells were incubated for 1h with 200 μM of Latrunculin B in synthetic media at 30°C and used directly for microscopy.

7.2.4 ACP labeling

ACP-Sag1 was grown ON and diluted at OD 0.1 the next morning YP media containing 2 % of raffinose. Protein expression was induced upon addition of 2 % Galactose and let grow for 4 h. Cells were washed twice in labelling buffer (50mM Tris-Cl pH 8.8, 100 mM NaCl, 10 mM MgCl2), labeling reaction was carried for 20 min at 30 textcelsius using 5 muem of Atto488-CoA(NEB) and 1 μM of ACP Synthase(NEB) was used (George et al., 2004). Reaction was performed in the dark and stopped by washing cell 2x with labeling buffer.

7.2.5 Coverslip treatment

Coverslips were cleaned with 1M NaOH overnight, washed twice with ddH_2O and stored under pure ethanol. To immobilise the cells coverslips were pre-coated with 2mg/ml of ConA (Sigma) prior usage (except for samples treated with zymolyase).

7.2.6 Canavanine uptake assay

Growth assay in canavanine containing media Yeast strains were grown on synthetic media plates lacking arginine and containing a final concentration of 5 μg /ml canavanine. ON culture of yeast cells were brought to an OD_{600} of 0.01 and ten-fold serial dilutions were prepared. Aliquots (5 μl) of cell suspensions were then spotted on plates and incubated at 30°C for two days. Anchor away technique was performed as described by (Haruki et al., 2008).

7.2.7 Iron depletion growth assay

Growth assay in iron depleted media ON cultures were diluted to OD_{600} of 0.01 and were grown in synthetic media containing a final concentration of 10 μg /ml bathophenanthroline disulfonate (BPS, Alfa Aesar). Subsequently OD_{600} was measured every 15 minutes during continuous shaking at 30°C for 30h using a plate reader (Bioscreen).

7.2.8 Mup1 endocytosis assay

Cells were grown ON and washed 3x with ddH_2O and diluted 1:10 in media lacking methionine. Cells were let grow for 3-4 h. Endocytosis of Mup1 was triggered by addition of 1mM methionine into the medium. Cells were imaged every 5min and fluorescence at the PM was measured using linescans.

7.2.9 Δ*Cho1* growth conditions and PS supplement

Cells were grown ON in the appropriate medium, supplemented with 1 mM of choline. Cells were diluted 1:10 next morning and let grow for 2-4 h. For recovery experiments, cells were supplemented with 20 μg /ml Lyso-PS for recovery experiments

7.2.10 Transformation of yeast

Cells were grown ON in appropriate and diluted the next morning 1:10 and let grow for 2-4 h. All steps are carried out in 1.5 ml reagent tubes. Yeast cells were washed 1x with 1 ml ddH_2O and 1x 1 ml SORB media. Supernatant was discarded and cells resuspendend in the remaining drop. For transformation 2 mul of denatured salmone sperm DNA and 10 mul of PCR product or integrative plasmids and 1 μl for CEN plasmids were added to the suspension. 250 μl of PEG mix was added to the transformation mix, carefully mixed and incubated for 60min at 30°C . Heat-shock was carried out for 15min at 42°C . Antibiotic resistant transformants were incubated in YPD media ON, while CEN plasmid containing transformants were plated immediately.

7.2.11 Induction of competence in yeast cells

Competence was induced in yeast cells for subsequent transformation. 1 mL SC-All medium was inoculated with a colony of yeast culture. The culture was incubated at 30°C over night at 180 rpm. Cells were diluted 1:10 with SC-All medium and further grown at 30°C for 4 h at 180 rpm. The cells were harvested at 0.6g for 1 min and washed with 1 mL ddH_2O with subsequent centrifugation at 0.6 g for 1 min. The supernatant was discarded, the pellet was resuspended in 1 mL SORB and again centrifuged at 0.6 g for 1 min. Competent cells were immediately used for transformation.

7.2.12 Recombinational cloning

Standard PCR was performed and the resulting fragment purified by gel elution. The entry vector was cut with SphI and the PCR product with overlapping sequences was used for standard transformation as described (Prado and Aguilera, 1994)(see 7.2.10). The centromeric plasmid was recovered using a standard plasmid preparation kit (7.2.13). Correct integration was confirmed by sequencing.

7.2.13 Yeast plasmid purification

Standard PCR was performed and the resulting fragment purified by gel elution. The entry vector was cut with SphI and the PCR product with overlapping sequences was used for standard transformation (see 7.2.10).

7.2.14 Bacterial methods

7.2.15 Induction of competence in *E. coli*

Competent DH5α *E. coli* cells were provided in 110 μL stocks. Competence was induced chemically. 5 mL YT medium were inoculated with plated DH5α colonies and incubated at 37°C overnight at 180 rpm. 50 mL YT medium were further inoculated with 2 mL preculture. 0.5 mL 1 M $MgCl_2$ and 0.5 mL 1 M $MgSO_4$ were added to a final concentration of 10 mM $MgCl_2$ and 10 mM $MgSO_4$. The culture was grown at 37°C for 2-3 h at 180 rpm until OD_{600} of 0.4-0.6. Cells were harvested at 4°C for 10 min at 3000 rpm. The

pelleted cells were resuspended and incubated for 30 min in 4°C cold 33 mL RF1 buffer. Cells were harvested again at 4°C for 10 min at 3000 rpm. Pelleted cells were resuspended and incubated for 15 min in 4°C cold 5 mL RF2 buffer. 110 μL aliquots were prepared in pre-cooled Eppendorf tubes. The competent cells were shock frozen in liquid nitrogen and stored at -80°C .

7.2.16 *E. coli* plasmid transformation

The entire ligation mixture or 1 μL plasmid DNA were mixed on ice with 50 μL of competent DH5α *E. coli* cells. The cells were transformed by heat-shock (Tab.7.1).

Table 7.1: *E. coli* Transformation

Step	Time	Temperature
Incubation	30 min	4°C
Heat-shock	90 s	42°C
Rescue	2 min	4°C

200 μL of YT medium were added after the heat-shock. The cells were grown for 1 h at room temperature. The culture was plated onto YT agar plates containing the respective antibiotics. Transformed cells were grown at 37°C over night.

7.2.17 Plasmid amplification and preparation

Transformed *E. coli* colonies were cultured and selected in 3 mL YT medium containing the respective antibiotics. Plasmid was isolated according to the plasmid extraction kit manufacturer (6.0.9).

7.2.18 Microscopy

7.2.19 Total internal reflection fluorescence microscopy

All images if not otherwise stated were acquired on a customised TIRF setup from Till Photonics based on a fully automated IMIC-stand with an Olympus 100x 1.45 NA objective.

DPSS lasers with output powers of 75 mW at 488 nm (Coherent Sapphire) and 75 mW at 561 nm (Cobolt Jive) were used as light sources. Lasers were selected through an AOTF and directed through a broadband fibre to the iMIC. A galvanometer-driven 2-axis scanner head was used to adjust incidence angles or FRAP position and an additional galvanometer was used to switch between epifluorescence, FRAP and TIRF. Images were collected with an Andor iXON DU-897 EM CCD camera. Acquisition was controlled by the Live Acquisition (Till Photonics) software package. For two-colour TIRFM experiments incidence angles were adjusted individually. Separate filters were used for detection of green and red fluorophores. Green fluorescent latex beads (Invitrogen) were mixed with each sample to correct for offset between different filters after acquisition. Images derived from green and red channels were aligned with sub pixel precision prior to analysis.

7.2.20 TIRF structured illumination microscopy (TIRF-SIM)

Total internal reflection fluorescence structured illumination microscopy (STIRF) was performed on a custom-made setup based on an inverted microscope (Leica DM-IRBE) according to (Fiolka et al., 2008). A 488 nm Argon-Ion Laser (2214-20SL, JDSU) was guided through an acousto-optic tenable filter (AOTF; Pegasus Optik), expanded by a 20x beam expander (SILL Optics) and reflected by a spatial light modulator (LCR-2500, Holoeye Photonics). Computer-generated phase gratings diffract the beam into the +/-1 diffraction orders. A polarisation filter and a motorised half-wave plate were used to ensure a high degree of linear s-polarisation. A lens doublet focused the beams and an aperture mask blocked all unwanted diffraction orders. The remaining first diffraction orders were guided by a 4f lens to opposite positions in the TIRF region of the back focal plane of the objective (HCX PL APO, 1.46 N.A. 100x, Leica). The two emanating beams create an evanescent wave with a sinusoidal excitation pattern. Fluorescence light was selected with a dichroic mirror (Chroma) and a 550/88 emission filter (Semrock). Modulated fluorescence images were recorded by a CCD camera (Hamamatsu C8484-05G). For one super-resolved image, nine raw images were acquired, corresponding to three grating orientations (0, 60°, 120°) in three phases (0°, 120°, 240°) each of the phase hologram displayed on the SLM. For reconstructions of the final images from the raw data a MATLAB-based algorithm provided by R. Heintzmann (University of Jena, Germany) was used (Hirvonen et al., 2009).

7.2.21 Widefield microscopy

Widefield imaging of both fixed samples and live cells were performed using an imaging system based on a standard Zeiss upright microscope equipped with an andor emccd camera.

7.2.22 Protein abundance measurements

Cells were grown over night in a 96-well microtiter plate, diluted 1:20 for another 2 h and transferred to 8-well glass bottom slides (ibidi). Z-stacks were taken for several random positions with a stepsize of 200 nm ($>$ 50 cells per strain). Intensity along the equator was normalised for background fluorescence and quantified with a custom-made Matlab program. The background corrected average intensity value was used for subsequent analysis.

7.2.23 Network factor calculation

To calculate network factors, intensity histograms of cropped TIRFM images were generated with 64 bins and minimal/maximal intensity values as lower/upper boundaries. The network factor was defined as the area above the cumulative histogram. For each protein at least 10 cells were analysed. The joint abundance or network factor of two proteins was calculated by summing the values for each of them.

7.3 Molecular biological methods

7.3.1 DNA precipitation

DNA precipitation buffer (3 M NaOAc, pH = 4.8) was added in 1/10 of sample volume, followed by 2x sample volume of 100% ethanol. The sample was incubated on ice for 1-2 hr, before being sedimented at 14000 rpm (Galaxy 16DH, VWR) for 10-15 mins. Supernatant was removed carefully by vacuum. Pellet was washed twice using 70% ethanol. After removal of ethanol, pellet was air-dried for 30-45 in RT, before being dissolved in appropriate volume of TE buffer.

7.3.2 Mini-preparation of plasmid DNA

The mini-preparation of plasmid DNA was carried out following the instructions provided in EZNA Plasmid Mini Kit for plasmid-miniprep kit and QIAGEN Plasmid Mini Kit.

7.3.3 Isolation of genomic DNA from *S. cerevisiae*

Cells were grown overnight at 30°C in 2-5 ml liquid YPD medium. Cultures were centrifuged at 1000 rcf for 2 mins. Supernatants were removed. Pellets were resuspended in 200 muel lysis buffer. 200 μl of TE buffer and 200 μl of phenol/chloroform were then added into the sample. An equal amount of glass-beads were added to the cell/buffer suspension and subsequently vortexed for 5-10 mins. Lysed suspension was sedimented at 14000 rpm for 10 mins. The mixtures were separated into three layers. The aqueous top layer was transferred into a fresh tube. DNA was purified using precipitation procedure described in 7.3.1. Dried pellets were dissolved in TE buffer containing 10 μg /ml RNAse A.

7.3.4 DNA-primer design

Oligonucleotides used as primers for *in vitro* amplifications were designed assuming a melting temperature of T_m=2°C perA/T-base +4°C perG/C-base to be at approximately 62°C . Oligonucleotides used as primers for gene deletion were designed according to (Janke et al., 2004). Test-primers used to validate correct integration were designed to be at 300 bp before or after the integration cassette and approximately 300 bp inside the cassette. All oligonucleotides used in this study were synthesised by metabion international AG (6.6). The primers were subsequently diluted to 100 μM as suggested by the manufacturer.

7.3.5 *In Vitro* DNA amplification by polymerase chain reaction

Polymerase Chain Reaction (PCR) was used to amplify DNA fragments. PCR products were used as plasmid inserts, integration cassettes and to validate integrated DNA.

Amplification of plasmid integration

Phusion Polymerase was used to create and amplify DNA constructs for plasmid insertion. The samples were prepared as listed below (Tab.7.2). Polymerase was added last. The listed program was performed using a thermocycler with heated lid (Tab.7.3). PCR products were analyzed and purified by 1% agarose gel electrophoresis. The relevant bands were excised and purified.

Table 7.2: Phusion®PCR reaction setup

Reagent	Volume	Final concentration
5x Phusion®HF Reaction Buffer	10.0 μL	-
dNTPs	1.0 μL	0.2 mM
Primer 5' FW	0.5 μL	1.0 μM
Primer 3' RV	0.5 μL	1.0 μM
Template DNA (Genomic or Plasmid)	1.0μL	approx. 1.0 ng
Phusion®Polymerase	1.0 μL	2 U
ddH_2O	36.0 μL	-
Total	50.0 μL	

Table 7.3: Phusion®PCR reaction cycle

Step	Cycles	Time	Temperature
Initial Denaturation	1x	5 min	95°C
Denaturation	32x	60 s	95°C
Annealing		30 s	56°C
Elongation		30 s - 90 s	72°C
Final Elongation	1x	10 min	72°C
Storage	1x	hold	4°C

Amplification of integrative cassettes

PCR reactions to amplify integrative cassettes were performed as described by (Janke et al., 2004). PCR products were analysed by agarose gel electrophoresis. The PCR product was directly used for yeast transformations (7.2.10).

Colony control PCR

Taq Polymerase was used to validate cassette integration. Two PCR were performed to test each gene deletion. For this purpose a segment reaching from upstream of the target into the integrated cassette and a segment reaching out of the cassette further downstream of the target was amplified. PCR products of correct size validate the replacement of the target. The samples were prepared as listed below (Tab.7.4). Polymerase was added after an initial denaturing step of 20min at 96°C . The listed program was performed using a thermocycler with heated lid (Tab.7.5). PCR products were analysed by 1% agarose gel electrophoresis (7.3.11).

Table 7.4: *Taq* colony PCR reaction setup

Reagent	Volume	Final concentration
10x *Taq* Reaction Buffer	10.0 μL	-
dNTPs	1.0 μL	0.2 mM
Primer 5' FW	0.5 μL	1.0 μM
Primer 3' RV	0.5 μL	1.0 μM
Taq Polymerase	2.0 μL	approx. 4 U
ddH_2O Inoculated with Colony Tip	36.0 μL	-
Total	50.0 μL	

Table 7.5: *Taq* colony PCR reaction cycle

Step	Cycles	Time	Temperature
Initial Denaturation	1x	20 min	96°C
Denaturation	32x	60 s	96°C
Annealing		30 s	56°C
Elongation		30 s - 90 s	72°C
Final Elongation	1x	10 min	72°C
Storage	1x	hold	4°C

7.3.6 *In Vitro* DNA restriction digestion

Restriction digestion for plasmid insertion

The target plasmid and the designated insert were digested for later ligation. The listed setups were incubated for 2h according to the manufacturer (Tab.7.6). Digestion products were purified via agarose gel electrophoresis.

Table 7.6: Restriction digestion setup

Reagent	Volume	Final concentration
10x Reaction Buffer (NEB 1-4)	3.0 μL	-
10x BSA	3.0 μL	3 μg
Restriction Enzyme I	1.0 μL	0.3 - 10.0 U depending on enzyme
Restriction Enzyme II	1.0 μL	0.3 - 10.0 U depending on enzyme
Plasmid	3.0 μL	1 - 3 μg
ddH_2O	19.0 μL	-
Total	30.0 μL	

Restriction digestion for plasmid validation

Plasmid was digested for analysis by agarose gel electrophoresis. The listed setups were incubated for 1h according to the manufacturer (Tab.7.7). Digestion products were analysed by agarose gel electrophoresis (7.3.11).

Table 7.7: Test restriction digestion setup

Reagent	Volume	Final concentration
10x Reaction Buffer (NEB 1-4)	2.0 μL	-
10x BSA	2.0 μL	2 μg
Restriction Enzyme	0.5 μL	0.2 - 5.0 U depending on enzyme
Plasmid	2.0 μL	0.5 - 2 μg
ddH_2O	13.5 μL	-
Total	20.0 μL	

7.3.7 *In Vitro* DNA ligation

Digested DNA was ligated using T4 DNA ligase according to the manufacturer. Vector and insert were ligated in a ratio of 1:3 for 2h at room temperature (Tab.7.8). Ligations were transformed in competent DH5α *E. coli* cells (7.2.15, 7.2.16).

Table 7.8: Ligation setup

Reagent	Volume	Final concentration
Vector	2.0 μL	50 nM
Insert	6.0 μL	150 nM
10x T4 Ligase Buffer	2.0 μL	-
T4 DNA Ligase	1.0 μL	5 U
ddH_2O	9.0 μL	-
Total	20.0 μL	

7.3.8 Plasmids and genomic tagging

The CEN plasmids pRS315 and pRS316 were used for C-terminal tagging. Constructs were generated using the following insertion sites: promoters, XhoI-PstI; genes, PstI-BamHI; fluorophores, BamHI-NotI. Primers for the TMS of Pmp1, Fet3 and Mid2 were directly ligated into the respective vectors. The FetPmp chimera was generated using recombination cloning in yeast (see met). Ras2 was cloned into a pRS306 derivative integrative vector using the following sites: promoter, BamHI-XbaI; gene, XhoI-KpnI; GFP, XbaI-XhoI. All constructs were verified by sequencing.

7.3.9 DNA sequencing

DNA was sequenced using sequencing primers. Sequencing was performed by the Microchemistry Core Facility (Tab.7.9).

Table 7.9: Sequencing Setup

Reagent	Volume	Final Concentration
Plasmid	3.0 μL	300 ng
Primer 1:10	1.0 μL	5 pM
ddH_2O	3.5 μL	-
Total	7.5 μL	

7.3.10 DNA concentration measurement

DNA concentration was measured spectro-photometrically using a NanoDrop according to the manufacturer.

7.3.11 Analytical agarose gel electrophoresis

DNA fragments can be separated according to their sizes by applying an electric field. Generally, agarose gels were prepared using between 0.5% - 2% agarose dissolved in 50ml electrophoresis buffer. The mixture was heated to using a microwave cooker to dissolve the agarose. The solution was chilled to 50°C -60°C before a final concentration of 0.5 μg /ml ethidium bromide was added. The solidified gel was then mounted onto an electrophoresis tank and submerged completed into electrophoresis buffer. DNA samples were mixed with 0.2 volumes of 6x DNA loading buffer and loaded into the gel. DNA was then separate by applying an electric field between two electrode for 30°C 45 mins at 100-120 V. Gels after eletrophoresis were then placed into a GeneFlash gel imaging system (Syngene Bio Imaging) to be photographed. DNA sequencing Plasmid DNA was sequenced using an ABI-3730 (Perkin Elmers) sequencer and ABI Big Dye 3.1 sequencing chemistry. The reactions were carried out by the Core Facility of Max-Planck Institute of Biochemistry.

Chapter 8

Appendix

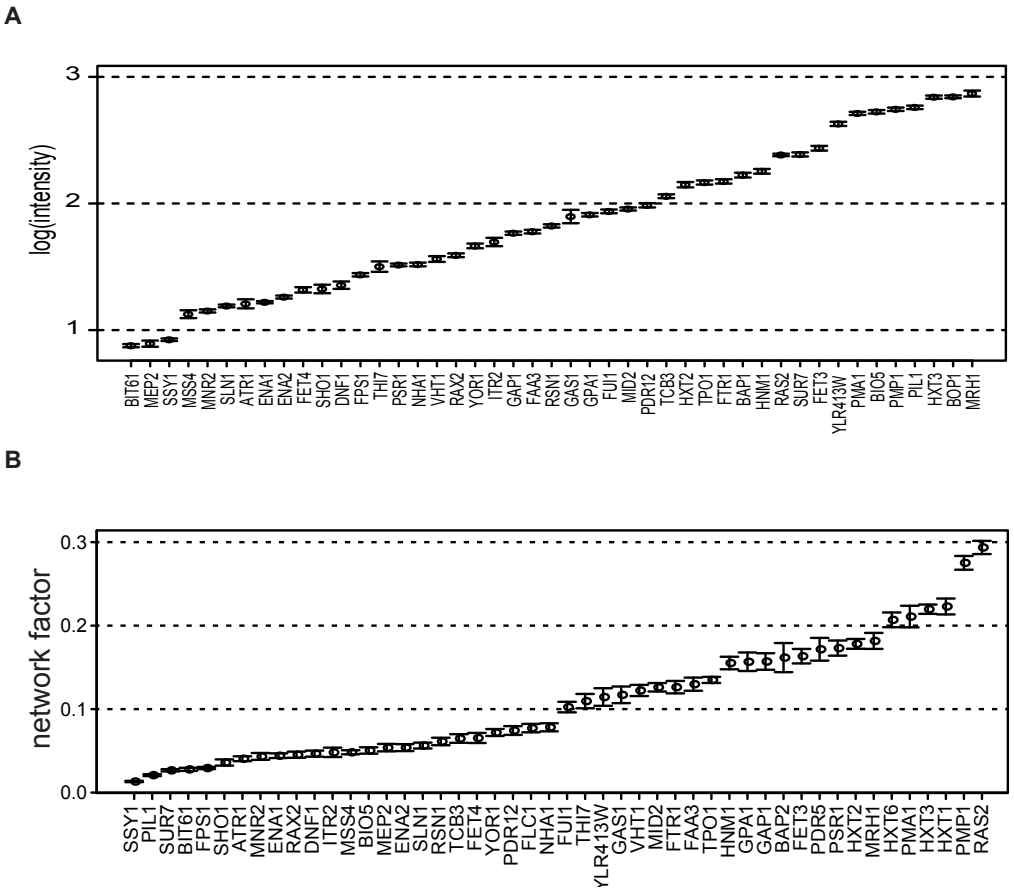

Figure 8.1: Protein expression quantification and network-factor A) Box plots showing the log of the protein expression screen. Each value is an average of at least 50 cells. B) Box plots showing the calculated network factors of the individual cells n> 10.

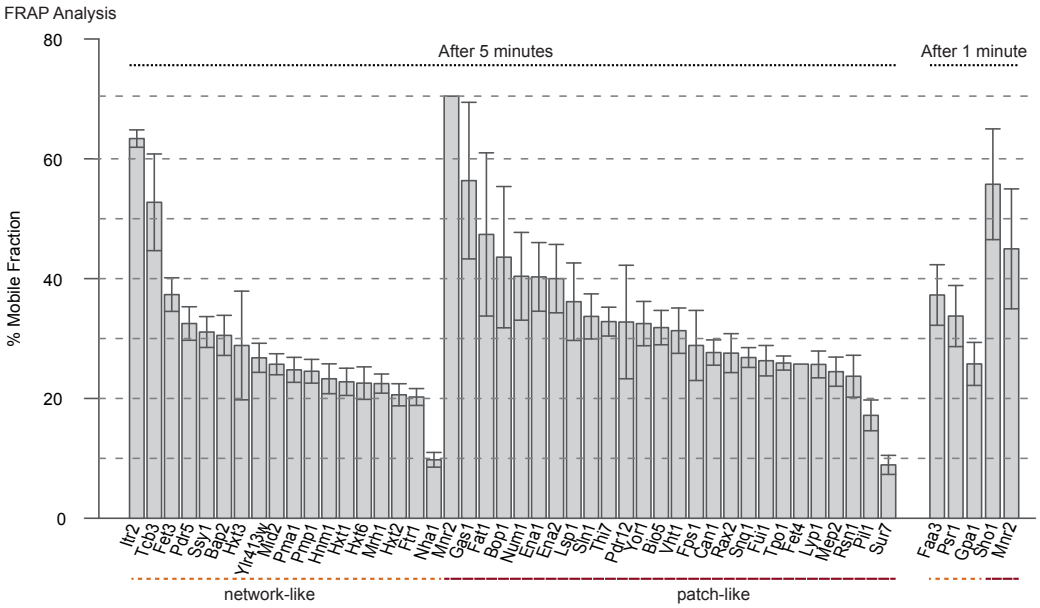

Figure 8.2: Immobile fraction of PM proteins Plots showing the recovery after 5 min for integral– and after 1 min for peripheral membrane proteins. Most proteins exhibit a very high immobile fraction.

Table 8.1: List of manually curated yeast PM proteins

Class	Functional group	Protein name	#TM domains	Lipid anchor
Transporter	Multidrug	ADP1	7	
Transporter	Amino Acids	AGP1	12	
Transporter	Amino Acids	AGP2	12	
Transporter	Amino Acids	AGP3	12	
Transporter	Amino Acids	ALP1	12	
Transporter	Ion	ALR1	2	
Transporter	Ion	ALR2	2	
Sensors	Stress	AQR1	12	
Transporter	Water	AQY1	7	
Transporter	Water	AQY2		
Transporter	Ion	ARN1	14	
Transporter	Ion	ARN2	14	
Transporter	Ion	ARR3	10	
Metabolism	Lipid Metabolism	ARV1	3	
Transporter	Anorganic acid	ATO3	6	
Transporter	Multidrug	ATR1	14	
Transporter	Lipid	AUS1	13	
Signalling	Bud Site SelectIon	AXL2	1	
Transporter	Multidrug	AZR1	14	
Transporter	Amino Acids	BAP2	12	
Transporter	Amino Acids	BAP3	12	
Signalling	Mating	BAR1		
Transporter	Vitamin	BIO5	12	
Signalling	Kinase Activity	BIT61		
Transporter	Ion	BOR1	9	
Signalling	Bud Site SelectIon	BUD8	2	
Signalling	Bud Site SelectIon	BUD9	2	
Transporter	Amino Acids	CAN1	12	
Transporter	Ion	CCH1	22	

Class	Functional group	Protein name	#TM domains	Lipid anchor
Unknown		CCM1		
Signalling	GTPase	CDC42		Prenylated
Transporter	Ion	CTR1	3	
Transporter	Ion	CTR3	2	
Unknown		CTS2	1	
Metabolism	Cell Wall Metabolism	CWH43	18	
Signalling	Hydrolase	DAL3		Prenylated
Transporter	Organic acid	DAL4	12	
Transporter	Organic acid	DAL5	12	
Metabolism	Cell Wall Metabolism	DCW1	1	
Transporter	Lipid	DET1		
Metabolism	Cell Wall Synthesis	DFG5	1	GPI Anchored
Transporter	Amino Acids	DIP5	12	
Metabolism	Lipid Metabolism	DNF1	10	
Metabolism	Lipid Metabolism	DNF2	9	
Metabolism	Lipid Metabolism	DRS2	10	
Transporter	Multidrug	DTR1	12	
Transporter	Organic acid	DUR3	15	
Unknown		ECM14		
Signalling	Cell Wall Integrity	ECM33		GPI Anchored
Transporter	Ion	ENA1	9	
Transporter	Ion	ENA2	9	
Transporter	Organic acid	ESBP6		
Metabolism	Cell Wall Synthesis	EXG2		GPI Anchored
Metabolism	Lipid Metabolism	FAA3		
Transporter	Lipid	FAT1	1	
Transporter	Organic acid	FCY2	12	
Transporter	Organic acid	FCY21	12	
Transporter	Organic acid	FCY22	12	
Transporter	Vitamin	FEN2	12	
Transporter	Ion	FET3	1	
Transporter	Ion	FET4	7	
Transporter	Ion	FLC1	11	
Transporter	Ion	FLC2	9	
Transporter	Organic acid	FLC3	9	
Metabolism	Flocculation	FLO1		GPI Anchored
Metabolism	Flocculation	FLO5	1	Flocculation
Metabolism	Flocculation	FLO9		Flocculation
Transporter	Multidrug	FLR1	12	
Metabolism	Eisosomes	FMP45	4	
Transporter	Small Carbohydrates	FPS1	6	
Transporter	Ion	FTR1	7	
Transporter	Organic acid	FUI1	12	
Transporter	Organic acid	FUR4	12	
Signalling	Mating	FUS1	1	
Transporter	Sugar	GAL2	12	
Transporter	Amino Acids	GAP1	12	
Metabolism	Cell Wall Metabolism	GAS1	1	
Metabolism	Cell Wall Metabolism	GAS2	1	
Metabolism	Cell Wall Metabolism	GAS4	1	
Transporter	Ion	GEF1	11	
Transporter	Small Carbohydrates	GIT1	12	
Transporter	Amino Acids	GNP1	12	
Signalling	GTPase	GPA1		PalmitoylatIon/Myristoyl
Signalling	GTPase	GPA2		Flocculation
Sensors	Broad nutritIon	GPR1	6	
Metabolism	Lipid Metabolism	GUP1	12	
Transporter	Small Carbohydrates	GUP2	10	
Transporter	Amino Acids	HIP1	12	
Sensors	Stress	HKR1	1	
Transporter	Amino Acids	HNM1	12	
Sensors	Stress	HOG1		
Transporter	Multidrug	HOL1	11	

Class	Functional group	Protein name	#TM domains	Lipid anchor
Transporter	Sugar	HXT1	12	
Transporter	Sugar	HXT10	12	
Transporter	Sugar	HXT11	12	
Transporter	Sugar	HXT12	11	
Transporter	Sugar	HXT13	12	
Transporter	Sugar	HXT14	12	
Transporter	Sugar	HXT15	12	
Transporter	Sugar	HXT16	12	
Transporter	Sugar	HXT17	12	
Transporter	Sugar	HXT2	12	
Transporter	Sugar	HXT3	12	
Transporter	Sugar	HXT4	12	
Transporter	Sugar	HXT5	12	
Transporter	Sugar	HXT6	12	
Transporter	Sugar	HXT7	12	
Transporter	Sugar	HXT8	12	
Transporter	Sugar	HXT9	12	
Transporter	Sugar	ITR1	12	
Transporter	Sugar	ITR2	12	
Transporter	Sugar	JEN1	12	
Metabolism	Cell Wall Synthesis	KRE1	2	
Metabolism	Cell Wall Metabolism	KRE9		
Transporter	Lipid	LEM3	2	
Metabolism	Eisosomes	LSP1		
Transporter	Amino Acids	LYP1	12	
Transporter	Sugar	MAL11	12	
Transporter	Sugar	MAL31	12	
Transporter	Organic acid	MCH1	12	
Transporter	Organic acid	MCH2	12	
Transporter	Organic acid	MCH4	12	
Transporter	Vitamin	MCH5	12	
Transporter	Anorganic acid	MEP1	11	
Transporter	Anorganic acid	MEP2	10	
Transporter	Anorganic acid	MEP3	11	
Signalling	Mating	MFA1		Prenylated
Signalling	Mating	MFA2		Prenylated
Transporter	Ion	MID1		
Sensors	Stress	MID2	1	
Signalling	Cell Wall Integrity	MKC7		GPI Anchored
Transporter	Organic acid	MMP1	12	
Transporter	Ion	MNR2	2	
Transporter	Sugar	MPH2		
Transporter	Sugar	MPH3	12	
Unknown		MRH1	7	
Sensors	Stress	MSB2	1	
Signalling	Kinase Activity	MSS4		
Sensors	Glucose	MTH1		
Sensors	Stress	MTL1	1	
Metabolism	Flocculation	MUC1		GPI Anchored
Transporter	Amino Acids	MUP1	12	
Transporter	Amino Acids	MUP3	12	
Unknown		NCE101	1	
Metabolism	Eisosomes	NCE102	4	
Transporter	Multidrug	NFT1	15	
Transporter	Ion	NHA1	13	
Transporter	Vitamin	NRT1	12	
Signalling	Cytoskeleton Binding	NUM1		PH Domain
Transporter	Peptides	OPT1	16	
Transporter	Peptides	OPT2	14	
Metabolism	Cell Wall Metabolism	PAU23/DAN2		
Transporter	Ion	PCA1	8	
Sensors	Stress	PDR1		
Transporter	Multidrug	PDR10	13	

Class	Functional group	Protein name	#TM domains	Lipid anchor
Transporter	Multidrug	PDR11	14	
Transporter	Multidrug	PDR12	13	
Transporter	Multidrug	PDR15	14	
Transporter	Multidrug	PDR5	13	
Transporter	Ion	PHO3		
Transporter	Ion	PHO5		
Transporter	Ion	PHO84	12	
Transporter	Ion	PHO87	13	
Transporter	Ion	PHO90	12	
Transporter	Ion	PHO91	12	
Metabolism	Eisosomes	PIL1		
Transporter	Ion	PMA1	10	
Transporter	Ion	PMA2	10	
Transporter	Ion	PMP1	1	
Transporter	Ion	PMP2		
Unknown		PMP3	2	
Signalling	Phosphatase Activity	PPZ1		
Sensors	Pheromone	PRM9	2	
Signalling	Phosphatase Activity	PSR1		PalmitoylatIon/Myristoyl
Signalling	Cell Wall Integrity	PST1	1	GPI Anchored
Signalling	Kinase Activity	PTK2	1	
Transporter	Peptides	PTR2	12	
Sensors	Amino Acids	PTR3		
Transporter	Amino Acids	PUT4	12	
Transporter	Multidrug	QDR1	12	
Transporter	Multidrug	QDR2	12	
Transporter	Multidrug	QDR3	12	
Signalling	GTPase	RAS2		Prenylated
Signalling	Bud Site SelectIon	RAX2	1	
Sensors	Glucose	RGT2	12	
Signalling	GTPase	RHO1		Prenylated
Signalling	GTPase	RHO2		Prenylated
Signalling	GTPase	RHO3		Prenylated
Signalling	GTPase	RHO4		Prenylated
Signalling	GTPase	RHO5		Prenylated
Signalling	Protease	RIM9	4	
Unknown		RRG8		
Metabolism	Lipid Metabolism	RSB1	7	
Unknown		RSN1	10	
Signalling	GTPase	RSR1		Prenylated
Transporter	Ion	SAM3	12	
Sensors	Stress	SHO1	4	
Signalling	Kinase Activity	SIP2		Myristoyl
Transporter	Ion	SIT1	14	
Signalling	Bud Site SelectIon	SKG6	1	
Sensors	Stress	SLG1/WSC1	1	
Sensors	Stress	SLN1	2	
Transporter	Ion	SMF1	11	
Transporter	Ion	SMF2	11	
Transporter	Ion	SMF3	11	
Unknown		SNA2	2	
Sensors	Glucose	SNF3	11	
Transporter	Multidrug	SNG1	6	
Transporter	Multidrug	SNQ2	14	
Signalling	SporulatIon	SPS2	1	GPI Anchored
Signalling	SporulatIon	SPS22		GPI Anchored
Transporter	Ion	SSU1	9	
Sensors	Amino Acids	SSY1	12	
Signalling	Mating	STE18		Prenylated
Sensors	Pheromone	STE6	10	
Transporter	Small Carbohydrates	STL1	12	
Transporter	Ion	SUL1	10	
Transporter	Ion	SUL2	10	

Class	Functional group	Protein name	#TM domains	Lipid anchor
Metabolism	Eisosomes	SUR7	4	
Transporter	Amino Acids	TAT1	12	
Transporter	Amino Acids	TAT2	12	
Metabolism	Lipid Metabolism	TCB1	2	
Unknown		TCB2	1	
Unknown		TCB3	1	
Transporter	Vitamin	THI7	12	
Transporter	Vitamin	THI73	12	
Transporter	Vitamin	TNA1	12	
Transporter	Ion	TOK1	10	
Transporter	Vitamin	TPN1	12	
Transporter	Amino Acids	TPO1	12	
Transporter	Amino Acids	TPO2	12	
Transporter	Amino Acids	TPO4	12	
Transporter	Ion	TRK1	10	
Transporter	Ion	TRK2	10	
Transporter	Organic acid	UGA4	12	
Transporter	Amino Acids	VBA5	14	
Transporter	Vitamin	VHT1	9	
Transporter	Sugar	VID22		
Unknown		VTH2	1	
Sensors	Stress	WSC2	1	
Sensors	Stress	WSC3	1	
Sensors	Stress	WSC4	1	
Unknown		YAL065C		
Unknown		YBL081W		
Unknown		YBR235W	11	
Transporter	Multidrug	YBT1	15	
Signalling	Kinase Activity	YCK1		Prenylated
Signalling	Kinase Activity	YCK2		Prenylated
Transporter	Amino Acids	YCT1	12	
Unknown		YDL199C	12	
Unknown		YDR387C	12	
Unknown		YER077C		
Unknown		YFL040W	12	
Unknown		YFL054C	6	
Unknown		YGL114W	14	
Unknown		YGR026W	5	
Transporter	Multidrug	YHK8	12	
Unknown		YHL008C	6	
Unknown		YIL060W		
Unknown		YIL166C	12	
Unknown		YIL171W	1	
Unknown		YJR012C	1	
Unknown		YKL187C	4	
Unknown		YLR149C		
Unknown		YLR413W	3	
Unknown	YMR034C	10		
Metabolism	Eisosomes	YNL194C	4	
Unknown		YNL320W	1	
Unknown		YNR048W	2	
Unknown		YOL075C		
Sensors	Stress	YOR1	11	
Sensors	Stress	YPD1		
Unknown		YPR003C	12	
Unknown		YPR117W	2	
Signalling	Protease	YPS1		GPI Anchored
Signalling	Protease	YPS3		GPI Anchored
Signalling	Protease	YPS6		GPI Anchored
Transporter	Ion	ZRT1	8	
Transporter	Ion	ZRT2	8	

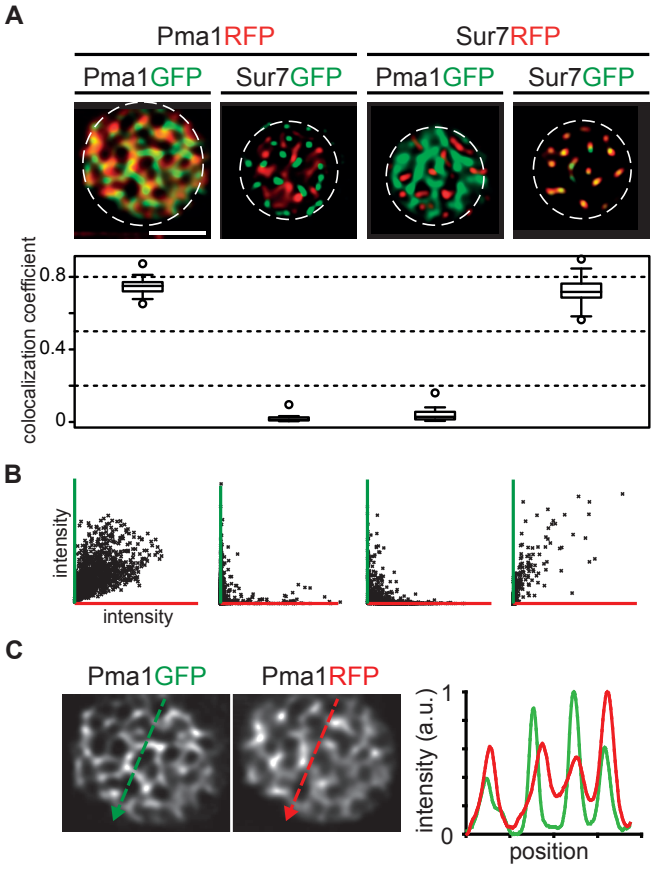

Figure 8.3: Co-localization controls The linear colocalization coefficient was experimentally evaluated. Sur7 and Pma1 form non-overlapping domains, which was consistent with low overlap coefficients < 0.2. Overlap coefficients for identical proteins were > 0.7. A) TIRFM images and Overlap coefficients. B) Scatter plots of images shown in A) C) Linescan over Pma1GFP-Pma1RFP shown in A). Scale bar: 2 μm .

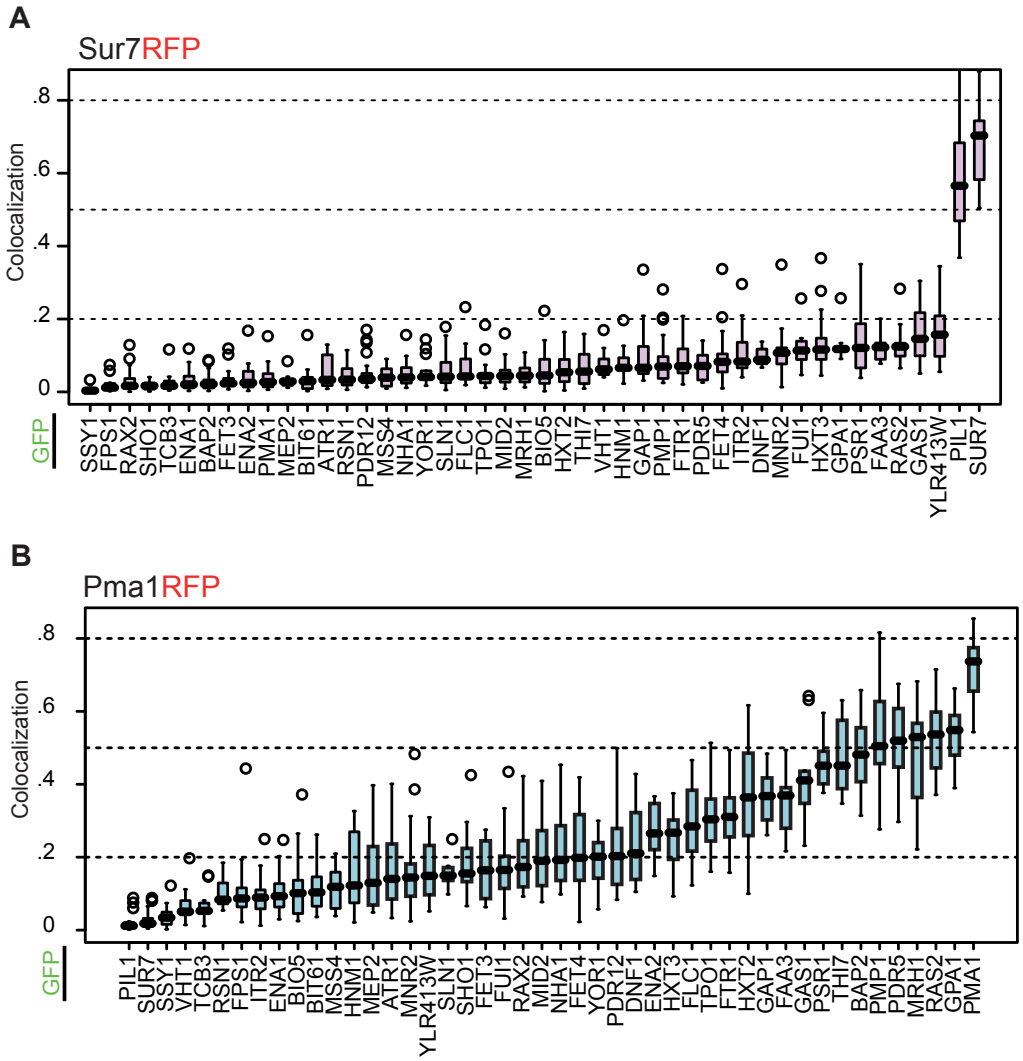

Figure 8.4: Colocalization of PM proteins with Sur7 and Pma1 Box plots of colocalization coefficients for all 46 proteins tested with A. Sur7RFP (pink) or B. Pma1RFP (light blue).

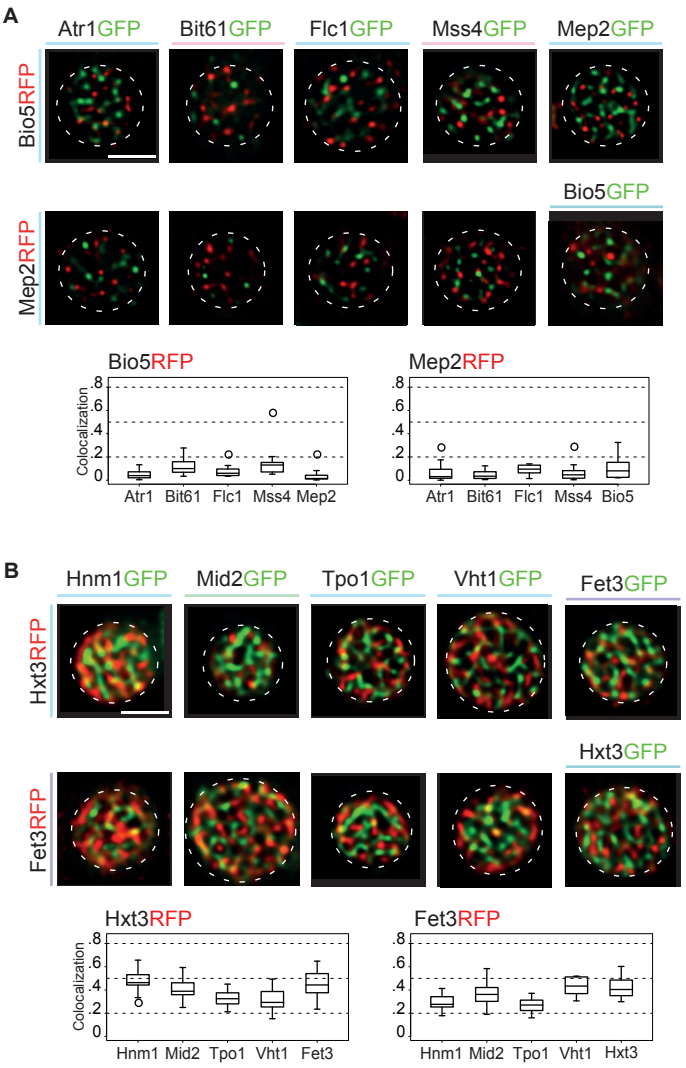

Figure 8.5: Colocalization of patch and network forming proteins against a protein subset A. Patch forming proteins Bio5RFP and Mep2RFP co-localised against 5 additional patch-like proteins. B. Network forming proteins Hxt3RFP and Fet3RFP were co-localised against 5 additional network forming proteins. Scale bar: 2 μm .

Table 8.2: Co-localisation results

RFPFusion-GFPFusion	Mean co-localisation	s.e.m. co-localisation	n
BIO5-ATR1	0.049	0.00745	21
BIO5-BIT61	0.12123	0.01465	22
BIO5-FLC1	0.07947	0.02154	7
BIO5-MEP2	0.0321	0.00813	24
BIO5-MSS4	0.14265	0.02602	18
BIO5-THI7	0.08155	0.0121	12
FET3-FET3	0.73345	0.03714	8
FET3-HNM1	0.29868	0.01856	13
FET3-HXT3	0.41697	0.0185	19
FET3-MID2	0.35966	0.02228	21
FET3-PMP1	0.42478	0.02259	16
FET3TM-PMP1	0.51655	0.0157	23
FET3-TPO1	0.27131	0.01883	13
FET3-VHT1	0.43201	0.02252	12
FETPMP-FET3	0.36462	0.05389	7
FETPMP-PMP1	0.62883	0.02607	16
HXT1-HXT2	0.38706	0.01422	30
HXT1-HXT3	0.57428	0.0223	17
HXT1-HXT6	0.59403	0.02471	13
HXT2-HXT1	0.43827	0.01467	31
HXT2-HXT3	0.52	0.01256	28
HXT2-HXT6	0.58368	0.02131	23
HXT3-FET3	0.44874	0.02201	26
HXT3-HNM1	0.47861	0.01365	41
HXT3-HXT1	0.65164	0.00974	25
HXT3-HXT2	0.4519	0.01784	20
HXT3-HXT6	0.50362	0.02042	19
HXT3-MID2	0.40757	0.01725	22
HXT3-TPO1	0.33005	0.01719	15
HXT3-VHT1	0.31338	0.01337	36
HXT6-HXT1	0.55534	0.01636	25
HXT6-HXT2	0.61311	0.01607	36
HXT6-HXT3	0.50662	0.02414	18
MEP2-ATR1	0.05954	0.0127	25
MEP2-BIO5	0.11423	0.04657	6
MEP2-BIT61	0.04579	0.0077	22
MEP2-FLC1	0.08979	0.01923	6
MEP2-MSS4	0.05911	0.01286	21
MEP2-THI7	0.21448	0.04839	5
MID2TM-PMP1	0.5923	0.0116	44
PMA1-ATR1	0.16361	0.0214	20
PMA1-BAP2	0.48474	0.02528	17
PMA1-BIO5	0.10974	0.0204	18
PMA1-BIT61	0.11172	0.01091	28
PMA1-DNF1	0.22957	0.02123	21
PMA1-ENA1	0.10183	0.01254	19
PMA1-ENA2	0.27753	0.02398	10
PMA1-FAA3	0.34401	0.01658	21
PMA1-FET3	0.16575	0.02457	10
PMA1-FET4	0.21649	0.0278	16
PMA1-FLC1	0.29472	0.04052	8
PMA1-FPS1	0.10145	0.01432	28
PMA1-FTR1	0.3131	0.01583	24
PMA1-FUI1	0.1699	0.0151	33
PMA1-GAP1	0.36087	0.02369	11
PMA1-GAS1	0.41707	0.03274	12
PMA1-GPA1	0.53323	0.02087	14
PMA1-HNM1	0.1644	0.0308	13
PMA1-HXT2	0.37346	0.02704	28
PMA1-HXT3	0.25403	0.01746	19
PMA1-ITR2	0.08957	0.01157	21

RFPFusion-GFPFusion	Mean co-localisation	s.e.m. co-localisation	n
PMA1-MEP2	0.15421	0.02278	19
PMA1-MID2	0.20784	0.029	13
PMA1-MNR2	0.15851	0.01621	35
PMA1-MRH1	0.47797	0.02453	28
PMA1-MSS4	0.11655	0.01315	18
PMA1-NHA1	0.21851	0.01899	30
PMA1-PDR12	0.23207	0.04064	11
PMA1-PDR5	0.51957	0.02789	15
PMA1-PIL1	0.0205	0.00573	16
PMA1-PMA1	0.72211	0.02523	12
PMA1-PMP1	0.52461	0.03113	18
PMA1-PSR1	0.45372	0.01844	12
PMA1-RAS2	0.53168	0.02315	19
PMA1-RAX2	0.19002	0.03469	9
PMA1-RSN1	0.09964	0.01381	10
PMA1-SHO1	0.18284	0.02354	15
PMA1-SLN1	0.15621	0.01309	9
PMA1-SSY1	0.03659	0.00431	30
PMA1-SUR7	0.0255	0.0039	29
PMA1-TCB3	0.06718	0.00986	13
PMA1-THI7	0.47581	0.03851	8
PMA1-TPO1	0.3025	0.01504	30
PMA1-VHT1	0.06382	0.01003	17
PMA1-YLR413W	0.1618	0.02041	14
PMA1-YOR1	0.19028	0.01428	23
PMP1TM-PMP1	0.7086	0.01158	45
SUR7-ATR1	0.057	0.01503	10
SUR7-BAP2	0.02626	0.00427	26
SUR7-BIO5	0.06189	0.01128	21
SUR7-BIT61	0.03118	0.00701	20
SUR7-DNF1	0.09588	0.01089	6
SUR7-ENA1	0.03131	0.00569	24
SUR7-ENA2	0.03751	0.00823	20
SUR7-FAA3	0.12425	0.01356	9
SUR7-FET3	0.03315	0.00606	19
SUR7-FET4	0.09754	0.01783	18
SUR7-FLC1	0.06974	0.01565	13
SUR7-FPS1	0.01748	0.00442	15
SUR7-FTR1	0.0916	0.01291	17
SUR7-FUI1	0.12192	0.02091	8
SUR7-GAP1	0.09294	0.01259	27
SUR7-GAS1	0.16213	0.02376	13
SUR7-GPA1	0.12894	0.01532	9
SUR7-HNM1	0.0763	0.00956	17
SUR7-HXT2	0.06312	0.00988	21
SUR7-HXT3	0.1263	0.00735	55
SUR7-ITR2	0.10822	0.01976	13
SUR7-MEP2	0.0305	0.0056	10
SUR7-MID2	0.04739	0.0054	31
SUR7-MNR2	0.11237	0.01586	18
SUR7-MRH1	0.04918	0.00766	15
SUR7-MSS4	0.04126	0.00666	16
SUR7-NHA1	0.04858	0.00645	25
SUR7-PDR12	0.04822	0.0075	26
SUR7-PDR5	0.07134	0.01198	11
SUR7-PIL1	0.58789	0.03267	22
SUR7-PMA1	0.03719	0.00594	28
SUR7-PMP1	0.08165	0.00932	39
SUR7-PSR1	0.14616	0.01987	21
SUR7-RAS2	0.1279	0.01016	21
SUR7-RAX2	0.02983	0.00698	19
SUR7-RSN1	0.0428	0.00627	22
SUR7-SHO1	0.01816	0.00333	14

RFPFusion-GFPFusion	Mean co-localisation	s.e.m. co-localisation	n
SUR7-SLN1	0.06006	0.00931	26
SUR7-SSY1	0.00643	0.00167	16
SUR7-SUR7	0.68271	0.01674	33
SUR7-TCB3	0.0256	0.00673	14
SUR7-THI7	0.0659	0.01246	15
SUR7-TPO1	0.04582	0.00636	27
SUR7-VHT1	0.07407	0.00879	15
SUR7-YLR413W	0.15834	0.02399	13
SUR7-YOR1	0.05572	0.00972	13

Table 8.3: Peripheral GFP signal

Protein	Membrane GFP signal mean	Membrane GFP signal s.e.m.	n
ATR1	18.5936	1.54370	44
BAP2	181.170	6.78977	95
BIO5	546.010	16.4510	64
BIT61	7.75522	0.20747	74
DNF1	24.3609	1.42807	38
ENA1	17.1211	0.33289	156
ENA2	18.6708	0.50987	63
FAA3	62.9679	2.01388	94
FET3	293.976	12.2312	85
FET4	22.5845	1.15606	70
FLC1	715.927	18.6934	89
FPS1	28.5165	0.90616	91
FTR1	160.522	7.00903	89
FUI1	90.8165	2.81574	89
GAP1	60.7383	1.76164	96
GAS1	117.665	19.4214	49
GPA1	84.6204	2.56172	81
HNM1	192.410	7.68090	82
HXT2	161.692	7.35843	132
HXT3	715.996	19.6198	86
ITR2	55.8913	3.43011	50
MEP2	9.43382	1.19295	82
MID2	94.4016	2.57711	111
MNR2	14.5656	0.40981	69
MRH1	799.356	32.5071	70
MSS4	14.4558	0.45090	66
NHA1	35.1393	1.43131	103
PDR12	105.964	4.35787	120
PDR5	360.206	56.5394	60
PIL1	595.249	18.7041	73
PMA1	540.287	15.6351	118
PMP1	582.697	17.3214	109
PSR1	33.7001	0.76429	102
RAS2	251.282	5.48924	157
RAX2	40.5953	1.36103	71
RSN1	70.0076	1.84268	129
SHO1	23.4282	1.60309	42
SLN1	15.9616	0.39319	94
SSY1	8.55658	0.19069	72
SUR7	256.616	9.30755	75
TCB3	119.990	3.78466	92
THI7	42.4928	4.84861	65
TPO1	156.093	5.55829	95
VHT1	40.6302	2.62546	72
YLR413W	449.988	14.2041	91
YOR1	49.6086	2.23768	77

Table 8.4: Network-Factor

Protein	Network-Factor mean	Network-Factor s.e.m.	n
ATR1	0.04055	0.00292	75
BAP2	0.16172	0.01743	14
BIO5	0.05044	0.00380	40
BIT61	0.02780	0.00185	92
DNF1	0.04667	0.00363	25
ENA1	0.04420	0.00281	38
ENA2	0.05386	0.00415	28
FAA3	0.12988	0.00788	22
FET3TM	0.22461	0.01203	25
FET3	0.16340	0.00867	78
FET4	0.06546	0.00603	29
FLC1	0.07724	0.00507	31
FPS1	0.02941	0.00132	37
FTR1	0.12630	0.00743	39
FUI1	0.10246	0.00630	34
GAP1	0.15703	0.00988	35
GAS1	0.11711	0.00995	20
GPA1	0.15676	0.01110	10
HNM1	0.15523	0.00751	73
HXT1	0.22296	0.00953	68
HXT2	0.17817	0.00586	127
HXT3	0.21972	0.00557	133
HXT6	0.20695	0.00884	46
ITR2	0.04821	0.00562	29
LACTC2	0.26086	0.01958	12
MEP2	0.05384	0.00444	46
MID2TM	0.21829	0.00674	42
MID2	0.12614	0.00507	70
MNR2	0.04334	0.00410	47
MRH1	0.18171	0.00958	43
MSS4	0.04828	0.00243	69
NHA1	0.07821	0.00482	50
PDR12	0.07436	0.00525	28
PDR5	0.17169	0.01362	21
PIL1	0.02093	0.00117	37
PLCD	0.26252	0.0082	8
PMA1	0.21089	0.01293	41
PMP1TM	0.24843	0.00637	48
PMP1	0.27546	0.00825	73
PSR1	0.17310	0.00907	28
RAS2	0.29388	0.0079	35
RAX2	0.04537	0.00369	29
RSN1	0.06122	0.00450	27
SHO1	0.03603	0.00373	25
SLN1	0.05634	0.00354	32
SSY1	0.01329	0.00077	43
SUR7	0.02668	0.00132	42
TCB3	0.06480	0.00515	23
THI7	0.10958	0.00857	36
TPO1	0.13498	0.00365	73
VHT1	0.12234	0.00667	64
YLR413W	0.11450	0.01052	21
YOR1	0.07197	0.00416	32

Table 8.5: Plasmids used in this study

Nummer	Plasmid	Origin
pFS001	pRS316 URA3 pFet3-Fet3-GFP	this study
pFS002	pRS315 LEU pFet3-Fet3-GFP	this study
pFS003	pRS316 URA3 pFet3-Fet3Chimera-GFP	this study
pFS004	pRS315 LEU pFet3-Fet3Chimera-RFP	this study
pFS005	pRS315 LEU pPma1-Mid2TM-RFP	this study
pFS006	pRS315 LEU pPma1-Pmp1TM-RFP	this study
pFS007	pRS315 LEU pPma1-Fet3TM-RFP	this study
pFS008	pRS315 LEU pPma1-Pma1-RFP	this study
pFS009	pRS316 URA3 pPma1-Pma1-GFP	this study
pFS010	pRS315 LEU pSur7-Sur7-RFP	this study
pFS011	pRS315 LEU pSur7-Sur7-GFP-Binder	this study
pFS012	pRL369 URA3 pRas2-Ras2-GFP	this study
pFS013	pRS426 URA3 GFP-PHx2 gift	from S. Emr24
pFS014	P416 GPD-URA3 Lactadherin-C2	Addgene plasmid 22853
pFS015	pRS316 pGAL1-ACP Sag1	gift fom N. Johnsson70

Protein Class	TIRFM	Membrane Abundance	Network Factor	Equator FRAP 5min.		Recovery	Colocalization with Sur7RFP		Colocalization with Pma1RFP		No. TMS
Atr1/Snq1**GFP** Transporter *Multidrug*	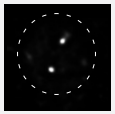	18.59±1.54 n: 44	0.04±0 n: 75	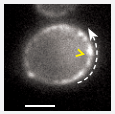	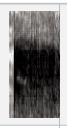 (44)	Recovery T/2: 45.6±14.4 Mf: 32±4 n: 7	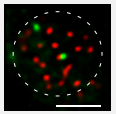	0.06±0.02 n: 10	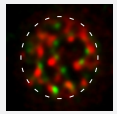	0.16±0.02 n: 19	14
Bap2GFP Transporter *Amino Acids*	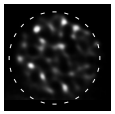	181.17±6.79 n: 95	0.16±0.02 n: 14	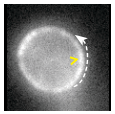	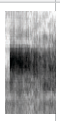 (10)	Recovery T/2: 40.1±5.2 Mf: 29±0 n: 3	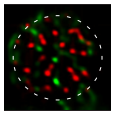	0.03±0.01 n: 26	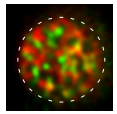	0.5±0.03 n: 14	12
Bio5GFP Transporter *Vitamin*	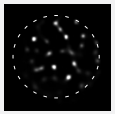	546.01±16.45 n: 64	0.05±0 n: 40	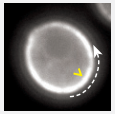	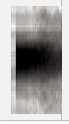 (20)	No Recovery	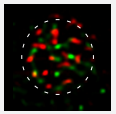	0.06±0.01 n: 21	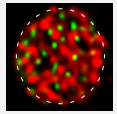	0.09±0.02 n: 13	12
Bit61GFP Signalling *Kinase Activity*	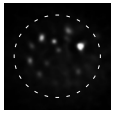	7.76±0.21 n: 74	0.03±0 n: 92	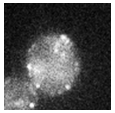	(signal too low)		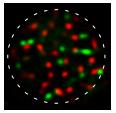	0.03±0.01 n: 20	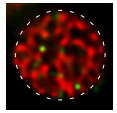	0.11±0.01 n: 28	-
Dnf1GFP Metabolism *Lipid Metabolism*	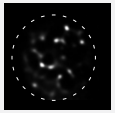	24.36±1.43 n: 38	0.05±0 n: 25	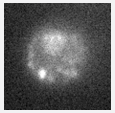	(signal too low)		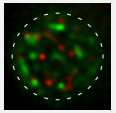	0.08±0.01 n: 4	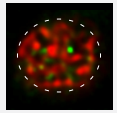	0.23±0.02 n: 21	10
Ena1GFP Transporter *Ion*	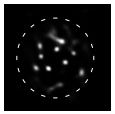	17.12±0.33 n: 156	0.04±0 n: 38	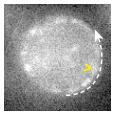	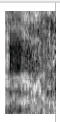 (12)	Techn. Limiting (no recovery)	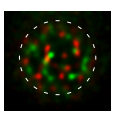	0.03±0.01 n: 24	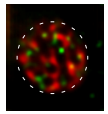	0.09±0.01 n: 14	9
Ena2GFP Transporter *Ion*	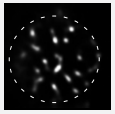	18.67±0.51 n: 63	0.05±0 n: 28	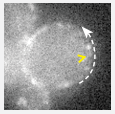	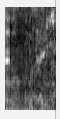 (15)	Techn. Limiting (no recovery)	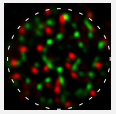	0.04±0.01 n: 20	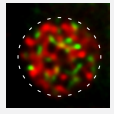	0.26±0.03 n: 8	9
Faa3GFP Metabolism *Lipid Metabolism*	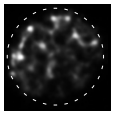	62.97±2.01 n: 94	0.13±0.01 n: 22	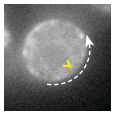	 (22)*	Techn. Limiting (no recovery)	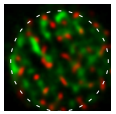	0.14±0.02 n: 6	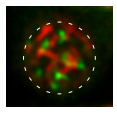	0.36±0.02 n: 16	-

Protein Class	TIRFM	Membrane Abundance	Network Factor	Equator FRAP 5min.	Recovery	Colocalization with Sur7RFP	Colocalization with Pma1RFP	No. TMS
Fet3GFP Metabolism *Oxidoreductase*	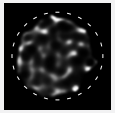	293.98±12.23 n: 85	0.16±0.01 n: 78	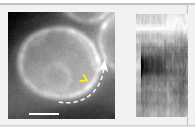 (24)	Recovery T/2: 35.3±4.4 Mf: 24±2 n: 6	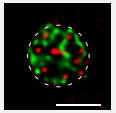 0.03±0.01 n: 19	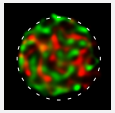 0.17±0.02 n: 10	1
Fet4GFP Transporter *Ion*	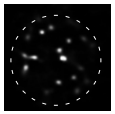	22.58±1.16 n: 70	0.07±0.01 n: 29	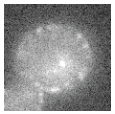 (signal too low)		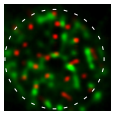 0.1±0.02 n: 18	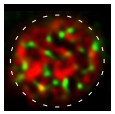 0.22±0.04 n: 11	7
Flc1/ Bop1GFP Transporter *Ion*	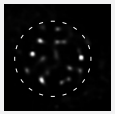	715.93±18.69 n: 89	0.08±0.01 n: 31	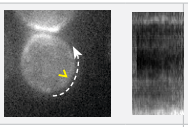 (7)	Techn. Limiting (no recovery)	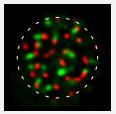 0.06±0.02 n: 12	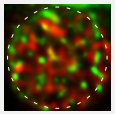 0.3±0.04 n: 6	11
Fps1GFP Transporter *Small Carbohydrates*	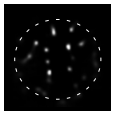	28.52±0.91 n: 91	0.03±0 n: 37	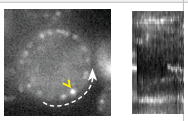 (15)	Techn. Limiting (no recovery)	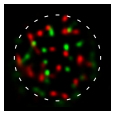 0.02±0 n: 14	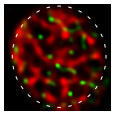 0.09±0.01 n: 23	6
Ftr1GFP Transporter *Ion*	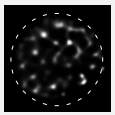	160.52±7.01 n: 89	0.13±0.01 n: 39	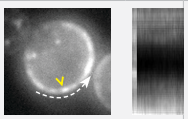 (24)	Techn. Limiting (no recovery)	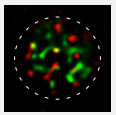 0.09±0.01 n: 16	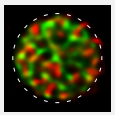 0.31±0.02 n: 23	7
Fui1GFP Transporter *Organic acid*	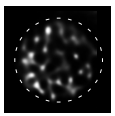	90.82±2.82 n: 89	0.1±0.01 n: 34	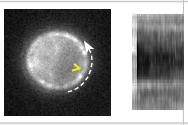 (21)	Recovery T/2: 19.0±4.9 Mf: 21±2 n: 5	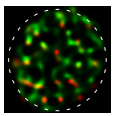 0.12±0.02 n: 8	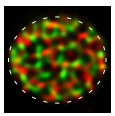 0.18±0.02 n: 26	12
Gap1GFP Transporter *Amino Acids*	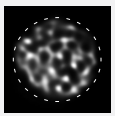	60.74±1.76 n: 96	0.16±0.01 n: 35	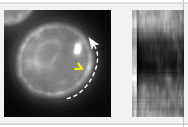 (13)	Recovery T/2: 19.9±2.9 Mf: 38±5 n: 4	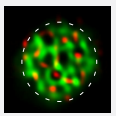 0.09±0.01 n: 26	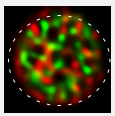 0.36±0.03 n: 9	12
Gas1GFP Metabolism *Cell Wall Metabolism*	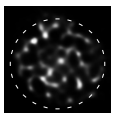	117.67±19.42 n: 49	0.12±0.01 n: 20	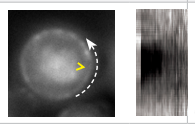 (6)	Recovery T/2: 28.9±10.9 Mf: 49±9 n: 3	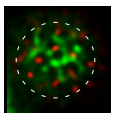 0.14±0.03 n: 9	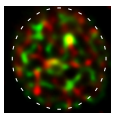 0.42±0.04 n: 11	1

Protein Class	TIRFM	Membrane Abundance	Network Factor	Equator FRAP 5min.	Recovery	Colocalization with Sur7RFP	Colocalization with Pma1RFP	No. TMS
Gpa1GFP Signalling *GTPase*	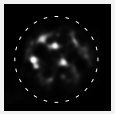	84.62±2.56 n: 81	0.16±0.01 n: 10	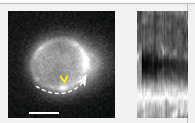 (23)*	No Recovery	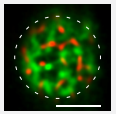 0.13±0.02 n: 9	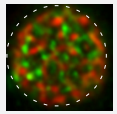 0.53±0.03 n: 10	l.a.
Hnm1GFP Transporter *Amino Acids*	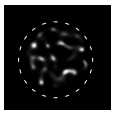	192.41±7.68 n: 82	0.16±0.01 n: 73	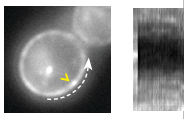 (17)	Recovery T/2: 25.4±11.0 Mf: 21±3 n: 4	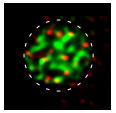 0.08±0.01 n: 15	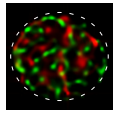 0.17±0.03 n: 11	12
Hxt2GFP Transporter *Sugar*	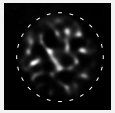	161.69±7.36 n: 132	0.18±0.01 n: 127	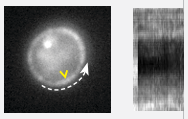 (28)	No Recovery	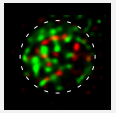 0.06±0.01 n: 16	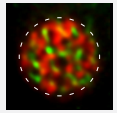 0.37±0.03 n: 27	12
Hxt3GFP Transporter *Sugar*	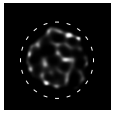	716±19.62 n: 86	0.22±0.01 n: 133	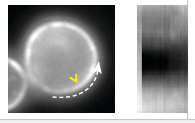 (18)	Recovery T/2: 45.5±5.3 Mf: 74±4 n: 3	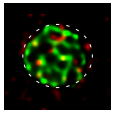 0.12±0.01 n: 45	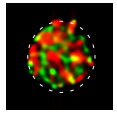 0.25±0.02 n: 19	12
Itr2GFP Transporter *Sugar*	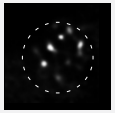	55.89±3.43 n: 50	0.05±0.01 n: 29	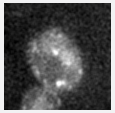 (signal too low)		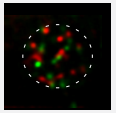 0.1±0.02 n: 10	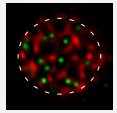 0.09±0.01 n: 19	12
Mep2GFP Transporter *Anorganic Acid*	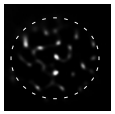	9.43±1.19 n: 82	0.05±0 n: 46	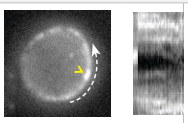 (18)	Techn. Limiting (no recovery)	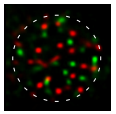 0.03±0.01 n: 10	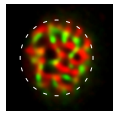 0.14±0.03 n: 14	10
Mid2GFP Sensors *Stress*	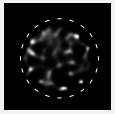	94.4±2.58 n: 111	0.13±0.01 n: 70	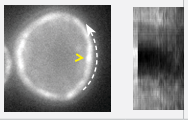 (33)	Recovery T/2: 58.3±17.2 Mf: 35±4 n: 5	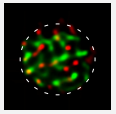 0.04±0 n: 24	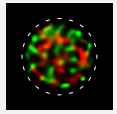 0.18±0.03 n: 9	1
Mnr2GFP Transporter *Ion*	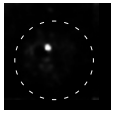	14.57±0.41 n: 69	0.04±0 n: 47	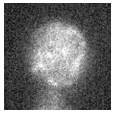 (signal too low)		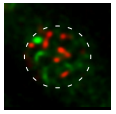 0.1±0.01 n: 16	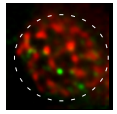 0.15±0.02 n: 31	2

Protein Class	TIRFM	Membrane Abundance	Network Factor	Equator FRAP 5min.		Recovery	Colocalization with Sur7RFP		Colocalization with Pma1RFP		No. TMS
Mrh1GFP Unknown	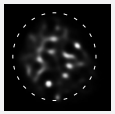	799.36±32.51 n: 70	0.18±0.01 n: 43	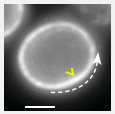	(22)	No Recovery	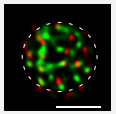	0.05±0.01 n: 15	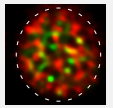	0.48±0.02 n: 28	7
Mss4GFP Signalling *Kinase Activity*	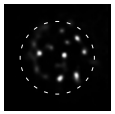	14.46±0.45 n: 66	0.05±0 n: 69	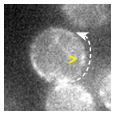	(9)	Techn. Limitation (no recovery)	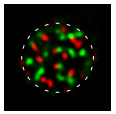	0.04±0.01 n: 16	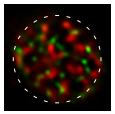	0.12±0.02 n: 14	-
Nha1GFP Transporter *Ion*	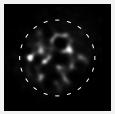	35.14±1.43 n: 103	0.08±0 n: 50	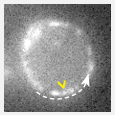	(4)	Techn. Limitation (no recovery)	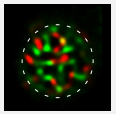	0.05±0.01 n: 23	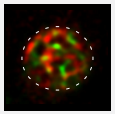	0.19±0.02 n: 27	13
Pdr5GFP Transporter *Multidrug*	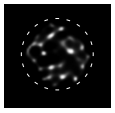	360.21±56.54 n: 60	0.17±0.01 n: 21	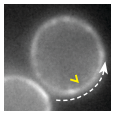	(25)	Recovery T/2: 36.7±9.9 Mf: 32±2 n: 5	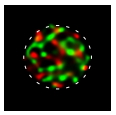	0.05±0.01 n: 21	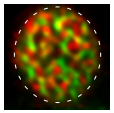	0.2±0.04 n: 7	13
Pdr12GFP Transporter *Multidrug*	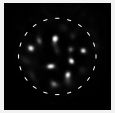	105.96±4.36 n: 120	0.07±0.01 n: 28	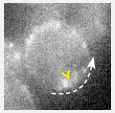	(6)	Techn. Limiting (no recovery)	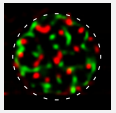	0.06±0.01 n: 8	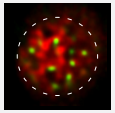	0.52±0.03 n: 13	13
Pil1GFP Metabolism *Eisosome*	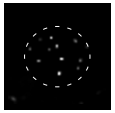	595.25±18.7 n: 73	0.02±0 n: 37	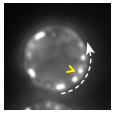	(12)	No Recovery	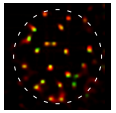	0.59±0.03 n: 22	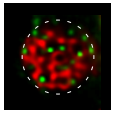	0.02±0.01 n: 15	-
Pma1GFP Transporter *Ion*	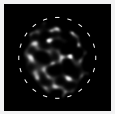	540.29±15.64 n: 118	0.21±0.01 n: 41	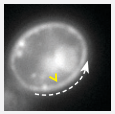	(19)	Recovery T/2: 12.5±3.3 Mf: 27±6 n: 4	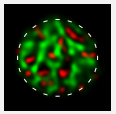	0.04±0.01 n: 23	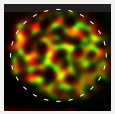	0.75±0.02 n: 9	10
Pmp1GFP Transporter *Ion*	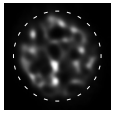	582.7±17.32 n: 109	0.28±0.01 n: 73	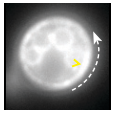	(19)	Recovery T/2: 5.8±1.2 Mf: 21±2 n: 7	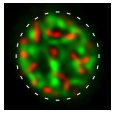	0.07±0.01 n: 31	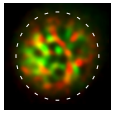	0.58±0.05 n: 7	1

Protein Class	TIRFM	Membrane Abundance	Network Factor	Equator FRAP 5min.		Recovery	Colocalization with Sur7RFP		Colocalization with Pma1RFP		No. TMS
Psr1GFP Signalling *Phosphatase Activity*	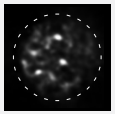	33.7±0.76 n: 102	0.17±0.01 n: 28	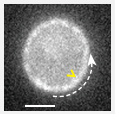	 (19)*	Techn. Limiting (no recovery)	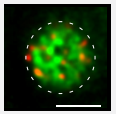	0.15±0.02 n: 16	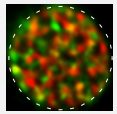	0.45±0.02 n: 12	l.a.
Ras2GFP Signalling *GTPase*	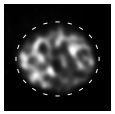	251.28±5.49 n: 157	0.29±0.01 n: 35	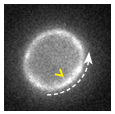	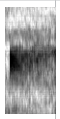 (29)*	Recovery T/2: 1.6±.3 Mf: 67±5 n: 4	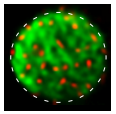	0.12±0.01 n: 18	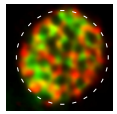	0.54±0.02 n: 17	l.a.
Rax2GFP Signalling *Bud Site Selection*	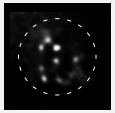	40.6±1.36 n: 71	0.05±0 n: 29	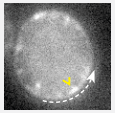	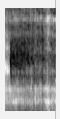 (21)	Techn. Limiting (no recovery)	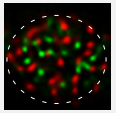	0.03±0.01 n: 19	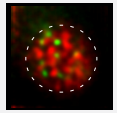	0.15±0.02 n: 10	1
Rsn1GFP Unknown	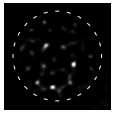	70.01±1.84 n: 129	0.06±0 n: 27	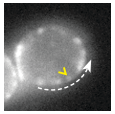	 (18)	Recovery T/2: 15.2±1.2 Mf: 27±4 n: 4	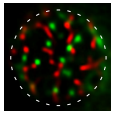	0.04±0.01 n: 17	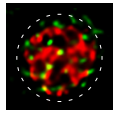	0.1±0.01 n: 10	10
Sho1GFP Sensors *Stress*	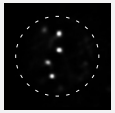	23.43±1.6 n: 42	0.04±0 n: 25	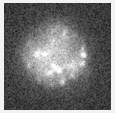	(signal too low)		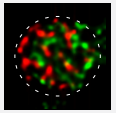	0.02±0 n: 14	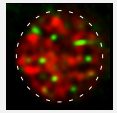	0.15±0.02 n: 11	4
Sln1GFP Sensors *Stress*	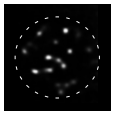	15.96±0.39 n: 94	0.06±0 n: 32	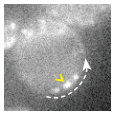	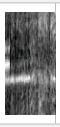 (9)	Techn. Limiting (no recovery)	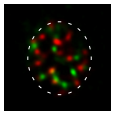	0.06±0.01 n: 24	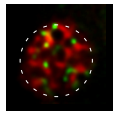	0.16±0.01 n: 8	2
Ssy1GFP Sensors *Amino Acids*	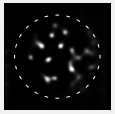	8.56±0.19 n: 72	0.01±0 n: 43	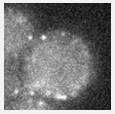	(signal too low)		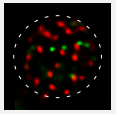	0.01±0 n: 16	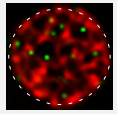	0.04±0 n: 27	12
Sur7GFP Metabolism *Eisosomes*	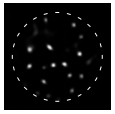	256.62±9.31 n: 75	0.03±0 n: 42	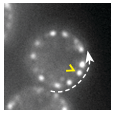	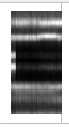 (7)	No Recovery	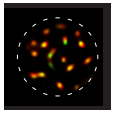	0.72±0.02 n: 20	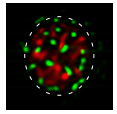	0.02±0.01 n: 12	4

Protein Class	TIRFM	Membrane Abundance	Network Factor	Equator FRAP 5min.		Recovery	Colocalization with Sur7RFP		Colocalization with Pma1RFP		No. TMS
Tcb3GFP Unknown	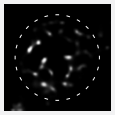	119.99±3.78 n: 92	0.06±0.01 n: 23	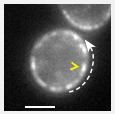	(9)	Recovery T/2: 49.3±8.4 Mf: 57±7 n: 7	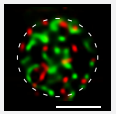	0.02±0 n: 11	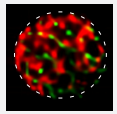	0.07±0.01 n: 12	1
Thi7GFP Transporter *Vitamin*	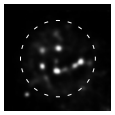	42.49±4.85 n: 65	0.11±0.01 n: 36	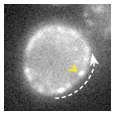	(35)	Recovery T/2: 20.3±3.5 Mf: 38±7 n: 3	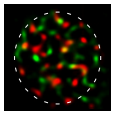	0.06±0.01 n: 12	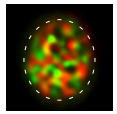	0.48±0.04 n: 8	12
Tpo1GFP Transporter *Amino Acids*	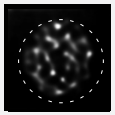	156.09±5.56 n: 95	0.13±0 n: 73	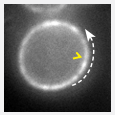	(49)	Recovery T/2: 31.2±4.1 Mf: 24±3 n: 11	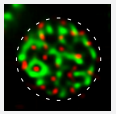	0.05±0.01 n: 23	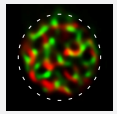	0.3±0.02 n: 27	12
Vht1GFP Transporter *Vitamin*	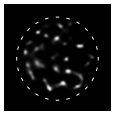	40.63±2.63 n: 72	0.12±0.01 n: 64	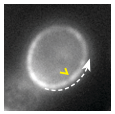	(15)	Recovery T/2: 24.1±10.5 Mf: 25±3 n: 4	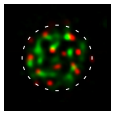	0.08±0.01 n: 14	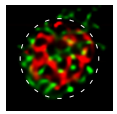	0.05±0.01 n: 14	9
YLR413WGFP Unknown	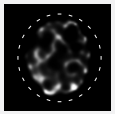	449.99±14.2 n: 91	0.11±0.01 n: 21	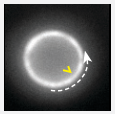	(13)	Recovery T/2: 50.2±12.2 Mf: 29±2 n: 5	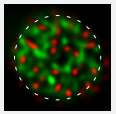	0.17±0.03 n: 10	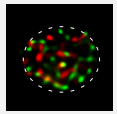	0.16±0.02 n: 11	3
Yor1GFP Sensors *Stress*	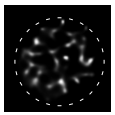	49.61±2.24 n: 77	.07±0 n: 32	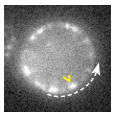	(18)	Techn. Limiting (no recovery)	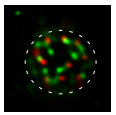	0.04±0.01 n: 9	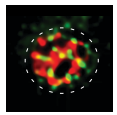	0.19±0.01 n: 23	11

Chapter 9

Abbreviations

AA	Amino acid
ATP–binding cassette	ABC
BAR	Bin Amphiphysin Rvs
BSP	Bathophenanthroline disulphonate
CL	Cardiolipin
ECM	Extra Cellular Matrix
ER	Endoplasmatic Reticulum
FRAP	Fluorescence Recovery after Photobleaching
FRET	Forster Resonance Energy Transfer
GB	GFP-binder
GFP	Green fluorescent protein
GPCRS	G protein coupled receptor
GPI	Glycosylphosphatidylinositol
HECT	Homologous to E6-associated protein C-terminus
IPC	Inositolphosphoceramide
KO	Knockout
L$_d$	Lipid disordered
L$_o$	Lipid ordered
LatB	Latrunculin B
LBD	Lipid-binding domain
MF	Mobile fraction

MHC	Major histocompatibility complex
$M(IP)_2C$	Manose di-inositolphosphate ceramide
MIPC	Manose inositol phosphoceramide
NPF	Nucleation promoting factors
n.d.	not determined
PALM	Particle Activation Light Microcopy
PALM	Photoactivated Localisation Microscopy
PCR	Polymerase chain reaction
PG	Phosphatidylglycerol
PH	Pleckstrin Homology
PI	Phosphatidylinositol
PL	Phospholipid
PM	plasma membrane
PS	Phosphatidylserine
PSF	Point spread function
RFP	Red fluorescent protein
RING	Really interesting new protein
SGD	*Saccharomyces* genome database
SIM	Structured illumination microscopy
SL	Sphingolipids
SRP	Signal recognition particle
STED	Stimulated Emission Depletion
TIRFM	Total internal reflection fluorescence microscopy
TM	Transmembrane
TMS	Transmembrane segment
TS	Temperature sensitive
Ub	Ubiquitin
WASP	Wiskott–Aldrich syndrome protein
WT	Wild type

Chapter 10

Curriculum Vitae

Personal Information

Name	Felix Spira
Address	Weissenburgerstr. 20, 80337 Munich
Email	spira@biochem.mpg.de
Date of Birth	28.01.1980
Place of Birth	Dillenburg, Germany
Nationality	German
Languages	German (mother tongue), English (fluent), Latin (latinum)

Education

03/2007 – present	PhD student at the Max Planck Institute of Biochemistry in Munich, supervisor Dr. Roland Wedlich-Soeldner
12/2006	Diploma in biology, *Rheinische-Friedrich-Wilhelms* University, Bonn, Germany
12/2005 – 11/2006	Diploma research year at the Center of Advanced European Studies and Research (caesar), Germany
07/2004 – 11/2005	Study of Biology at the *Rheinische-Friedrich-Wilhelms* University, Bonn, supervisor Dr. Hanjo Hennemann
07/2003 – 06/2004	Exchange year,Uppsala University, Uppsala, Sweden
10/2000 – 2/2003	Undergraduate studies in biology at the *Rheinische-Friedrich-Wilhelms* University, Bonn, Germany
1998 – 1999	Social service *evangelische Kirchengemeinde Adenau* protestant church, Adenau, Germany
1995 – 1998	Gymnasium *Erich - Klausener - Gymnasium*, Adenau, Germany; degree: Abitur

Teaching Experience

2011	BioImaging practical - Total Internal Reflection Microscopy
2007 – 2012	Supervision of several students, including Master and Bachelor thesis

Meetings and Conferences

16/08/2011 – 20/08/2011	Cold Spring Harbor, Yeast: Poster Presentation
17/03/2011 – 20/03/2011	Seeing is believing: Oral Presentation
10/10/2010 – 13/10/2010	Patchy Prague: Oral Presentation
04/09/2010 – 07/09/2010	EMBO Meeting Barcelona, Spain: Poster Presentation
10/01/2010 – 15/01/2010	Keystone Conference, Molecular Basis for Biological Membrane Organisation and Dynamics (A5): Poster Presentation
29/08/2009 – 01/09/2009	EMBO Meeting Amsterdam, Netherlands: Poster Presentation
01/12/2007 – 05/12/2007	ASCB 47th Annual Meeting Washington, USA: Poster Presentation

Publications

Felix Spira, Nikola S. Mueller, Gisela Beck, Philipp von Olshausen, Joachim Beig, Roland Wedlich-Soldner. Patchwork organization of the yeast plasma membrane into numerous coexisting domains, NCB (under revision)

Felix Spira, Julia Dominguez-Escobar,Nikola Mueller, Roland Wedlich-Soldner. Visualization of cortex organization and dynamics in microorganisms using Total Internal Reflection Fluorescence microscopy, Jove

Nikola Mueller, Roland Wedlich-Soldner, **Felix Spira**. Lateral organization of biological membranes by protein-lipid interactions, MMB (review, under revision)

Chapter 11

Author contribution

All FRAP analyses were conducted with a Matlab GUI developed by Nikola Müller. Nikola Müller contributed greatly to the successful completion of the membrane organisation project. She developed the tools for handling of large datasets. In addition she developed the linearised manders overlap coefficient and analysed the co-localisation data. Correlation analysis, network-factor calculations, determination of peripheral GFP signals, as well as data-mining were performed by Nikola Müller. She contributed either by generating/analysing the data and creating the following figures (Figure 3.2 - Figure 3.20). Super-resolution images were acquired in collaboration with Philipp von Olshausen in Freiburg.

Chapter 12

Declaration

Declaration according to the "Promotionsordnung der LMU München für die Fakultät Biologie"

Hiermit erkläre ich, dass die vorgelegte Arbeit in der Zeit vom 1.03.2007 bis März 2012 in der Arbeitsgruppe zelluläre Dynamik und Musterbildung von Dr. Roland Wedlich-Söldner am Max-Planck-Institut für Biochemie in Martinsried entstanden ist. Die Arbeit wird erstmalig einer Prüfungskommission vorgelegt und weiterhin habe ich weder an einem anderen Ort eine Promotion angestrebt noch angemeldet noch versucht eine Doktorprüfung abzulegen. Ich versichere hiermit an Eides statt, dass die vorgelegte Dissertation von mir selbständig und ohne unerlaubte Hilfe angefertigt wurde.

München, den 19. März 2012, Felix Spira

Chapter 13

Danksagung

Ich möchte all den Menschen danken, die wissenschaftlich und persönlich ihren Beitrag zu dieser Arbeit geleistet haben. Besonderer Dank gilt meinen Betreuern und Gutachtern:
Dr. Roland Wedlich-Söldner, der mir ermöglicht hat an diesem Projekt zu arbeiten und der mir immer mit Rat und Tat zur Seite stand und es mir erlaubte auch eigene Ideen zu verwirklichen.
Prof. Dr. Stefan Jentsch, dass er die Rolle meines Doktorvaters übernommen hat.
Prof. Dr. Charles David für die Erstellung des Zweitgutachtens.
Allen weiteren Mitgliedern der Prüfungskommission.

Meinem Kollaborationspartner Philipp von Oelshausen für super-resolution Bildern von Membranproteinen und einem “Teufelsritt” auf seinem Rad durch Freiburg.

Markus, für jahrlange Freundschaft und Unterstützung in allen Lebenslagen und der mir Hilft den Blick auf das wesentliche nicht zu verlieren.
Maurits, für gute Gespräche und einem unverfälschten kritischen Blick und Urteile mit Augenmaß.
Nils, ohne den ich meine Arbeit nicht beendet hätte, Kaffee in unserem Wohnzimmer und schöne Touren in den Bergen.

Britta, für eine schöne gemeinsame Zeit.

Volker und Daniel aus der Kletter-WG für eine lustige und entspannte Zeit.

Nikola, für die spannende Zeit die wir mit dem Membranprojekt verbracht haben, die Entdeckung des Alignierbuttons, fortwährende Unterstützung in allen Lebenslagen und eine treue Boulderpartnerin.

Roland, für fortwährende Klettermotivation, seine ehrliche konstruktive Art und viele schöne Skitouren.
Julia, für eine extrem lustige und schöne Zeit und die Erkenntnis das Jogaschuhe nicht immer nötig sind.
Gisela, für ihre Hilfe bei den aller-kniffligsten Klonierungen, Bodenständigkeit und ihre herzliche Art.

Anoope für seine lustige und unverfälschte Art.

Tina, für den Austausch von guter Musik und diverser Konzertbesuche.

Christoph, für den Beweis das Balkan Beat doch eine ernstzunehmende Musikrichtung darstellt und ziellosem Schwadronieren.

Alvaro, für ehrliche Diskussion über das Membranprojekt.
Michael für viele Diskussionen und eine gute Zeit

Scheibenbremsenmela und Orthovoxfrank für eine lustige Zeit in der Dachauer, guter Musik, vielen Konzertbesuchen und überhaupt schönen Abenden.

Frauke für Wein auf dem Balkon, treue Umzugshelferin und Hilfe in jeder Lebenslage.

den ehemaligen MPI-/Labormitgliedern, Garwin, Janina und Steffi, sowie dem Walther Labor für die gute Zeit auch über die Laborgrenzen hinaus.

Meiner Familie: Meinen Eltern und meinen Geschwistern für ihre bedingungslose Unterstützung in allen Lebenslagen.

Bibliography

Daniel Abankwa, Alemayehu A Gorfe, and John F Hancock. Mechanisms of ras membrane organization and signalling: Ras on a rocker. *Cell Cycle*, 7(17):2667–2673, Sep 2008.

E. Abbe. Beitraege zur theorie des mikroskops und der mikroskopischen wahrnehmung. *Archiv fuer Mikroskopische Anatomie*, 9:413–418, 1873. ISSN 0176-7364. 10.1007/BF02956173.

Fumiyoshi Abe and Toshiki Hiraki. Mechanistic role of ergosterol in membrane rigidity and cycloheximide resistance in saccharomyces cerevisiae. *Biochim Biophys Acta*, 1788 (3):743–752, Mar 2009. doi: 10.1016/j.bbamem.2008.12.002.

Soheil Aghamohammadzadeh and Kathryn R Ayscough. Differential requirements for actin during yeast and mammalian endocytosis. *Nat Cell Biol*, 11(8):1039–1042, Aug 2009. doi: 10.1038/ncb1918.

Pablo S Aguilar, Florian Frohlich, Michael Rehman, Mike Shales, Igor Ulitsky, Agustina Olivera-Couto, Hannes Braberg, Ron Shamir, Peter Walter, Matthias Mann, Christer S Ejsing, Nevan J Krogan, and Tobias C Walther. A plasma-membrane e-map reveals links of the eisosome with sphingolipid metabolism and endosomal trafficking. *Nat Struct Mol Biol*, 17(7):901–908, Jul 2010. doi: 10.1038/nsmb.1829.

M. Ahmad and H. Bussey. Yeast arginine permease: nucleotide sequence of the can1 gene. *Curr Genet*, 10(8):587–592, 1986.

Sergey A Akimov, Vladimir A J Frolov, Peter I Kuzmin, Joshua Zimmerberg, Yuri A Chizmadzhev, and Fredric S Cohen. Domain formation in membranes caused by lipid wetting of protein. *Phys Rev E Stat Nonlin Soft Matter Phys*, 77(5 Pt 1):051901, May 2008.

Francisco J Alvarez, Lois M Douglas, Adam Rosebrock, and James B Konopka. The sur7 protein regulates plasma membrane organization and prevents intracellular cell wall growth in candida albicans. *Mol Biol Cell*, 19(12):5214–5225, Dec 2008. doi: 10.1091/mbc.E08-05-0479.

Olaf S Andersen and Roger E Koeppe. Bilayer thickness and membrane protein function: an energetic perspective. *Annu Rev Biophys Biomol Struct*, 36:107–130, 2007. doi: 10.1146/annurev.biophys.36.040306.132643.

R. G. Anderson. Caveolae: where incoming and outgoing messengers meet. *Proc Natl Acad Sci U S A*, 90(23):10909–10913, Dec 1993.

Richard G W Anderson and Ken Jacobson. A role for lipid shells in targeting proteins to caveolae, rafts, and other lipid domains. *Science*, 296(5574):1821–1825, Jun 2002. doi: 10.1126/science.1068886.

Allison Armstrong and Kodi S Ravichandran. Phosphatidylserine receptors: what is the new rage? *EMBO Rep*, 12(4):287–288, Apr 2011. doi: 10.1038/embor.2011.41.

D. Axelrod. Selective imaging of surface fluorescence with very high aperture microscope objectives. *J Biomed Opt*, 6(1):6–13, Jan 2001. doi: 10.1117/1.1335689.

D. Axelrod, N. L. Thompson, and T. P. Burghardt. Total internal inflection fluorescent microscopy. *J Microsc*, 129(Pt 1):19–28, Jan 1983.

Daniel Axelrod and Geneva M Omann. Combinatorial microscopy. *Nat Rev Mol Cell Biol*, 7(12):944–952, Dec 2006. doi: 10.1038/nrm2062.

Luis A Bagatolli, John H Ipsen, Adam C Simonsen, and Ole G Mouritsen. An outlook on organization of lipids in membranes: Searching for a realistic connection with the organization of biological membranes. *Prog Lipid Res*, May 2010a. doi: 10.1016/j.plipres.2010.05.001.

Luis A Bagatolli, John H Ipsen, Adam C Simonsen, and Ole G Mouritsen. An outlook on organization of lipids in membranes: searching for a realistic connection with the organization of biological membranes. *Prog Lipid Res*, 49(4):378–389, Oct 2010b. doi: 10.1016/j.plipres.2010.05.001.

Michele Bastiani and Robert G Parton. Caveolae at a glance. *J Cell Sci*, 123(Pt 22): 3831–3836, Nov 2010. doi: 10.1242/jcs.070102.

Naima Belgareh-Touze, Sebastien Leon, Zoi Erpapazoglou, Marta Stawiecka-Mirota, Daniele Urban-Grimal, and Rosine Haguenauer-Tsapis. Versatile role of the yeast ubiquitin ligase rsp5p in intracellular trafficking. *Biochem Soc Trans*, 36(Pt 5):791–796, Oct 2008. doi: 10.1042/BST0360791.

B. Benito, E. Moreno, and R. Lagunas. Half-life of the plasma membrane atpase and its activating system in resting yeast cells. *Biochim Biophys Acta*, 1063(2):265–268, Apr 1991.

Doris Berchtold and Tobias C Walther. Torc2 plasma membrane localization is essential for cell viability and restricted to a distinct domain. *Mol Biol Cell*, 20(5):1565–1575, Mar 2009. doi: 10.1091/mbc.E08-10-1001.

Eric Betzig, George H Patterson, Rachid Sougrat, O. Wolf Lindwasser, Scott Olenych, Juan S Bonifacino, Michael W Davidson, Jennifer Lippincott-Schwartz, and Harald F Hess. Imaging intracellular fluorescent proteins at nanometer resolution. *Science*, 313 (5793):1642–1645, Sep 2006. doi: 10.1126/science.1127344.

Thorsten Brach, Tanja Specht, and Marko Kaksonen. Reassessment of the role of plasma membrane domains in the regulation of vesicular traffic in yeast. *J Cell Sci*, Jan 2011. doi: 10.1242/jcs.078519.

D. A. Brown and J. K. Rose. Sorting of gpi-anchored proteins to glycolipid-enriched membrane subdomains during transport to the apical cell surface. *Cell*, 68(3):533–544, Feb 1992.

A. E. Carlsson, A. D. Shah, D. Elking, T. S. Karpova, and J. A. Cooper. Quantitative analysis of actin patch movement in yeast. *Biophys J*, 82(5):2333–2343, May 2002. doi: 10.1016/S0006-3495(02)75579-3.

George M Carman and Gil-Soo Han. Regulation of phospholipid synthesis in the yeast saccharomyces cerevisiae. *Annu Rev Biochem*, 80:859–883, Jun 2011. doi: 10.1146/annurev-biochem-060409-092229.

P. J. Casey. Protein lipidation in cell signaling. *Science*, 268(5208):221–225, Apr 1995.

D Chapman. *BIOLOGICAL MEMBRANES*. 1984. ISBN 978-0-12-168546-1.

Stephanie Charrin, FranÃğois le Naour, Olivier Silvie, Pierre-Emmanuel Milhiet, Claude Boucheix, and Eric Rubinstein. Lateral organization of membrane proteins: tetraspanins spin their web. *Biochem J*, 420(2):133–154, Jun 2009. doi: 10.1042/BJ20082422.

Abhishek Chaudhuri, Bhaswati Bhattacharya, Kripa Gowrishankar, Satyajit Mayor, and Madan Rao. Spatiotemporal regulation of chemical reactions by active cytoskeletal remodeling. *Proc Natl Acad Sci U S A*, 108(36):14825–14830, Sep 2011. doi: 10.1073/pnas.1100007108.

Jose Angel Clemente-Ramos, Rebeca MartÃŋn-GarcÃŋa, Mohammad R Sharifmoghadam, Mami Konomi, Masako Osumi, and M-Henar Valdivieso. The tetraspan protein dni1p is required for correct membrane organization and cell wall remodelling during mating in schizosaccharomyces pombe. *Mol Microbiol*, 73(4):695–709, Aug 2009. doi: 10.1111/j.1365-2958.2009.06800.x.

Gene Ontology Consortium. The gene ontology in 2010: extensions and refinements. *Nucleic Acids Res*, 38(Database issue):D331–D335, Jan 2010a. doi: 10.1093/nar/gkp1018.

UniProt Consortium. The universal protein resource (uniprot) in 2010. *Nucleic Acids Res*, 38(Database issue):D142–D148, Jan 2010b. doi: 10.1093/nar/gkp846.

F. Cornelius. Modulation of na,k-atpase and na-atpase activity by phospholipids and cholesterol. i. steady-state kinetics. *Biochemistry*, 40(30):8842–8851, Jul 2001.

Unal Coskun and Kai Simons. Membrane rafting: From apical sorting to phase segregation. *FEBS Lett*, Dec 2009. doi: 10.1016/j.febslet.2009.12.043.

Unal Coskun and Kai Simons. Cell membranes: the lipid perspective. *Structure*, 19(11): 1543–1548, Nov 2011. doi: 10.1016/j.str.2011.10.010.

L. Ashley Cowart and Lina M Obeid. Yeast sphingolipids: recent developments in understanding biosynthesis, regulation, and function. *Biochim Biophys Acta*, 1771(3):421–431, Mar 2007. doi: 10.1016/j.bbalip.2006.08.005.

Arupratan Das, Brian D Slaughter, Jay R Unruh, William D Bradford, Richard Alexander, Boris Rubinstein, and Rong Li. Flippase-mediated phospholipid asymmetry promotes

fast cdc42 recycling in dynamic maintenance of cellÂăpolarity. *Nat Cell Biol*, 14(3): 304–310, 2012. doi: 10.1038/ncb2444.

Armaity P Davierwala, Jennifer Haynes, Zhijian Li, Renee L Brost, Mark D Robinson, Lisa Yu, Sanie Mnaimneh, Huiming Ding, Hongwei Zhu, Yiqun Chen, Xin Cheng, Grant W Brown, Charles Boone, Brenda J Andrews, and Timothy R Hughes. The synthetic genetic interaction spectrum of essential genes. *Nat Genet*, 37(10):1147–1152, Oct 2005. doi: 10.1038/ng1640.

Jorge Bernardino de la Serna, Greger Oradd, Luis A Bagatolli, Adam C Simonsen, Derek Marsh, Goran Lindblom, and Jesus Perez-Gil. Segregated phases in pulmonary surfactant membranes do not show coexistence of lipid populations with differentiated dynamic properties. *Biophys J*, 97(5):1381–1389, Sep 2009. doi: 10.1016/j.bpj.2009.06.040.

P. F. Devaux. Protein involvement in transmembrane lipid asymmetry. *Annu Rev Biophys Biomol Struct*, 21:417–439, 1992. doi: 10.1146/annurev.bb.21.060192.002221.

J. R. Didsbury, R. J. Uhing, and R. Snyderman. Isoprenylation of the low molecular mass gtp-binding proteins rac 1 and rac 2: possible role in membrane localization. *Biochem Biophys Res Commun*, 171(2):804–812, Sep 1990.

Julia Dominguez-Escobar, Arnaud Chastanet, Alvaro H Crevenna, Vincent Fromion, Roland Wedlich-Soldner, and Rut Carballido-LÃşpez. Processive movement of mreb-associated cell wall biosynthetic complexes in bacteria. *Science*, 333(6039):225–228, Jul 2011. doi: 10.1126/science.1203466.

Adam D Douglass and Ronald D Vale. Single-molecule microscopy reveals plasma membrane microdomains created by protein-protein networks that exclude or trap signaling molecules in t cells. *Cell*, 121(6):937–950, Jun 2005. doi: 10.1016/j.cell.2005.04.009.

Vincent Dupres, Yves F DufrÃłne, and Jurgen J Heinisch. Measuring cell wall thickness in living yeast cells using single molecular rulers. *ACS Nano*, 4(9):5498–5504, Sep 2010. doi: 10.1021/nn101598v.

Christian Eggeling, Christian Ringemann, Rebecca Medda, Gunter Schwarzmann, Konrad Sandhoff, Svetlana Polyakova, Vladimir N Belov, Birka Hein, Claas von Middendorff, Andreas Schonle, and Stefan W Hell. Direct observation of the nanoscale dynamics of

membrane lipids in a living cell. *Nature*, 457(7233):1159–1162, Feb 2009. doi: 10.1038/nature07596.

D. Eide, S. Davis-Kaplan, I. Jordan, D. Sipe, and J. Kaplan. Regulation of iron uptake in saccharomyces cerevisiae. the ferrireductase and fe(ii) transporter are regulated independently. *J Biol Chem*, 267(29):20774–20781, Oct 1992.

Sharon Eisenberg, Alison J Beckett, Ian A Prior, Frank J Dekker, Christian Hedberg, Herbert Waldmann, Marcelo Ehrlich, and Yoav I Henis. Raft protein clustering alters n-ras membrane interactions and activation pattern. *Mol Cell Biol*, 31(19):3938–3952, Oct 2011. doi: 10.1128/MCB.05570-11.

Christer S Ejsing, Julio L Sampaio, Vineeth Surendranath, Eva Duchoslav, Kim Ekroos, Robin W Klemm, Kai Simons, and Andrej Shevchenko. Global analysis of the yeast lipidome by quantitative shotgun mass spectrometry. *Proc Natl Acad Sci U S A*, 106(7): 2136–2141, Feb 2009. doi: 10.1073/pnas.0811700106.

James I Elliott, Annmarie Surprenant, Federica M Marelli-Berg, Joanne C Cooper, Robin L Cassady-Cain, Carol Wooding, Kenneth Linton, Denis R Alexander, and Christopher F Higgins. Membrane phosphatidylserine distribution as a non-apoptotic signalling mechanism in lymphocytes. *Nat Cell Biol*, 7(8):808–816, Aug 2005. doi: 10.1038/ncb1279.

K. Emoto and M. Umeda. An essential role for a membrane lipid in cytokinesis. regulation of contractile ring disassembly by redistribution of phosphatidylethanolamine. *J Cell Biol*, 149(6):1215–1224, Jun 2000.

Helge Ewers, Winfried Romer, Alicia E Smith, Kirsten Bacia, Serge Dmitrieff, Wengang Chai, Roberta Mancini, Jurgen Kartenbeck, Valerie Chambon, Ludwig Berland, Ariella Oppenheim, Gunter Schwarzmann, Ten Feizi, Petra Schwille, Pierre Sens, Ari Helenius, and Ludger Johannes. Gm1 structure determines sv40-induced membrane invagination and infection. *Nat Cell Biol*, 12(1):11–8; sup pp 1–12, Jan 2010. doi: 10.1038/ncb1999.

Gregory D Fairn, Martin Hermansson, Pentti Somerharju, and Sergio Grinstein. Phosphatidylserine is polarized and required for proper cdc42 localization and for development of cell polarity. *Nat Cell Biol*, Oct 2011. doi: 10.1038/ncb2351.

Reto Fiolka, Markus Beck, and Andreas Stemmer. Structured illumination in total internal reflection fluorescence microscopy using a spatial light modulator. *Opt Lett*, 33(14):1629–1631, Jul 2008.

Hana Flegelova and Hana Sychrova. Mammalian nhe2 na(+)/h+ exchanger mediates efflux of potassium upon heterologous expression in yeast. *FEBS Lett*, 579(21):4733–4738, Aug 2005. doi: 10.1016/j.febslet.2005.07.046.

Florian Frohlich, Karen Moreira, Pablo S Aguilar, Nina C Hubner, Matthias Mann, Peter Walter, and Tobias C Walther. A genome-wide screen for genes affecting eisosomes reveals nce102 function in sphingolipid signaling. *J Cell Biol*, 185(7):1227–1242, Jun 2009. doi: 10.1083/jcb.200811081.

T. Fujimoto, M. Hayashi, M. Iwamoto, and Y. Ohno-Iwashita. Crosslinked plasmalemmal cholesterol is sequestered to caveolae: analysis with a new cytochemical probe. *J Histochem Cytochem*, 45(9):1197–1205, Sep 1997.

Akikazu Fujita, Jinglei Cheng, Kumi Tauchi-Sato, Tadaomi Takenawa, and Toyoshi Fujimoto. A distinct pool of phosphatidylinositol 4,5-bisphosphate in caveolae revealed by a nanoscale labeling technique. *Proc Natl Acad Sci U S A*, 106(23):9256–9261, Jun 2009. doi: 10.1073/pnas.0900216106.

Takahiro Fujiwara, Ken Ritchie, Hideji Murakoshi, Ken Jacobson, and Akihiro Kusumi. Phospholipids undergo hop diffusion in compartmentalized cell membrane. *J Cell Biol*, 157(6):1071–1081, Jun 2002. doi: 10.1083/jcb.200202050.

B. Gagny, A. Wiederkehr, P. Dumoulin, B. Winsor, H. Riezman, and R. Haguenauer-Tsapis. A novel eh domain protein of saccharomyces cerevisiae, ede1p, involved in endocytosis. *J Cell Sci*, 113 (Pt 18):3309–3319, Sep 2000.

H. J. Galla and E. Sackmann. Chemically induced lipid phase separation in model membranes containing charged lipids: a spin label study. *Biochim Biophys Acta*, 401(3): 509–529, Sep 1975.

Oriol Gallego, Matthew J Betts, Jelena Gvozdenovic-Jeremic, Kenji Maeda, Christian Matetzki, Carmen Aguilar-Gurrieri, Pedro Beltran-Alvarez, Stefan Bonn, Carlos Fernandez-Tornero, Lars Juhl Jensen, Michael Kuhn, Jamie Trott, Vladimir Rybin, Christoph W Muller, Peer Bork, Marko Kaksonen, Robert B Russell, and Anne-Claude

Gavin. A systematic screen for protein-lipid interactions in saccharomyces cerevisiae. *Mol Syst Biol*, 6:430, Nov 2010. doi: 10.1038/msb.2010.87.

Alok Gambhir, Gyongyi Hangyas-Mihalyne, Irina Zaitseva, David S Cafiso, Jiyao Wang, Diana Murray, Srinivas N Pentyala, Steven O Smith, and Stuart McLaughlin. Electrostatic sequestration of pip2 on phospholipid membranes by basic/aromatic regions of proteins. *Biophys J*, 86(4):2188–2207, Apr 2004. doi: 10.1016/S0006-3495(04)74278-2.

Sourav Ganguly, Pushpendra Singh, Raman Manoharlal, Rajendra Prasad, and Amitabha Chattopadhyay. Differential dynamics of membrane proteins in yeast. *Biochem Biophys Res Commun*, Jul 2009. doi: 10.1016/j.bbrc.2009.07.054.

K. Gawrisch, J. A. Barry, L. L. Holte, T. Sinnwell, L. D. Bergelson, and J. A. Ferretti. Role of interactions at the lipid-water interface for domain formation. *Mol Membr Biol*, 12(1):83–88, 1995.

Nathalie George, Horst Pick, Horst Vogel, Nils Johnsson, and Kai Johnsson. Specific labeling of cell surface proteins with chemically diverse compounds. *J Am Chem Soc*, 126(29):8896–8897, Jul 2004. doi: 10.1021/ja048396s.

Sina Ghaemmaghami, Won-Ki Huh, Kiowa Bower, Russell W Howson, Archana Belle, Noah Dephoure, Erin K O'Shea, and Jonathan S Weissman. Global analysis of protein expression in yeast. *Nature*, 425(6959):737–741, Oct 2003. doi: 10.1038/nature02046.

Concepcion Gomez-Mouton, Rosa Ana Lacalle, Emilia Mira, Sonia Jimenez-Baranda, Domingo F Barber, Ana C Carrera, Carlos MartÃŋnez-A, and Santos MaÃśes. Dynamic redistribution of raft domains as an organizing platform for signaling during cell chemotaxis. *J Cell Biol*, 164(5):759–768, Mar 2004. doi: 10.1083/jcb.200309101.

M. L. Greenberg and D. Axelrod. Anomalously slow mobility of fluorescent lipid probes in the plasma membrane of the yeast saccharomyces cerevisiae. *J Membr Biol*, 131(2): 115–127, Jan 1993.

Guido Grossmann, Miroslava Opekarova, Jan Malinsky, Ina Weig-Meckl, and Widmar Tanner. Membrane potential governs lateral segregation of plasma membrane proteins and lipids in yeast. *EMBO J*, 26(1):1–8, Jan 2007. doi: 10.1038/sj.emboj.7601466.

Guido Grossmann, Jan Malinsky, Wiebke Stahlschmidt, Martin Loibl, Ina Weig-Meckl, Wolf B Frommer, Miroslava Opekarova, and Widmar Tanner. Plasma membrane microdomains regulate turnover of transport proteins in yeast. *J Cell Biol*, 183(6):1075–1088, Dec 2008. doi: 10.1083/jcb.200806035.

Xue Li Guan, Cleiton M Souza, Harald Pichler, Gisele Dewhurst, Olivier Schaad, Kentaro Kajiwara, Hirotomo Wakabayashi, Tanya Ivanova, Guillaume A Castillon, Manuele Piccolis, Fumiyoshi Abe, Robbie Loewith, Kouichi Funato, Markus R Wenk, and Howard Riezman. Functional interactions between sphingolipids and sterols in biological membranes regulating cell physiology. *Mol Biol Cell*, 20(7):2083–2095, Apr 2009. doi: 10.1091/mbc.E08-11-1126.

M. G. Gustafsson. Surpassing the lateral resolution limit by a factor of two using structured illumination microscopy. *J Microsc*, 198(Pt 2):82–87, May 2000.

A. T. Hammond, F. A. Heberle, T. Baumgart, D. Holowka, B. Baird, and G. W. Feigenson. Crosslinking a lipid raft component triggers liquid ordered-liquid disordered phase separation in model plasma membranes. *Proc Natl Acad Sci U S A*, 102(18):6320–6325, May 2005. doi: 10.1073/pnas.0405654102.

Scott B Hansen, Xiao Tao, and Roderick MacKinnon. Structural basis of pip2 activation of the classical inward rectifier k+ channel kir2.2. *Nature*, 477(7365):495–498, Sep 2011. doi: 10.1038/nature10370.

T. Harder and K. Simons. Clusters of glycolipid and glycosylphosphatidylinositol-anchored proteins in lymphoid cells: accumulation of actin regulated by local tyrosine phosphorylation. *Eur J Immunol*, 29(2):556–562, Feb 1999. doi: 62;3.0.CO;2-2.

Hirohito Haruki, Junichi Nishikawa, and Ulrich K Laemmli. The anchor-away technique: rapid, conditional establishment of yeast mutant phenotypes. *Mol Cell*, 31(6):925–932, Sep 2008. doi: 10.1016/j.molcel.2008.07.020.

Ramanujan S Hegde and Robert J Keenan. Tail-anchored membrane protein insertion into the endoplasmic reticulum. *Nat Rev Mol Cell Biol*, 12(12):787–798, Dec 2011. doi: 10.1038/nrm3226.

Rainer Heintzmann and Christoph G. Cremer. Laterally modulated excitation microscopy: improvement of resolution by using a diffraction grating. volume 3568, pages 185–196. SPIE, 1999. doi: 10.1117/12.336833.

S. W. Hell and J. Wichmann. Breaking the diffraction resolution limit by stimulated emission: stimulated-emission-depletion fluorescence microscopy. *Opt Lett*, 19(11):780–782, Jun 1994.

Martin E Hemler. Tetraspanin functions and associated microdomains. *Nat Rev Mol Cell Biol*, 6(10):801–811, Oct 2005. doi: 10.1038/nrm1736.

Samuel T Hess, Mukesh Kumar, Anil Verma, Jane Farrington, Anne Kenworthy, and Joshua Zimmerberg. Quantitative electron microscopy and fluorescence spectroscopy of the membrane distribution of influenza hemagglutinin. *J Cell Biol*, 169(6):965–976, Jun 2005. doi: 10.1083/jcb.200412058.

Samuel T Hess, Thanu P K Girirajan, and Michael D Mason. Ultra-high resolution imaging by fluorescence photoactivation localization microscopy. *Biophys J*, 91(11):4258–4272, Dec 2006. doi: 10.1529/biophysj.106.091116.

Ewald H Hettema, Javier Valdez-Taubas, and Hugh R B Pelham. Bsd2 binds the ubiquitin ligase rsp5 and mediates the ubiquitination of transmembrane proteins. *EMBO J*, 23(6): 1279–1288, Mar 2004. doi: 10.1038/sj.emboj.7600137.

L. Hicke, B. Zanolari, and H. Riezman. Cytoplasmic tail phosphorylation of the alpha-factor receptor is required for its ubiquitination and internalization. *J Cell Biol*, 141(2): 349–358, Apr 1998.

S. High and B. M. Abell. Tail-anchored protein biosynthesis at the endoplasmic reticulum: the same but different. *Biochem Soc Trans*, 32(Pt 5):659–662, Nov 2004. doi: 10.1042/BST0320659.

T. Hikiji, K. Miura, K. Kiyono, I. Shibuya, and A. Ohta. Disruption of the cho1 gene encoding phosphatidylserine synthase in saccharomyces cerevisiae. *J Biochem*, 104(6): 894–900, Dec 1988.

Liisa M Hirvonen, Kai Wicker, Ondrej Mandula, and Rainer Heintzmann. Structured illumination microscopy of a living cell. *Eur Biophys J*, 38(6):807–812, Jul 2009. doi: 10.1007/s00249-009-0501-6.

Richard K Hite, Zongli Li, and Thomas Walz. Principles of membrane protein interactions with annular lipids deduced from aquaporin-0 2d crystals. *EMBO J*, 29(10):1652–1658, May 2010. doi: 10.1038/emboj.2010.68.

Thomas Huber, Ana V Botelho, Klaus Beyer, and Michael F Brown. Membrane model for the g-protein-coupled receptor rhodopsin: hydrophobic interface and dynamical structure. *Biophys J*, 86(4):2078–2100, Apr 2004. doi: 10.1016/S0006-3495(04)74268-X.

Won-Ki Huh, James V Falvo, Luke C Gerke, Adam S Carroll, Russell W Howson, Jonathan S Weissman, and Erin K O'Shea. Global analysis of protein localization in budding yeast. *Nature*, 425(6959):686–691, Oct 2003. doi: 10.1038/nature02026.

O. Jensen Ingrell, M. Miller and N. Blom. Netphosyeast: Prediction of protein phosphorylation sites in yeast. *Bioinf*, pages 375–382, 2007.

J. N. Israelachvili. Refinement of the fluid-mosaic model of membrane structure. *Biochim Biophys Acta*, 469(2):221–225, Sep 1977.

P. Jacobs, J. C. Jauniaux, and M. Grenson. A cis-dominant regulatory mutation linked to the argb-argc gene cluster in saccharomyces cerevisiae. *J Mol Biol*, 139(4):691–704, Jun 1980.

Ken Jacobson, Ole G Mouritsen, and Richard G W Anderson. Lipid rafts: at a crossroad between cell biology and physics. *Nat Cell Biol*, 9(1):7–14, Jan 2007. doi: 10.1038/ncb0107-7.

P. W. Janes, S. C. Ley, and A. I. Magee. Aggregation of lipid rafts accompanies signaling via the t cell antigen receptor. *J Cell Biol*, 147(2):447–461, Oct 1999.

Carsten Janke, Maria M Magiera, Nicole Rathfelder, Christof Taxis, Simone Reber, Hiromi Maekawa, Alexandra Moreno-Borchart, Georg Doenges, Etienne Schwob, Elmar Schiebel, and Michael Knop. A versatile toolbox for pcr-based tagging of yeast genes: new fluorescent proteins, more markers and promoter substitution cassettes. *Yeast*, 21 (11):947–962, Aug 2004. doi: 10.1002/yea.1142.

Khuloud Jaqaman, Hirotaka Kuwata, Nicolas Touret, Richard Collins, William S Trimble, Gaudenz Danuser, and Sergio Grinstein. Cytoskeletal control of cd36 diffusion promotes its receptor and signaling function. *Cell*, 146(4):593–606, Aug 2011. doi: 10.1016/j.cell.2011.06.049.

Beata Jastrzebska, Aleksander Debinski, Slawomir Filipek, and Krzysztof Palczewski. Role of membrane integrity on g protein-coupled receptors: Rhodopsin stability and function. *Prog Lipid Res*, 50(3):267–277, Jul 2011. doi: 10.1016/j.plipres.2011.03.002.

Morten Jensen and Ole G Mouritsen. Lipids do influence protein function-the hydrophobic matching hypothesis revisited. *Biochim Biophys Acta*, 1666(1-2):205–226, Nov 2004. doi: 10.1016/j.bbamem.2004.06.009.

Nicoletta Kahya, Deborah A Brown, and Petra Schwille. Raft partitioning and dynamic behavior of human placental alkaline phosphatase in giant unilamellar vesicles. *Biochemistry*, 44(20):7479–7489, May 2005. doi: 10.1021/bi047429d.

Hermann-Josef Kaiser, Daniel Lingwood, Ilya Levental, Julio L Sampaio, Lucie Kalvodova, Lawrence Rajendran, and Kai Simons. Order of lipid phases in model and plasma membranes. *Proc Natl Acad Sci U S A*, 106(39):16645–16650, Sep 2009. doi: 10.1073/pnas.0908987106.

Hermann-Josef Kaiser, Adam Orlowski, Tomasz RÃşg, Thomas K M Nyholm, Wengang Chai, Ten Feizi, Daniel Lingwood, Ilpo Vattulainen, and Kai Simons. Lateral sorting in model membranes by cholesterol-mediated hydrophobic matching. *Proc Natl Acad Sci U S A*, 108(40):16628–16633, Oct 2011. doi: 10.1073/pnas.1103742108.

Marko Kaksonen, Yidi Sun, and David G Drubin. A pathway for association of receptors, adaptors, and actin during endocytic internalization. *Cell*, 115(4):475–487, Nov 2003.

Marko Kaksonen, Christopher P Toret, and David G Drubin. A modular design for the clathrin- and actin-mediated endocytosis machinery. *Cell*, 123(2):305–320, Oct 2005. doi: 10.1016/j.cell.2005.09.024.

Pawel Kaliszewski and Teresa Zoadek. The role of rsp5 ubiquitin ligase in regulation of diverse processes in yeast cells. *Acta Biochim Pol*, 55(4):649–662, 2008.

Pakorn Kanchanawong, Gleb Shtengel, Ana M Pasapera, Ericka B Ramko, Michael W Davidson, Harald F Hess, and Clare M Waterman. Nanoscale architecture of integrin-based cell adhesions. *Nature*, 468(7323):580–584, Nov 2010. doi: 10.1038/nature09621.

Lena Karotki, Juha T Huiskonen, Christopher J Stefan, Natasza E Ziflkowska, Robyn Roth, Michal A Surma, Nevan J Krogan, Scott D Emr, John Heuser, Kay Grunewald,

and Tobias C Walther. Eisosome proteins assemble into a membrane scaffold. *J Cell Biol*, 195(5):889–902, Nov 2011. doi: 10.1083/jcb.201104040.

Matthew Kirkham and Robert G Parton. Clathrin-independent endocytosis: new insights into caveolae and non-caveolar lipid raft carriers. *Biochim Biophys Acta*, 1746(3):349–363, Dec 2005.

Martin Klammer, David N Messina, Thomas Schmitt, and Erik L L Sonnhammer. Metatm - a consensus method for transmembrane protein topology prediction. *BMC Bioinformatics*, 10:314, 2009. doi: 10.1186/1471-2105-10-314.

T. A. Klar and S. W. Hell. Subdiffraction resolution in far-field fluorescence microscopy. *Opt Lett*, 24(14):954–956, Jul 1999.

A. Kusumi, Y. Sako, and M. Yamamoto. Confined lateral diffusion of membrane receptors as studied by single particle tracking (nanovid microscopy). effects of calcium-induced differentiation in cultured epithelial cells. *Biophys J*, 65(5):2021–2040, Nov 1993.

Akihiro Kusumi, Chieko Nakada, Ken Ritchie, Kotono Murase, Kenichi Suzuki, Hideji Murakoshi, Rinshi S Kasai, Junko Kondo, and Takahiro Fujiwara. Paradigm shift of the plasma membrane concept from the two-dimensional continuum fluid to the partitioned fluid: high-speed single-molecule tracking of membrane molecules. *Annu Rev Biophys Biomol Struct*, 34:351–378, 2005. doi: 10.1146/annurev.biophys.34.040204.144637.

Elsa Lauwers and Bruno Andre. Association of yeast transporters with detergent-resistant membranes correlates with their cell-surface location. *Traffic*, 7(8):1045–1059, Aug 2006. doi: 10.1111/j.1600-0854.2006.00445.x.

Elsa Lauwers, Christophe Jacob, and Bruno Andre. K63-linked ubiquitin chains as a specific signal for protein sorting into the multivesicular body pathway. *J Cell Biol*, 185 (3):493–502, May 2009. doi: 10.1083/jcb.200810114.

Elsa Lauwers, Zoi Erpapazoglou, Rosine Haguenauer-Tsapis, and Bruno Andre. The ubiquitin code of yeast permease trafficking. *Trends Cell Biol*, 20(4):196–204, Apr 2010. doi: 10.1016/j.tcb.2010.01.004.

A.G. Lee. Annular events: lipid-protein interactions. *Trends in Biochemical Sciences*, 2 (10):231 – 233, 1977. ISSN 0968-0004. doi: 10.1016/0968-0004(77)90117-7.

Anthony G Lee. How lipids affect the activities of integral membrane proteins. *Biochim Biophys Acta*, 1666(1-2):62–87, Nov 2004. doi: 10.1016/j.bbamem.2004.05.012.

Anthony G Lee. How lipids and proteins interact in a membrane: a molecular approach. *Mol Biosyst*, 1(3):203–212, Sep 2005. doi: 10.1039/b504527d.

Anthony G Lee. Biological membranes: the importance of molecular detail. *Trends Biochem Sci*, 36(9):493–500, Sep 2011. doi: 10.1016/j.tibs.2011.06.007.

J. Y. Lehtonen, J. M. Holopainen, and P. K. Kinnunen. Evidence for the formation of microdomains in liquid crystalline large unilamellar vesicles caused by hydrophobic mismatch of the constituent phospholipids. *Biophys J*, 70(4):1753–1760, Apr 1996a. doi: 10.1016/S0006-3495(96)79738-2.

J. Y. Lehtonen, M. Rytomaa, and P. K. Kinnunen. Characteristics of the binding of tacrine to acidic phospholipids. *Biophys J*, 70(5):2185–2194, May 1996b. doi: 10.1016/S0006-3495(96)79784-9.

Mark A Lemmon. Membrane recognition by phospholipid-binding domains. *Nat Rev Mol Cell Biol*, 9(2):99–111, Feb 2008. doi: 10.1038/nrm2328.

Ilya Levental, Daniel Lingwood, Michal Grzybek, Unal Coskun, and Kai Simons. Palmitoylation regulates raft affinity for the majority of integral raft proteins. *Proc Natl Acad Sci U S A*, 107(51):22050–22054, Dec 2010. doi: 10.1073/pnas.1016184107.

Charles H Lin, Jason A MacGurn, Tony Chu, Christopher J Stefan, and Scott D Emr. Arrestin-related ubiquitin-ligase adaptors regulate endocytosis and protein turnover at the cell surface. *Cell*, 135(4):714–725, Nov 2008. doi: 10.1016/j.cell.2008.09.025.

Daniel Lingwood and Kai Simons. Lipid rafts as a membrane-organizing principle. *Science*, 327(5961):46–50, Jan 2010. doi: 10.1126/science.1174621.

Daniel Lingwood, Hermann-Josef Kaiser, Ilya Levental, and Kai Simons. Lipid rafts as functional heterogeneity in cell membranes. *Biochem Soc Trans*, 37(Pt 5):955–960, Oct 2009. doi: 10.1042/BST0370955.

Martin Loibl, Guido Grossmann, Vendula Stradalova, Andreas Klingl, Reinhard Rachel, Widmar Tanner, Jan Malinsky, and Miroslava Opekarova. C terminus of nce102 deter-

mines the structure and function of microdomains in the saccharomyces cerevisiae plasma membrane. *Eukaryot Cell*, 9(8):1184–1192, Aug 2010. doi: 10.1128/EC.00006-10.

Shaoying Lu, Mingxing Ouyang, Jihye Seong, Jin Zhang, Shu Chien, and Yingxiao Wang. The spatiotemporal pattern of src activation at lipid rafts revealed by diffusion-corrected fret imaging. *PLoS Comput Biol*, 4(7):e1000127, 2008. doi: 10.1371/journal.pcbi.1000127.

Mary Luckey. *Membrane structural biology: with biochemical and biophysical foundations*. 2008. ISBN 978-0-521-85655-3.

Benjamin B Machta, Stefanos Papanikolaou, James P Sethna, and Sarah L Veatch. Minimal model of plasma membrane heterogeneity requires coupling cortical actin to criticality. *Biophys J*, 100(7):1668–1677, Apr 2011. doi: 10.1016/j.bpj.2011.02.029.

Katerina Malinska, Jan Malinska, Miroslava Opekarova, and Widmar Tanner. Visualization of protein compartmentation within the plasma membrane of living yeast cells. *Mol Biol Cell*, 14(11):4427–4436, Nov 2003. doi: 10.1091/mbc.E03-04-0221.

Katerina Malinska, Jan Malinsky, Miroslava Opekarova, and Widmar Tanner. Distribution of can1p into stable domains reflects lateral protein segregation within the plasma membrane of living s. cerevisiae cells. *J Cell Sci*, 117(Pt 25):6031–6041, Dec 2004. doi: 10.1242/jcs.01493.

E.M.M. Manders, F.J. Verbeek, and J.A. Aten. Measurement of co-localization of object in dual-colour confocal images. *J Microsc*, pages 375–382, 1993.

C. Marchal, R. Haguenauer-Tsapis, and D. Urban-Grimal. A pest-like sequence mediates phosphorylation and efficient ubiquitination of yeast uracil permease. *Mol Cell Biol*, 18 (1):314–321, Jan 1998.

Sebastian Maurer-Stroh, Birgit Eisenhaber, and Frank Eisenhaber. N-terminal n-myristoylation of proteins: refinement of the sequence motif and its taxon-specific differences. *J Mol Biol*, 317(4):523–540, Apr 2002. doi: 10.1006/jmbi.2002.5425.

Thomas J McIntosh, Adriana Vidal, and Sidney A Simon. Sorting of lipids and transmembrane peptides between detergent-soluble bilayers and detergent-resistant rafts. *Biophys J*, 85(3):1656–1666, Sep 2003. doi: 10.1016/S0006-3495(03)74595-0.

A. D. McLachlan. Repeating sequences and gene duplication in proteins. *J Mol Biol*, 64 (2):417–437, Mar 1972.

Stuart McLaughlin and Diana Murray. Plasma membrane phosphoinositide organization by protein electrostatics. *Nature*, 438(7068):605–611, Dec 2005. doi: 10.1038/nature04398.

Christien J Merrifield, Morris E Feldman, Lei Wan, and Wolfhard Almers. Imaging actin and dynamin recruitment during invagination of single clathrin-coated pits. *Nat Cell Biol*, 4(9):691–698, Sep 2002. doi: 10.1038/ncb837.

O. G. Mouritsen and M. Bloom. Mattress model of lipid-protein interactions in membranes. *Biophys J*, 46(2):141–153, Aug 1984. doi: 10.1016/S0006-3495(84)84007-2.

Debdyuti Mukhopadhyay and Howard Riezman. Proteasome-independent functions of ubiquitin in endocytosis and signaling. *Science*, 315(5809):201–205, Jan 2007. doi: 10.1126/science.1127085.

Dorothy I Mundy, Thomas Machleidt, Yun shu Ying, Richard G W Anderson, and George S Bloom. Dual control of caveolar membrane traffic by microtubules and the actin cytoskeleton. *J Cell Sci*, 115(Pt 22):4327–4339, Nov 2002.

Kotono Murase, Takahiro Fujiwara, Yasuhiro Umemura, Kenichi Suzuki, Ryota Iino, Hidetoshi Yamashita, Mihoko Saito, Hideji Murakoshi, Ken Ritchie, and Akihiro Kusumi. Ultrafine membrane compartments for molecular diffusion as revealed by single molecule techniques. *Biophys J*, 86(6):4075–4093, Jun 2004. doi: 10.1529/biophysj.103.035717.

Klaus Natter, Peter Leitner, Alexander Faschinger, Heimo Wolinski, Stephen McCraith, Stanley Fields, and Sepp D Kohlwein. The spatial organization of lipid synthesis in the yeast saccharomyces cerevisiae derived from large scale green fluorescent protein tagging and high resolution microscopy. *Mol Cell Proteomics*, 4(5):662–672, May 2005. doi: 10.1074/mcp.M400123-MCP200.

Elina Nikko and Hugh R B Pelham. Arrestin-mediated endocytosis of yeast plasma membrane transporters. *Traffic*, 10(12):1856–1867, Dec 2009. doi: 10.1111/j.1600-0854.2009.00990.x.

Elina Nikko, James A Sullivan, and Hugh R B Pelham. Arrestin-like proteins mediate ubiquitination and endocytosis of the yeast metal transporter smf1. *EMBO Rep*, 9(12): 1216–1221, Dec 2008. doi: 10.1038/embor.2008.199.

Jorg Nikolaus, Silvia Scolari, Elisa Bayraktarov, Nadine Jungnick, Stephanie Engel, Anna Pia Plazzo, Martin Stockl, Rudolf Volkmer, Michael Veit, and Andreas Herrmann. Hemagglutinin of influenza virus partitions into the nonraft domain of model membranes. *Biophys J*, 99(2):489–498, Jul 2010. doi: 10.1016/j.bpj.2010.04.027.

A. H. O'Keeffe, J. M. East, and A. G. Lee. Selectivity in lipid binding to the bacterial outer membrane protein ompf. *Biophys J*, 79(4):2066–2074, Oct 2000. doi: 10.1016/S0006-3495(00)76454-X.

M. Opekarova and W. Tanner. Nystatin changes the properties of transporters for arginine and sugars. an in vitro study. *FEBS Lett*, 350(1):46–50, Aug 1994.

Miroslava Opekarova, Katerina Malinska, Linda Novakova, and Widmar Tanner. Differential effect of phosphatidylethanolamine depletion on raft proteins: further evidence for diversity of rafts in saccharomyces cerevisiae. *Biochim Biophys Acta*, 1711(1):87–95, Jun 2005. doi: 10.1016/j.bbamem.2005.02.015.

Unn Ortegren, Margareta Karlsson, Natascha Blazic, Maria Blomqvist, Fredrik H Nystrom, Johanna Gustavsson, Pam Fredman, and Peter Stralfors. Lipids and glycosphingolipids in caveolae and surrounding plasma membrane of primary rat adipocytes. *Eur J Biochem*, 271(10):2028–2036, May 2004. doi: 10.1111/j.1432-1033.2004.04117.x.

S. Ozcan and M. Johnston. Function and regulation of yeast hexose transporters. *Microbiol Mol Biol Rev*, 63(3):554–569, Sep 1999.

Robert G Parton and Kai Simons. The multiple faces of caveolae. *Nat Rev Mol Cell Biol*, 8(3):185–194, Mar 2007. doi: 10.1038/nrm2122.

Irina Pozdnyakova and Pernilla Wittung-Stafshede. Non-linear effects of macromolecular crowding on enzymatic activity of multi-copper oxidase. *Biochim Biophys Acta*, 1804(4): 740–744, Apr 2010. doi: 10.1016/j.bbapap.2009.11.013.

F. Prado and A. Aguilera. New in-vivo cloning methods by homologous recombination in yeast. *Curr Genet*, 25(2):180–183, Feb 1994.

G. C. Prendergast. Farnesyltransferase inhibitors: antineoplastic mechanism and clinical prospects. *Curr Opin Cell Biol*, 12(2):166–173, Apr 2000.

Derek C Prosser, Theodore G Drivas, Lymarie Maldonado-Baez, and Beverly Wendland. Existence of a novel clathrin-independent endocytic pathway in yeast that depends on rho1 and formin. *J Cell Biol*, 195(4):657–671, Nov 2011. doi: 10.1083/jcb.201104045.

Britta Qualmann, Dennis Koch, and Michael Manfred Kessels. Let's go bananas: revisiting the endocytic bar code. *EMBO J*, 30(17):3501–3515, 2011. doi: 10.1038/emboj.2011.266.

F. Reggiori, E. Canivenc-Gansel, and A. Conzelmann. Lipid remodeling leads to the introduction and exchange of defined ceramides on gpi proteins in the er and golgi of saccharomyces cerevisiae. *EMBO J*, 16(12):3506–3518, Jun 1997. doi: 10.1093/emboj/16.12.3506.

Steve L Reichow and Tamir Gonen. Lipid-protein interactions probed by electron crystallography. *Curr Opin Struct Biol*, 19(5):560–565, Oct 2009. doi: 10.1016/j.sbi.2009.07.012.

Jian Ren, Longping Wen, Xinjiao Gao, Changjiang Jin, Yu Xue, and Xuebiao Yao. Csspalm 2.0: an updated software for palmitoylation sites prediction. *Protein Eng Des Sel*, 21(11):639–644, Nov 2008. doi: 10.1093/protein/gzn039.

Patrick J Roberts, Natalia Mitin, Patricia J Keller, Emily J Chenette, James P Madigan, Rachel O Currin, Adrienne D Cox, Oswald Wilson, Paul Kirschmeier, and Channing J Der. Rho family gtpase modification and dependence on caax motif-signaled posttranslational modification. *J Biol Chem*, 283(37):25150–25163, Sep 2008. doi: 10.1074/jbc.M800882200.

Amy F Roth, Junmei Wan, Aaron O Bailey, Beimeng Sun, Jason A Kuchar, William N Green, Brett S Phinney, John R Yates, and Nicholas G Davis. Global analysis of protein palmitoylation in yeast. *Cell*, 125(5):1003–1013, Jun 2006. doi: 10.1016/j.cell.2006.03.042.

Eric Rubinstein. The complexity of tetraspanins. *Biochem Soc Trans*, 39(2):501–505, Apr 2011. doi: 10.1042/BST0390501.

Andreas Ruepp, Alfred Zollner, Dieter Maier, Kaj Albermann, Jean Hani, Martin Mokrejs, Igor Tetko, Ulrich Goldener, Gertrud Mannhaupt, Martin Munsterkletter, and H. Werner Mewes. The funcat, a functional annotation scheme for systematic classification of proteins from whole genomes. *Nucleic Acids Res*, 32(18):5539–5545, 2004. doi: 10.1093/nar/gkh894.

Koji Saito, Konomi Fujimura-Kamada, Hisatoshi Hanamatsu, Utako Kato, Masato Umeda, Keith G Kozminski, and Kazuma Tanaka. Transbilayer phospholipid flipping regulates cdc42p signaling during polarized cell growth via rga gtpase-activating proteins. *Dev Cell*, 13(5):743–751, Nov 2007. doi: 10.1016/j.devcel.2007.09.014.

Y. Sako and A. Kusumi. Compartmentalized structure of the plasma membrane for receptor movements as revealed by a nanometer-level motion analysis. *J Cell Biol*, 125(6):1251–1264, Jun 1994.

Sumana Sanyal, Christian G Frank, and Anant K Menon. Distinct flippases translocate glycerophospholipids and oligosaccharide diphosphate dolichols across the endoplasmic reticulum. *Biochemistry*, 47(30):7937–7946, Jul 2008. doi: 10.1021/bi800723n.

I. F. Sbalzarini and P. Koumoutsakos. Feature point tracking and trajectory analysis for video imaging in cell biology. *J Struct Biol*, 151(2):182–195, Aug 2005. doi: 10.1016/j.jsb.2005.06.002.

Lothar Schermelleh, Rainer Heintzmann, and Heinrich Leonhardt. A guide to super-resolution fluorescence microscopy. *J Cell Biol*, 190(2):165–175, Jul 2010. doi: 10.1083/jcb.201002018.

P. Schwille, J. Korlach, and W. W. Webb. Fluorescence correlation spectroscopy with single-molecule sensitivity on cell and model membranes. *Cytometry*, 36(3):176–182, Jul 1999.

Silvia Scolari, Stephanie Engel, Nils Krebs, Anna Pia Plazzo, Rodrigo F M De Almeida, Manuel Prieto, Michael Veit, and Andreas Herrmann. Lateral distribution of the transmembrane domain of influenza virus hemagglutinin revealed by time-resolved fluorescence imaging. *J Biol Chem*, 284(23):15708–15716, Jun 2009. doi: 10.1074/jbc.M900437200.

Prabuddha Sengupta, Tijana Jovanovic-Talisman, Dunja Skoko, Malte Renz, Sarah L Veatch, and Jennifer Lippincott-Schwartz. Probing protein heterogeneity in the plasma membrane using palm and pair correlation analysis. *Nat Methods*, 8(11):969–975, Nov 2011. doi: 10.1038/nmeth.1704.

R. Serrano. Characterization of the plasma membrane atpase of saccharomyces cerevisiae. *Mol Cell Biochem*, 22(1):51–63, Nov 1978.

Pranav Sharma, Rajat Varma, R. C. Sarasij, Ira, Karine Gousset, G. Krishnamoorthy, Madan Rao, and Satyajit Mayor. Nanoscale organization of multiple gpi-anchored proteins in living cell membranes. *Cell*, 116(4):577–589, Feb 2004.

Frances J Sharom. Flipping and flopping-lipids on the move. *IUBMB Life*, Jul 2011. doi: 10.1002/iub.515.

Hayley J Sharpe, Tim J Stevens, and Sean Munro. A comprehensive comparison of transmembrane domains reveals organelle-specific properties. *Cell*, 142(1):158–169, Jul 2010. doi: 10.1016/j.cell.2010.05.037.

Jialan Shi, Christian W Heegaard, Jan T Rasmussen, and Gary E Gilbert. Lactadherin binds selectively to membranes containing phosphatidyl-l-serine and increased curvature. *Biochim Biophys Acta*, 1667(1):82–90, Nov 2004. doi: 10.1016/j.bbamem.2004.09.006.

K. Simons and E. Ikonen. Functional rafts in cell membranes. *Nature*, 387(6633):569–572, Jun 1997. doi: 10.1038/42408.

S. J. Singer and G. L. Nicolson. The fluid mosaic model of the structure of cell membranes. *Science*, 175(23):720–731, Feb 1972.

O. Soetens, J. O. De Craene, and B. Andre. Ubiquitin is required for sorting to the vacuole of the yeast general amino acid permease, gap1. *J Biol Chem*, 276(47):43949–43957, Nov 2001. doi: 10.1074/jbc.M102945200.

Hae Won Sohn, Pavel Tolar, and Susan K Pierce. Membrane heterogeneities in the formation of b cell receptor-lyn kinase microclusters and the immune synapse. *J Cell Biol*, 182 (2):367–379, Jul 2008. doi: 10.1083/jcb.200802007.

I. A. Sparkes, K. Graumann, A. Martiniere, J. Schoberer, P. Wang, and A. Osterrieder. Bleach it, switch it, bounce it, pull it: using lasers to reveal plant cell dynamics. *J Exp Bot*, 62(1):1–7, Jan 2011. doi: 10.1093/jxb/erq351.

Olivier Staub and Daniela Rotin. Role of ubiquitylation in cellular membrane transport. *Physiol Rev*, 86(2):669–707, Apr 2006. doi: 10.1152/physrev.00020.2005.

T. P. Stauffer, S. Ahn, and T. Meyer. Receptor-induced transient reduction in plasma membrane ptdins(4,5)p2 concentration monitored in living cells. *Curr Biol*, 8(6):343–346, Mar 1998.

Helen E M Stimpson, Christopher P Toret, Aaron T Cheng, Barbara S Pauly, and David G Drubin. Early-arriving syp1p and ede1p function in endocytic site placement and formation in budding yeast. *Mol Biol Cell*, Sep 2009. doi: 10.1091/mbc.E09-05-0429.

Vendula Stradalova, Wiebke Stahlschmidt, Guido Grossmann, Michaela Blazikova, Reinhard Rachel, Widmar Tanner, and Jan Malinsky. Furrow-like invaginations of the yeast plasma membrane correspond to membrane compartment of can1. *J Cell Sci*, Jul 2009. doi: 10.1242/jcs.051227.

S. E. Sund, J. A. Swanson, and D. Axelrod. Cell membrane orientation visualized by polarized total internal reflection fluorescence. *Biophys J*, 77(4):2266–2283, Oct 1999.

M. Swaisgood and M. Schindler. Clonal selection by fluorescence redistribution after photobleaching (frap)–a "fast" lateral mobility fibroblast mutant (e7g1). *Exp Cell Res*, 180 (2):529–536, Feb 1989.

Michael M Tamkun, Kristen M S O'connell, and Annah S Rolig. A cytoskeletal-based perimeter fence selectively corrals a sub-population of cell surface kv2.1 channels. *J Cell Sci*, 120(Pt 14):2413–2423, Jul 2007. doi: 10.1242/jcs.007351.

Widmar Tanner, Jan Malinsky, and Miroslava Opekarova. In plant and animal cells, detergent-resistant membranes do not define functional membrane rafts. *Plant Cell*, 23(4):1191–1193, Apr 2011. doi: 10.1105/tpc.111.086249.

Kirill Tarassov, Vincent Messier, Christian R Landry, Stevo Radinovic, Mercedes M Serna Molina, Igor Shames, Yelena Malitskaya, Jackie Vogel, Howard Bussey, and Stephen W Michnick. An in vivo map of the yeast protein interactome. *Science*, 320(5882):1465–1470, Jun 2008. doi: 10.1126/science.1153878.

Junko Y Toshima, Jun ichi Nakanishi, Kensaku Mizuno, Jiro Toshima, and David G Drubin. Requirements for recruitment of a g protein-coupled receptor to clathrin-coated pits in budding yeast. *Mol Biol Cell*, 20(24):5039–5050, Dec 2009. doi: 10.1091/mbc.E09-07-0541.

Bebhinn Treanor and Facundo D Batista. Organisation and dynamics of antigen receptors: implications for lymphocyte signalling. *Curr Opin Immunol*, Apr 2010. doi: 10.1016/j.coi.2010.03.009.

Bebhinn Treanor, David Depoil, Andreas Bruckbauer, and Facundo D Batista. Dynamic cortical actin remodeling by erm proteins controls bcr microcluster organization and integrity. *J Exp Med*, 208(5):1055–1068, May 2011. doi: 10.1084/jem.20101125.

Esa K J Tuominen, Carmichael J A Wallace, and Paavo K J Kinnunen. Phospholipid-cytochrome c interaction: evidence for the extended lipid anchorage. *J Biol Chem*, 277 (11):8822–8826, Mar 2002. doi: 10.1074/jbc.M200056200.

D. Tyteca, L. D'Auria, P. Van Der Smissen, T. Medts, S. Carpentier, J. C. Monbaliu, P. de Diesbach, and P. J. Courtoy. Three unrelated sphingomyelin analogs spontaneously cluster into plasma membrane micrometric domains. *Biochim Biophys Acta*, 1798(5): 909–927, May 2010. doi: 10.1016/j.bbamem.2010.01.021.

Maho Uchida, Rosa R Mourino-Perez, and Robert W Roberson. Live-cell imaging of microtubule dynamics in hyphae of neurospora crassa. *Methods Mol Biol*, 638:259–268, 2010. doi: 10.1007/978-1-60761-611-$5_1$9.

Yasuhiro M Umemura, Marija Vrljic, Stefanie Y Nishimura, Takahiro K Fujiwara, Kenichi G N Suzuki, and Akihiro Kusumi. Both mhc class ii and its gpi-anchored form undergo hop diffusion as observed by single-molecule tracking. *Biophys J*, 95(1):435–450, Jul 2008. doi: 10.1529/biophysj.107.123018.

Javier Valdez-Taubas and Hugh R B Pelham. Slow diffusion of proteins in the yeast plasma membrane allows polarity to be maintained by endocytic cycling. *Curr Biol*, 13(18):1636–1640, Sep 2003.

M. E. van der Rest, A. H. Kamminga, A. Nakano, Y. Anraku, B. Poolman, and W. N. Konings. The plasma membrane of saccharomyces cerevisiae: structure, function, and biogenesis. *Microbiol Rev*, 59(2):304–322, Jun 1995.

G. van Meer, E. H. Stelzer, R. W. Wijnaendts van Resandt, and K. Simons. Sorting of sphingolipids in epithelial (madin-darby canine kidney) cells. *J Cell Biol*, 105(4):1623–1635, Oct 1987.

Gerrit van Meer. Dynamic transbilayer lipid asymmetry. *Cold Spring Harb Perspect Biol*, 3 (5), May 2011. doi: 10.1101/cshperspect.a004671.

Adriana Vidal and Thomas J McIntosh. Transbilayer peptide sorting between raft and nonraft bilayers: comparisons of detergent extraction and confocal microscopy. *Biophys J*, 89(2): 1102–1108, Aug 2005. doi: 10.1529/biophysj.105.062380.

Gema Vizcay-Barrena, Stephen E D Webb, Marisa L Martin-Fernandez, and Zoe A Wilson. Subcellular and single-molecule imaging of plant fluorescent proteins using total internal reflection fluorescence microscopy (tirfm). *J Exp Bot*, 62(15):5419–5428, Nov 2011. doi: 10.1093/jxb/err212.

Elizabeth J Wallace, Nigel M Hooper, and Peter D Olmsted. Effect of hydrophobic mismatch on phase behavior of lipid membranes. *Biophys J*, 90(11):4104–4118, Jun 2006. doi: 10.1529/biophysj.105.062778.

Christopher Walsh. *Posttranslational Modification of Proteins: Tools for Functional Proteomics*. 2006. ISBN 978-0-89603-678-9.

Tobias C Walther, Jason H Brickner, Pablo S Aguilar, Sebastian Bernales, Carlos Pantoja, and Peter Walter. Eisosomes mark static sites of endocytosis. *Nature*, 439(7079):998–1003, Feb 2006. doi: 10.1038/nature04472.

Jennifer C Waters. Accuracy and precision in quantitative fluorescence microscopy. *J Cell Biol*, 185(7):1135–1148, Jun 2009. doi: 10.1083/jcb.200903097.

Jasper Weinberg and David G Drubin. Clathrin-mediated endocytosis in budding yeast. *Trends Cell Biol*, 22(1):1–13, Jan 2012. doi: 10.1016/j.tcb.2011.09.001.

Daniel Wipf, Uwe Ludewig, Mechthild Tegeder, Doris Rentsch, Wolfgang Koch, and Wolf B Frommer. Conservation of amino acid transporters in fungi, plants and animals. *Trends Biochem Sci*, 27(3):139–147, Mar 2002.

Goragot Wisedchaisri, Steve L Reichow, and Tamir Gonen. Advances in structural and functional analysis of membrane proteins by electron crystallography. *Structure*, 19(10): 1381–1393, Oct 2011. doi: 10.1016/j.str.2011.09.001.

Laxman Yetukuri, Kim Ekroos, Antonio Vidal-Puig, and Matej Oresic. Informatics and computational strategies for the study of lipids. *Mol Biosyst*, 4(2):121–127, Feb 2008. doi: 10.1039/b715468b.

Tony Yeung, Gary E Gilbert, Jialan Shi, John Silvius, Andras Kapus, and Sergio Grinstein. Membrane phosphatidylserine regulates surface charge and protein localization. *Science*, 319(5860):210–213, Jan 2008. doi: 10.1126/science.1152066.

Michael E Young, Tatiana S Karpova, Britta Braegger, Darcy M Moschenross, Georgeann K Wang, Roger Schneiter, Felix T Wieland, and John A Cooper. The sur7p family defines novel cortical domains in saccharomyces cerevisiae, affects sphingolipid metabolism, and is involved in sporulation. *Mol Cell Biol*, 22(3):927–934, Feb 2002.

Jerry H Yu, Alvaro H Crevenna, Mario Bettenbuhl, Tina Freisinger, and Roland Wedlich-Soldner. Cortical actin dynamics driven by formins and myosin v. *J Cell Sci*, 124(Pt 9): 1533–1541, May 2011. doi: 10.1242/jcs.079038.

Tobias Zech, Christer S Ejsing, Katharina Gaus, Ben de Wet, Andrej Shevchenko, Kai Simons, and Thomas Harder. Accumulation of raft lipids in t-cell plasma membrane domains engaged in tcr signalling. *EMBO J*, 28(5):466–476, Mar 2009. doi: 10.1038/emboj.2009.6.

Vadim Zinchuk and Olga Grossenbacher-Zinchuk. Recent advances in quantitative colocalization analysis: focus on neuroscience. *Prog Histochem Cytochem*, 44(3):125–172, 2009. doi: 10.1016/j.proghi.2009.03.001.

Natasza E Ziolkowska, Lena Karotki, Michael Rehman, Juha T Huiskonen, and Tobias C Walther. Eisosome-driven plasma membrane organization is mediated by bar domains. *Nat Struct Mol Biol*, 18(7):854–856, Jul 2011. doi: 10.1038/nsmb.2080.